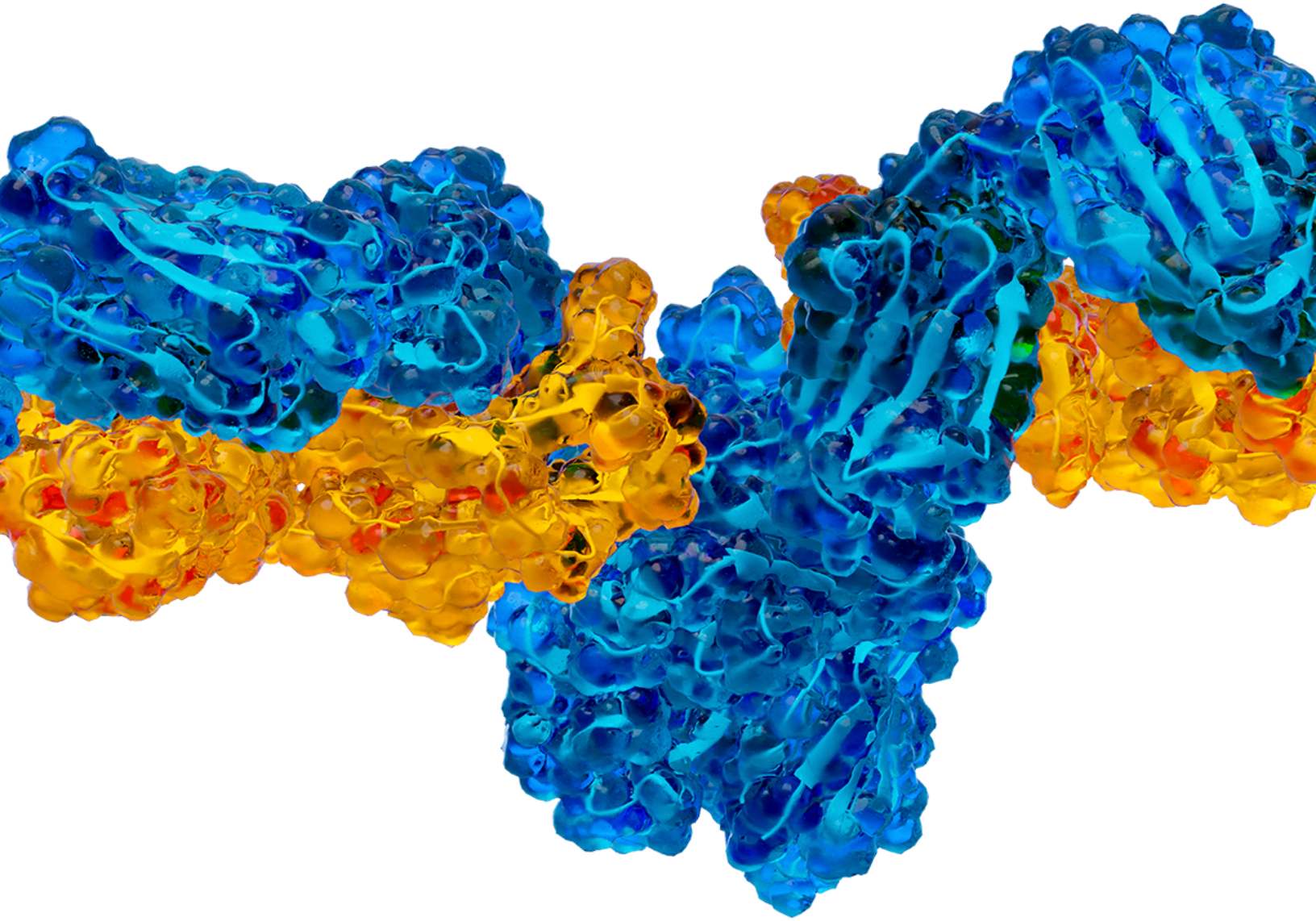

Harnessing icIEF to Unlock Protein-Based Therapeutics

ARTICLE COLLECTION

WILEY Analytical Science

Sponsored by:

bio-techne® | proteinsimple

FLEX YOUR FREEDOM

- Freedom to do more with your fractions
- Freedom from laborious IEX workflows
- Freedom to do more with your time
- Freedom to do more with your budget

Explore MauriceFlex

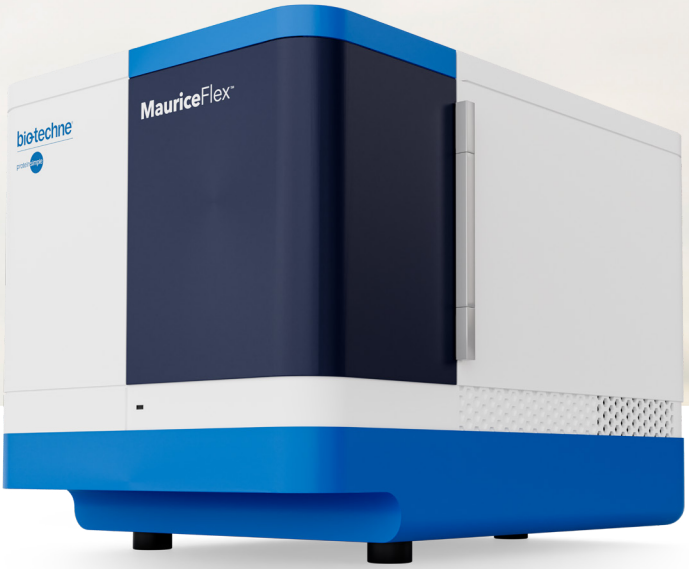

bio-techne® | proteinsimple

Contents

Introduction

The development of biotherapeutics has revolutionized modern medicine by providing new treatment options for a wide range of diseases. These biomolecules are often complex, heterogeneous, and fragile, which makes their production, purification, and delivery challenging. Methods to assess the surface charge of lipid nanoparticles and charge heterogeneity of proteins and antibodies are key to quality assurance in the biochemical industry.

The imaged capillary isoelectric focused (icIEF) technique utilizes imaging to visualize the separation of analytes along the length of the capillary, allowing for accurate determination of the pI of each molecule. This method is particularly useful in the biopharmaceutical industry for quality control and process development of protein-based drugs.

Seth Madren *et al.* (2022), report the results of an assessment that aimed to assess the robustness and precision of the iCE3 and Maurice platforms across numerous different bioanalytical laboratories. In this study they performed charge heterogeneity analysis of the National Institute of Standards and Technology (NIST) mAb and a rhPD-L1-Fc fusion protein.

Next, Finja Krebs *et al.* (2022) show how icEIF methods can successfully be used in quality and stability assessments of mRNA vaccines. Their focus was on investigating various storage times at different temperatures and freeze-thaw cycles, as well as the ability of the methods to distinguish lipid compositions and measure batch-to-batch variability.

The next study, by John W. Loughney *et al.* (2019) report on the development of an icIEF method to characterize the surface charge of mRNA lipid nanoparticle vaccines. This method is capable of distinguishing the pI of LNPs manufactured with one or more different ionizable lipids to confirm LNP identity in a manufacturing setting. Additionally, the method is quantitative and stability-indicating making it suitable for both process and formulation development.

Christin Scheller *et al.* (2021) have done a comparative study of CE-SDS, SDS-PAGE, and Simple Western methods for the shift of apparent molecular mass in glycosylated proteins. They found large deviations for some methods and offer some possible explanations for this.

The studies conclude with a whitepaper from Bio-Techne that highlights the possibilities the MauriceFlex system offers for icIEF Fractionation.

Through the methods and applications presented in this article collection, we aim to educate researchers on new technologies and techniques about icIEF. For more information, we encourage you to visit Bio-Techne to learn more and explore options to enhance your research.

Dr. Martin Graf-Utzmann
Editor at Wiley Analytical Science

References

Madren, S., McElroy, W., Schultz-Kuszak, K., Boumajny, B., Shu, Y., Sautter, S., Zhao, H.C., Schadock-Hewitt, A., Chumsae, C., Ball, N., Zhang, X., Rish, K., Zhang, S., Wurm, C., Cai, S., Bauer, S.P., Stella, C., Zheng, L., Roper, B., Michels, D.A., Wu, G., Kocjan, B., Birk, M., Erdmann, S.E., He, X., Whittaker, B., Song, Y., Barrett, H., Strozyk, K., Jing, Y., Huang, L., Mhatre, V., McLean, P., Yu, T., Yang, H. and Mattila, M. (2022), Global intercompany assessment of ICIEF platform comparability for the characterization of therapeutic proteins. ELECTROPHORESIS, 43: 1050-1058. https://doi.org/10.1002/elps.202100348

Krebs, F, Burger, U, Dörks, S, Kramer, M, Wätzig, H. (2022), Two quality and stability indicating imaged CIEF methods for mRNA vaccines. ELECTROPHORESIS, 43: 1971– 1983. https://doi.org/10.1002/elps.202200123

Loughney, J.W., Minsker, K., Ha, S. and Rustandi, R.R. (2019), Development of an imaged capillary isoelectric focusing method for characterizing the surface charge of mRNA lipid nanoparticle vaccines. ELECTROPHORESIS, 40: 2602-2609. https://doi.org/10.1002/elps.201900063

Scheller, C., Krebs, F., Wiesner, R., Wätzig, H. and Oltmann-Norden, I. (2021), A comparative study of CE-SDS, SDS-PAGE, and Simple Western—Precision, repeatability, and apparent molecular mass shifts by glycosylation. ELECTROPHORESIS, 42: 1521-1531. https://doi.org/10.1002/elps.202100068

Electrophoresis 2022, *43*, 1050–1058

Seth Madren[1]
Will McElroy[2]
Kristin Schultz-Kuszak[3]
Boris Boumajny[4]
Yao Shu[5]
Sabine Sautter[6]
Helen C. Zhao[7]
Abby Schadock-Hewitt[7]
Chris Chumsae[7]
Nancy Ball[8]
Xiaoying Zhang[8]
Kimberly Rish[8]
Shukui Zhang[9]
Christine Wurm[10]
Sumin Cai[11]
Scott P. Bauer[11]
Cinzia Stella[12]
Laura Zheng[12]
Brian Roper[12]
David A. Michels[12]
Gang Wu[13]
Bostjan Kocjan[14]
Matej Birk[14]
Simon Erik Erdmann[15]
Xiaoping He[16]
Brad Whittaker[17]
Yvonne Song[17]
Hannah Barrett[18]
Kevin Strozyk[19]
Ye Jing[20]
Long Huang[21]
Vishal Mhatre[22]
Paul McLean[22]
Tiantian Yu[23]
Huijuan Yang[23]
Minna Mattila[24]

[1]Technical Development, Biogen Research Triangle Park, Durham, NC, USA

Received November 1, 2021
Revised February 7, 2022
Accepted February 17, 2022

Research Article

Global intercompany assessment of ICIEF platform comparability for the characterization of therapeutic proteins

An international team spanning 19 sites across 18 biopharmaceutical and *in vitro* diagnostics companies in the United States, Europe, and China, along with one regulatory agency, was formed to compare the precision and robustness of imaged CIEF (ICIEF) for the charge heterogeneity analysis of the National Institute of Standards and Technology (NIST) mAb and a rhPD-L1-Fc fusion protein on the iCE3 and the Maurice instruments. This information has been requested to help companies better understand how these instruments compare and how to transition ICIEF methods from iCE3 to the Maurice instrument. The different laboratories performed ICIEF on the NIST mAb and rhPD-L1-Fc with both the iCE3 and Maurice using analytical methods specifically developed for each of the molecules. After processing the electropherograms, statistical evaluation of the data was performed to determine consistencies within and between laboratory and outlying information. The apparent isoelectric point (p*I*) data generated, based on two-point calibration, for the main isoform of the NIST mAb showed high precision between laboratories, with RSD values of less than 0.3% on both instruments. The SDs for the NIST mAb and the rhPD-L1-Fc charged variants percent peak area values for both instruments are less than 1.02% across different laboratories. These results validate the appropriate use of both the iCE3 and Maurice for ICIEF in the biopharmaceutical industry in support of process development and regulatory submissions of biotherapeutic molecules. Further, the data comparability between the iCE3 and Maurice illustrates that the Maurice platform is a next-generation replacement for the iCE3 that provides comparable data.

Keywords:
Antibody / Biopharmaceutical analysis / Fusion protein / ICIEF / Imaged capillary Isoelectric focusing
DOI 10.1002/elps.202100348

Additional supporting information may be found online in the Supporting Information section at the end of the article.

1 Introduction

There is a pressing need for robust analytical techniques to monitor and control protein drug product quality, owing to the rapid development and commercialization of mAbs, fusion proteins, biosimilars, etc., over the last 15 years. Charge heterogeneity is deemed a critical product quality attribute by regulatory agencies and must be evaluated due to the potential impact of acidic and basic isoforms on pharmacokinetics, biological activity, and long-term storage [1,2]. Charge heterogeneity can be monitored by a wide range of analytical methods that are based on LC [3] or electrophoresis [4]. Among the electrophoretic-based methods, CIEF has become the most common method used in the biopharmaceutical industry to characterize charge heterogeneity [4,5].

In conventional CIEF methods, the analyte is focused inside a capillary and then mobilized past a detection window. While the mobilization of the analyte is required for detection with this technique, it can reduce the resolution of the separation by disturbing the focused bands. Imaged CIEF (ICIEF)

Correspondence: Dr. Seth Madren, Technical Development, Biogen, Research Triangle Park, Durham, NC, USA.
E-mail: seth.madren@biogen.com

Abbreviations: **ICIEF**, imaged CIEF; **ISO**, International Organization for Standardization; **NIST**, National Institute of Standards and Technology; **PD-L1**, programmed death-ligand 1

Color online: See article online to view Fig. 1 in color.

was developed to eliminate the need for the mobilization step. In ICIEF, focusing of the analyte occurs in a capillary and is monitored by a whole-capillary detection system at 280 nm. As a result, the different charge variants of a sample can be simultaneously recorded by the whole-capillary detector without disturbing the separation resolution, which can result in improved reproducibility compared to conventional CIEF. In addition, since there is no need for a lengthy mobilization step, the analysis time of ICIEF methods is significantly shorter, typically less than 10 min.

Because of its short run times and high resolution, ICIEF has increasingly been adopted by pharmaceutical and biotechnology industries as a primary tool for determining charge heterogeneity and identity of therapeutic proteins [6–10]. Along with the evolution of therapeutics, the technology for ICIEF detection has improved over the years. In 2011, the results of an interlaboratory collaboration with 11 independent biopharmaceutical companies in North America and Europe to evaluate the robustness of ICIEF for the charge heterogeneity analysis of a mAb using the iCE280 instrument were reported [11]. The apparent p*I* data generated for each resolved charge isoform showed excellent precision between instruments and across laboratories with RSD values of less than 0.8%. Similarly, the RSD for the charge variants percent peak area values were less than 11% across different laboratories. As the system gained popularity, improvements to the auto sampler and injector of the iCE280 were made, giving rise to the iCE3. In 2018, another intercompany study in China evaluated the iCE3 comparability between sites, with the goal of setting ICIEF as a compendial method [10]. Importantly, it was the first study of this nature that followed ICH guidelines to validate the ICIEF method and used a therapeutic monoclonal antibody instead of a reference molecule. Ten laboratories across eight different companies participated in that study, and the method was found to perform strongly on specificity, precision, accuracy, linearity, range, and limit of quantitation. Based on these results, the ICIEF method was validated as an identity and purity assay for the characterization of protein charge and stability studies of therapeutic mAbs. Studies such as these are critical for the acceptance of ICIEF by both industry and regulators because, while the method has been around for over 20 years, LC-based methods have existed significantly longer [3,12].

Just as improvements to the operation of the iCE280 resulted in the iCE3, additional improvements to the instrumentation have recently resulted in the Maurice. The cartridge for the iCE3 contains a capillary for focusing and imaging, reservoirs for the electrolytes, and capillaries for fluidic connection to the system. The cartridge for the Maurice contains these same components but in addition, it also contains all the fluidic connections required for sample injection and cartridge flushing, and the electrodes required for focusing. These changes to the cartridge result in simplified operation and reduces the number of instrumentation failures by moving the most common failure points from the instrument to the cartridge, which is frequently replaced. The significant changes in the instrument operation that result from this new cartridge has raised concerns regarding the comparability of the two systems have arisen. To demonstrate the comparability between iCE3 and Maurice, a global multi-lab study was conducted with a team of 19 companies, including biopharmaceutical companies, an *in vitro* diagonistics company, and a regulatory agency located in the United States, Europe, and China. This study evaluated the well-characterized National Institute of Standards and Technology monoclonal antibody (NISTmAb) reference material, and a programmed death-ligand 1 (PD-L1) fusion protein using both the iCE3 and Maurice instruments. Intra- and interlaboratory precision and robustness of the ICIEF method for the two different molecules on both instruments were evaluated to (i) determine the apparent p*I* and (ii) the relative distribution of the sample charge variants. The goals of this interlaboratory study are to (1) further facilitate regulatory and industrial acceptance of ICIEF as a reliable technology to assess the purity of therapeutic proteins as it relates to charge heterogeneity, (2) demonstrate the comparability of the iCE3 and Maurice instruments, and (3) demonstrate the ease of transitioning iCE3 methods to the Maurice.

2 Materials and methods

2.1 Samples and chemicals

All samples and chemicals used in this study were provided to the participants by Protein Simple.

NISTmAb (PN RM 8671) is a humanized IgG1κ monoclonal antibody and was obtained from the Materials Measurement Laboratory at NIST. The recombinant human PD-L1/B7-H1 Fc chimera protein (PN 156-B7-01M) was obtained from R&D systems (Minneapolis, MN). Pharmalyte 3–10 (PN GE17-0456-01) and Pharmalyte 8–10.5 (PN GE17-0455-01) were obtained from Millipore Sigma. SimpleSol protein solubilizer for cIEF (PN 046–575), Maurice cIEF cartridges (PN PS-MC02-C), iCE3 FC cartridge (PN 101701), electrolyte kit (0.08 M H_3PO_4 in 0.1% in methyl cellulose and 0.1 M NaOH in 0.1% methyl cellulose) (PN 102506), 500 mM arginine (PN 042–691), 1% methyl cellulose (PN 101876), 0.5% methyl cellulose (PN 102505), p*I* marker 4.05 (PN 046-029), p*I* marker 9.99 (PN 046-034), and p*I* marker 8.4 (PN 046-033) were obtained from Protein Simple.

2.2 Sample preparation

The NISTmAb sample solutions were prepared by adding 12 μL of NISTmAb at 10 mg/mL into a 1.5 mL microfuge tube containing 108 μL of deionized water. The solution was mixed by pipetting and was stored at 4°C on ice until ready for use. The rhPD-L1-Fc sample was prepared to a final concentration of 0.5 mg/mL.

The NISTmAb ampholyte mixture was prepared by adding the following reagents in a 1.5 mL microfuge tube: 592 μL of deionized water, 45 μL of Pharmalyte 8–10.5, 15 μL

of Pharmalyte 5–8, 15 μL of 500 mM arginine, 525 μL of 1% methylcellulose, 4 μL of p*I* marker 8.4, and 4 μL of p*I* marker 9.99. The microfuge tube was then vortexed for 10 s, followed by centrifugation for 3 min at 10 000 × *g*.

The rhPD-L1-Fc ampholyte mixture was prepared by adding the following reagents in a 1.5 mL microfuge tube: 600 μL of SimpleSol protein solubilizer, 34 μL of Pharmalyte 3–10, 11 μL of Pharmalyte 5–8, 525 μL of 1% methylcellulose, 22 μL of water, 4 μL of p*I* marker 8.4, and 4 μL of p*I* marker 4.05. The microfuge tube was then vortexed for 10 s, followed by centrifugation for 3 min at 10 000 × *g*.

Two preparations of each protein were prepared by mixing the ampholyte solutions with the respective antibody sample solutions. Note that 360 μL of both ampholyte solutions were each aliquoted into two 1.5 mL microcentrifuge tubes, one for the sample protein and the other for the blank. For NISTmAb analysis, 60 μL of 1 mg/mL NISTmAb was added to one microcentrifuge tube, while 60 μL of deionized water was added to another tube to serve as a blank. Similarly, for rhPD-L1-Fc analysis, 60 μL of rhPD-L1-Fc at 1 mg/mL was added to one tube, while 60 μL of the sample buffer was added to another tube serving as blank. All tubes were then vortexed for 5 s, followed by centrifugation for roughly 20 s. If the Prince autosampler was connected to the iCE3 system, 150 μL of each final sample was added to sample vials for the iCE3 and 150 μL of each final sample was added to a 96-well plate for the Maurice. If the Alcott autosampler was used, then 80 μL of final samples were added to a 96-well plate for the Maurice and the remaining sample volume was added to the sample vials for the iCE3. All Maurice and iCE3 96-well plates and vials with final samples were centrifuged for 1 min at 3000 × *g*.

2.3 Imaged capillary electrophoretic conditions

All participants in this study used the iCE3 and Maurice instruments from ProteinSimple. The iCE3 instrument employed a UV detector at 280 nm and an Alcott 720 Autosampler or PrinCE Next Microinjector. The Maurice instrument allowed UV absorbance at 280 nm. The sample compartments for the instruments were set at 10°C. For the analysis of NISTmAb, the samples were loaded into the cartridge and focused by using a potential of 1500 V for 1 min, and then at 3000 V for 12 min. For rhPD-L1-Fc analysis, the samples were focused using a potential of 1500 V for 1 min, followed by 3000 V for 10 min. Each sample was injected six times.

2.4 Data management and peak integration

As there were certain sites that did not use the Empower software, all unprocessed electropherograms were blinded and electronically transferred to ProteinSimple where the data were processed using Empower. The following data attributes were determined from the data supplied by the participants: apparent p*I*, percent peak area, intermediate precision, specificity, and repeatability. Three study coordinators representing United States, Europe, and China managed the experiments across the labs in each region.

Figure 1 shows the integrations for the NISTmAb and rhPD-L1-Fc. The NISTmAb was processed comparably to previous work [13,14] with three charge regions: acidic, main, and basic. The largest peak was identified as the main isoform and the region of the profile with a lower p*I* was considered acidic isoforms and the region of the profile with a higher p*I* was considered basic isoforms. rhPD-L1-Fc was divided into five peak groups. The two peak groups with the highest p*I* were then grouped together. The most basic peak was used for a relative migration time reference for component identification. The jump in the absorbance in the acidic region was used as the break between Group A and Group B. This jump was the most consistent feature of the rhPD-L1-Fc peak profile. Group B was always the next six peaks and Group C was always the next four more basic peaks. Group D was the remaining basic peaks.

2.5 Statistical data evaluation and outlier analysis

The statistical analysis was performed based on the principles of the International Organization for Standardization (ISO) 5725-2 Guide [15]. The processed data were critically evaluated to identify outliers. There are two possible types of outliers: (1) results collected from a single laboratory may deviate from the rest of the data collected at the lab, meaning their results are too low or too high compared the other values; and (2) data from a single laboratory may deviate in either repeatability or in mean values compared to the other labs. Unequal repeatability values deviate from a fundamental assumption in the statistical analysis, specifically homogeneity of variances.

To test for homogeneity of variances, the Cohran's test was utilized to detect outliers within laboratory variances. This test is calculated as:

$$C = \frac{s^2_{\max}}{\sum_{i=1}^{p} s_i^2}, \tag{1}$$

where $s^2_{\max}$ is the highest variance in the data set and s_i^2 is the variance of the laboratory being evaluated. The criteria for the outlier rejection were taken from the ISO 5725-2 Guideline. Variances significant at $\alpha = 0.01$ were considered outliers and were removed from the dataset, while stragglers (variances significant at $\alpha = 0.05$) were kept in for further calculations. Critical *C* values can be found in ISO 5725-2.

To test for outliers in the mean values of the relative peak areas, a two-sided Grubb's test was used. The test is calculated as:

$$G = \frac{\left|\bar{\bar{\gamma}}_{ij} - \bar{\gamma}_i\right|}{s}, \tag{2}$$

where $\bar{\gamma}_i$ is the laboratory mean, $\bar{\bar{\gamma}}_{ij}$ is the grand mean of all laboratories, and *s* is the standard deviation (SD) for all of the mean values. The value of *G* is compared to the critical val-

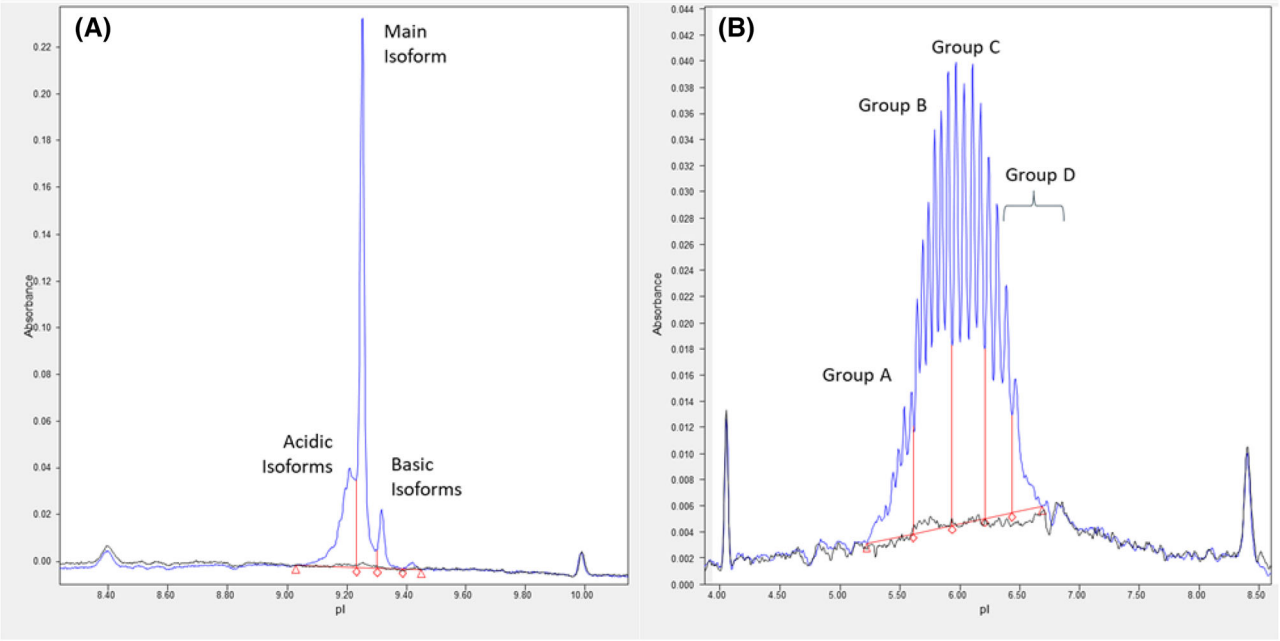

Figure 1. Example electropherograms obtained for (A) NISTmAb and (B) rhPD-L1-Fc, each overlaid with their respective formulation blank injections. Baselines for peak integration were selected to best agree with signal from blank injections.

ues for the test. Values larger than the critical value for the Grubb's test are considered outliers.

The grand mean, SD, and percent RSD for the relative peak areas for each peak were calculated after removing all outlying values.

3 Results and discussion

Figure 1 shows representative electropherograms for the NISTmAb and rhPD-L1-Fc sample and the integration protocols used for the relative peak area determinations. Consistent electrophoretic profiles were obtained by all laboratories on both the iCE3 and Maurice (Figs. S2–S19).

3.1 Qualitative comparison of the NISTmAb

The NISTmAb was selected as a model mAb for this study because it is a commercially available mAb with well-controlled characteristics that has been studied extensively previously [13,14]. The ICIEF profile for the NISTmAb contains a main isoform peak, which is the most abundant peak in the profile. Isoforms with apparent p*I* values greater than the main peak are considered basic and isoforms with apparent p*I* values less than the main peak are considered acidic. To evaluate the focusing of the NIST mAb on both the iCE3 and Maurice, the apparent p*I* for the main peak was compared. The apparent p*I* of a protein is determined by including markers of known p*I* values with the samples. Both the iCE3 and Maurice automatically calculate the p*I* values for the peak assuming a linear pH gradient between the p*I* markers. Therefore, the apparent p*I* value of a peak is highly dependent on the ability of the instrument to focus the ampholytes and the sample in a reproducible manner. To compare the focusing of the Maurice to the iCE3, the apparent p*I* value for the main isoform was calculated for each laboratory (Table 1). Both systems were able to achieve similar apparent p*I* across all laboratories with a %RSD between labs of <0.3%, even though two lots of Pharmalyte were used for both NISTmAb and rhPD-L1-Fc. This confirms that both instruments can reproducibly focus the NISTmAb across sites, with multiple analysts and multiple instruments. Both systems measured the p*I* value for the main isoform as 9.26, confirming that both systems focus the NIST mAb in a similar manner.

3.2 Quantitative comparison of the NISTmAb

The electropherograms collected at each laboratory were processed to determine the relative peak area for these acidic, main, and basic regions (Table S1). The data were used to determine the means and SD of the relative peak area of each region for each laboratory. The Cochran's and Grubb's tests were then applied to the data to identify any outlying results.

To detect outliers in the data, the Cochran's and Grubb's tests were applied to the data. The Cochran's test was used to identify data with variabilities that were significantly higher than the other labs. The Cochran's value (*C*) was determined by Eq. (1) for each region for each laboratory. The results for the relative peak area for each laboratory are shown in Fig. 2. It can be observed that results from laboratories 4, 7, and 14 show large *C* values, which are greater than the 1% critical value of 0.192 and should be rejected. All data from the iCE3

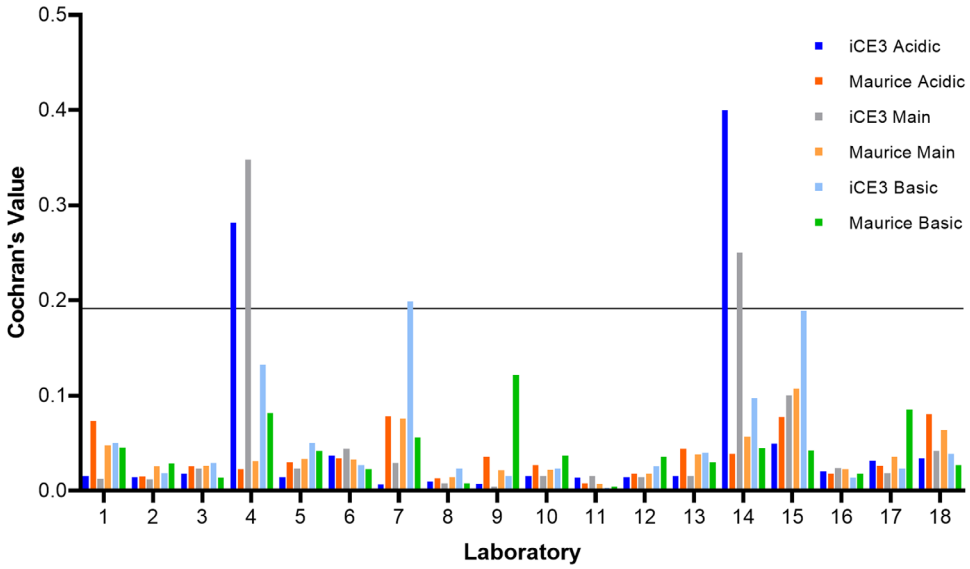

Figure 2. Cochran's *C* values to determine outliers in laboratory consistency within the NISTmAb dataset. The line represents the 1% critical value of 0.196.

Table 1. Apparent p*I* of the NIST mAb main isoform measured by each laboratory using both the iCE3 and Maurice instruments

Laboratory	Average apparent p*I* value	
	iCE3	Maurice
1	9.25	9.28
2	9.27	9.27
3	9.27	9.27
4	9.25	9.32
5	9.29	9.25
6	9.27	9.25
7	9.29	9.28
8	9.25	9.26
9	9.26	9.26
10	9.27	9.25
11	9.27	9.26
14	9.23	9.24
15	9.24	9.25
17	9.21	9.22
18	9.29	9.27
19	9.32	9.26
20	9.24	9.20
21	9.26	9.25
Mean	9.26	9.26
SD	0.025	0.026
%RSD	0.27	0.28

instrument were rejected from laboratories 4 and 14 since both the acidic and main peak values failed the Cochran's test. The basic region for the iCE3 instrument was rejected for lab 7. To detect outliers in the mean values for the relative peak areas, a two-sided Grubb's test was utilized. Data that had been rejected by the Cochran's test were not included in this analysis. The *G* value was determined by Eq. (2) for each region for each laboratory. The results of the Grubb's test are shown in Fig. S1. The Grubb's test does not reject any of the data in the study.

The data for laboratory 4 showed poor resolution of the basic isoforms for early injections but improved over the course of the experiment. For laboratory 14, the high variability can be attributed to a shoulder peak on the main isoform that is observed for some injections but not all of them. For laboratory 7, the high variability can be attributed to the second basic peak falling below the noise threshold for several injections. Fluctuations in the focusing of a protein are not uncommon in ICIEF and while a robust method can reduce the impact of these fluctuations, they are difficult to eliminate due to the complexity of the charge profile and the large number of possible root causes. Since the fluctuations are only observed on iCE3 systems, the sources of variability associated with the sample matrix and pharmalyte. A common source of variability that is only present on the iCE3 is hydrodynamic flow due to a poor fluid seal where the cartridge interfaces with the system. While major leaks are easily detected, minor leaks can occur intermittently before the highly viscus methylcellulose can seal the leaks temporarily. The cartridge for the Maurice eliminates this interface, eliminating this potential source of variability.

After the rejection of outliers by the Cochran's test, the remaining data were used to compare the results obtained on the Maurice to the results obtained on the iCE3. Figure 3 compares the relative percent area for the acidic, main, and basic isoforms measured on both instruments. The grand means of the relative peak areas for the acidic, main, and basic isoforms measured on the iCE3 (32.0%, 59.3% and 8.7%, respectively) agree with the values measured on the Maurice (32.0%, 59.2%, and 8.9%, respectively). The precisions of all three regions are comparable (Table S2) and the standard deviation of the data collected on the iCE3 (<0.91) is comparable to data collected on the Maurice (<1.02). The box plots in Fig. 3 show significant overlap of the data collected on both instruments,

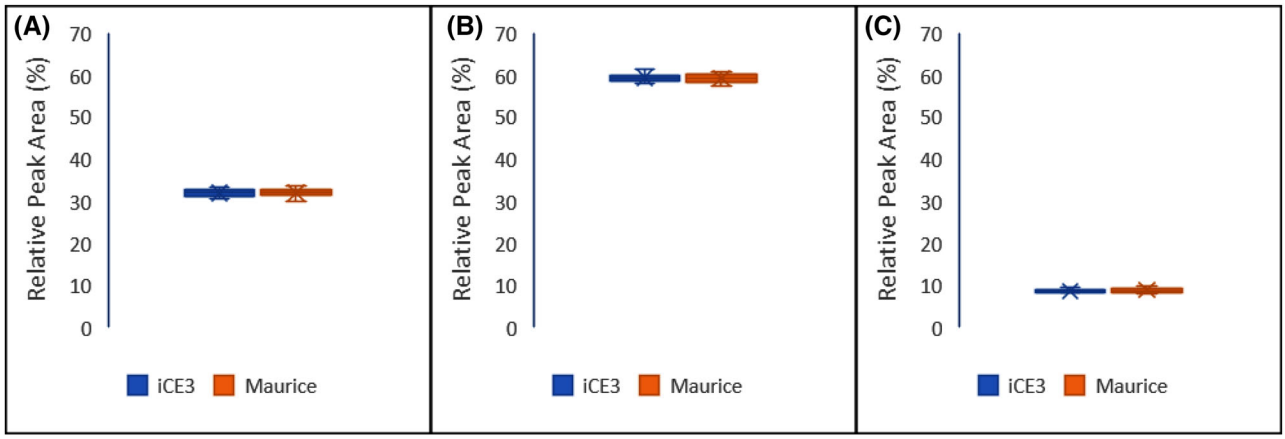

Figure 3. Box plots for the relative peak area for the acidic (A), main peak (B), and basic (C) isoforms for the NISTmAb.

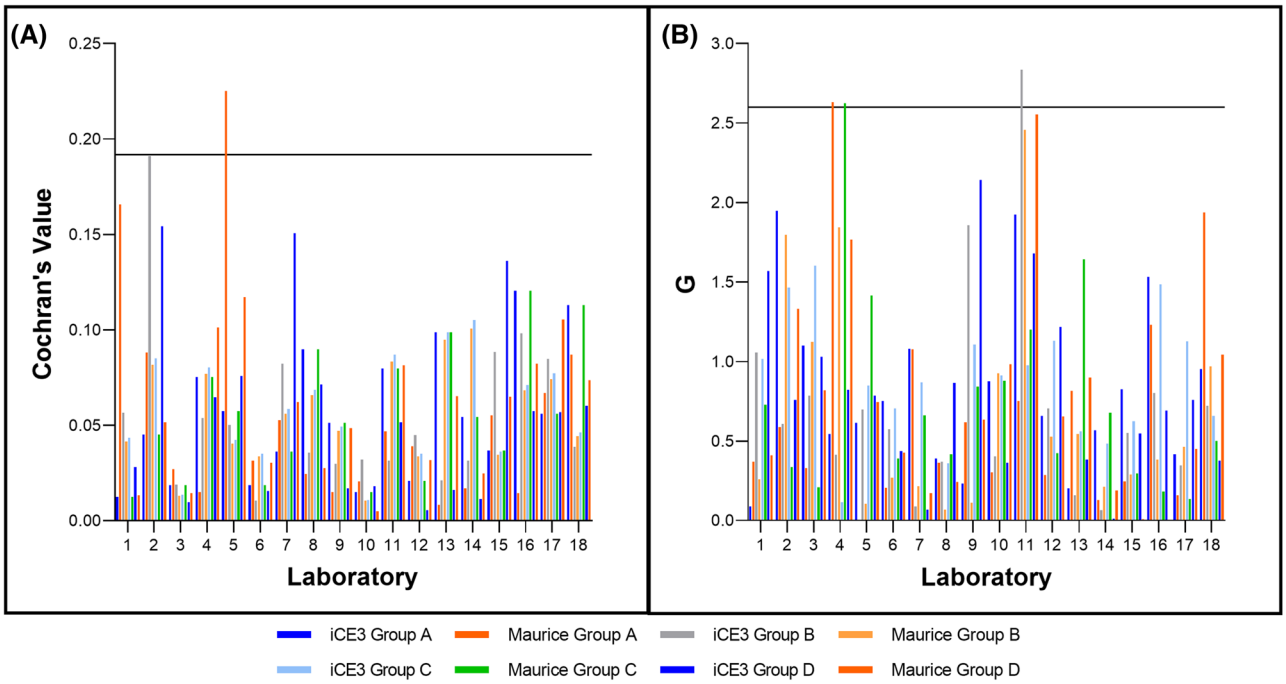

Figure 4. Cochran's *C* values (A) and Grubb's *G* values (B) to determine outliers in laboratory consistency within the rhPD-L1-Fc dataset. The line represents the 1% critical value for both statistical analyses.

supporting that the data from the Maurice are comparable to the data collected on the iCE3.

3.3 Comparison of rhPD-L1-Fc

Previously published round robin studies evaluating the performance of ICIEF [10,11] has used a mAb as the model protein. However, the use of ICIEF is not limited to mAbs. The fusion protein rhPD-L1-Fc was selected as a model for therapeutic proteins that have ICIEF profiles that are significantly more complex than routinely observed for mAbs. While not a therapeutic protein itself, rhPD-L1-Fc is a commercially available critical reagent that has been used as a reference standard for the characterization of other therapeutic proteins [16,17]. The ICIEF profile of the fusion protein rhPD-L1-Fc consists of over a dozen well-resolved peaks. Due to the complexity of its charge heterogeneity, the profile was grouped into five sections, with the two sections with the highest p*I* value combined into a single group, group D. Determination of apparent p*I* is not practical for such profiles and thus was not measured for this study. However, since the droplines for several sections in the profile are based on the number of peaks observed, the precision and robustness of the quantitative results is dependent on consistent focusing of the protein.

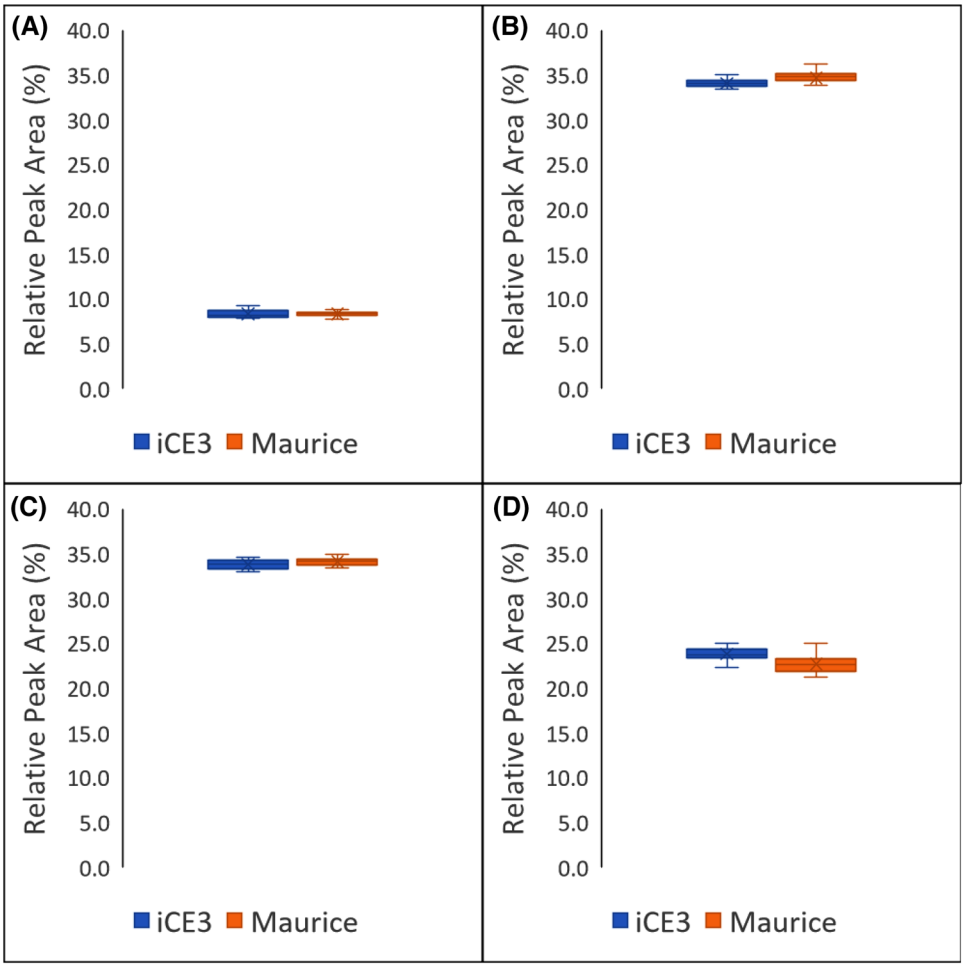

Figure 5. Box plots for the relative peak area for Group A (A), B (B), C (C), and D (D) of rhPD-L1-Fc.

The electropherograms collected at each laboratory were processed to determine the relative peak area for groups A, B, C, and D (Table S3). The data were used to determine the means and SD of the relative peak area of each region for each laboratory. As with the NIST mAb, the Cochran's and Grubb's tests were then applied to the data to identify any outlying results. The results of the Cochran's test for the relative peak area for each laboratory are shown in Fig. 4. It can be observed that results from laboratories 1 and 5 show large *C* values, which are greater than the 1% critical value of 0.196 and should be rejected. The group B data on the Maurice and group C data on the iCE3 for laboratory 1 were above the critical value and rejected. Since the high variability is observed on both the iCE3 and the Maurice, it is likely contamination in the pharmalyte or sample used for the analysis. The group A data on the Maurice for laboratory 5 was also rejected. This seems to be caused by a hump in the most acidic region of the profile. The rhPD-L1-Fc data from the Maurice has a lower intensity and therefore more sensitive to variability than the iCE3. To detect outliers in the mean values for the relative peak areas, the Grubb's test was utilized. As with the NISTmAb, data that had been rejected by the Cochran's test were not included in this analysis. The results of the Grubb's test are shown in Fig. 4. Results for group A and C on the Maurice from laboratory 4 have *G* values are above the critical value and are rejected. The intensity of the profile from the Maurice is much less than the other laboratories and is the likely reason for the out of trend results. Results for group B on the iCE3 and region D from laboratory 11 were also rejected. As with the data for laboratory 1, since data from both the Maurice and iCE3 are outliers, it seems likely that a contamination in the pharmalyte or sample is responsible. Due to the nature of the study (with testing sites across the world and test occurring over the course of multiple months), it is not feasible to identify the contamination with high confidence. However, since only two laboratories are outliers, it does not seem to be a systematic issue.

After the rejection of outliers by the Cochran's and Grubb's test, the remaining data were used to compare the results obtained on the Maurice to the results obtained on the iCE3. Figure 5 compares the relative percent area for the groups A, B, C, and D. The grand means of the relative peak areas for groups A, B, C, and D measured on the iCE3 (8.2%, 34.5%, 33.9%, and 23.6%, respectively) agree with the values measured on the Maurice (8.4%, 34.7%, 34.2% and 22.6%, respectively). The precisions of all three regions are comparable

(Table S4) and the standard deviation of the data collected on the iCE3 (<0.81) is comparable to data collected on the Maurice (<0.93). The box plots in Fig. 3 show significant overlap of the data collected on both instruments, supporting that the data from the Maurice are comparable to the data collected on the iCE3.

4 Concluding remarks

This manuscript describes an interlaboratory study to determine the performance and comparability of iCE3 and Maurice systems. To evaluate this, each site across North America, Europe, and Asia ran the same method using supplied materials, while data were processed by a single lab. The data included in this manuscript show that both the iCE3 and the Maurice systems can perform ICIEF in a robust manner to monitor charge heterogeneity of monoclonal antibodies and fusion proteins. The electropherograms for both the NISTmAb and the rhPD-L1-Fc are consistent across all laboratories and between both the iCE3 and the Maurice instruments. The iCE3 and Maurice instruments produce identical apparent p*I* values for the main isoform and comparable relative peak areas for the acidic, main, and basic isoforms for the NISTmAb. Both instruments also produce comparable quantitative results for rhPD-L1-Fc.

The authors would like to thank ProteinSimple, a Bio-Techne brand, for providing all the materials used in this study. The authors would also like to thank Ed Chase, Baburaj Kunnummal, Chris Heger, Susan Bilsborrow, Michael Eggers, and Manisha Pratap for assistance in study organization and design.

Protein Simple, the manufacturer of the iCE3 and Maurice, provided all required reagents to the participating labs and developed the focusing conditions used for the study. They were also involved in the study design and processing the blinded data.

Data availability statement

The data that support the findings of this study are available from the corresponding author upon reasonable request.

5 References

[1] Khawli, L. A., Goswami, S., Hutchinson, R., Kwong, Z. W., Yang, J., Wang, X., Yao, Z., Sreedhara, A., Cano, T., Tesar, D., Nijem, I., Allison, D. E., Wong, P. Y., Kao, Y.-H., Quan, C., Joshi, A., Harris, R. J., Motchnik, P., *MAbs* 2010, *2*, 613–624.

[2] Rudge, S. R., Nims, R. W., in *ICH Quality Guidelines: An Implementation Guide*, John Wiley & Sons, Inc., Hoboken, NJ 2017, pp. 467–486.

[3] Fekete, S., Beck, A., Veuthey, J. L., Guillarme, D., *J. Pharm. Biomed. Anal.* 2015, *113*, 43–55.

[4] Kumar, R., Guttman, A., Rathore, A. S., *Electrophoresis* 2022, *43*, 143–166.

[5] Sastre Toraño, J., Ramautar, R., de Jong, G., *J. Chromatogr. B: Anal. Technol. Biomed. Life Sci.* 2019, *1118–1119*, 116–136.

[6] Meert, C. D., Brady, L. J., Guo, A., Balland, A., *Anal. Chem.* 2010, *82*, 3510–3518.

[7] He, X. Z., Que, A. H., Mo, J. J., *Electrophoresis* 2009, *30*, 714–722.

[8] Zhang, J., Yip, H., Katta, V., *Anal. Biochem.* 2011, *410*, 234–243.

[9] Sosic, Z., Houde, D., Blum, A., Carlage, T., Lyubarskaya, Y., *Electrophoresis* 2008, *29*, 4368–4376.

[10] Wu, G., Yu, C., Wang, W., Wang, L., *Electrophoresis* 2018, *39*, 2091–2098.

[11] Salas-Solano, O., Babu, K., Park, S. S., Zhang, X., Zhang, L., Sosic, Z., Boumajny, B., Zeng, M., Cheng, K.-C., Reed-Bogan, A., Cummins-Bitz, S., Michels, D. A., Parker, M., Bonasia, P., Hong, M., Cook, S., Ruesch, M., Lamb, D., Bolyan, D., Kiessig, S., Allender, D., Nunnally, B., *Chromatographia* 2011, *73*, 1137–1144.

[12] Lucy, C. A., *J. Chromatogr. A* 2003, *1000*, 711–724.

[13] Turner, A., Schiel, J. E., *Anal. Bioanal. Chem.* 2018, *410*, 2079–2093.

[14] Michels, D. A., Ip, A. Y., Dillon, T. M., Brorson, K., Lute, S., Chavez, B., Prentice, K. M., Brady, L. J., Miller, K. J., in *State-of-the-Art and Emerging Technologies for Therapeutic Monoclonal Antibody Characterization Volume 2. Biopharmaceutical Characterization: The NISTmAb Case Study*, American Chemical Society, Washington DC 2015, pp. 237–284.

[15] ISO/IEC, *International Organization for Standardization, Accuracy (Trueness and Precision) of Measurements Methods and Results (ISO/IEC Standard 5725-2)*. 2019.

[16] Osa, A., Uenami, T., Koyama, S., Fujimoto, K., Okuzaki, D., Takimoto, T., Hirata, H., Yano, Y., Yokota, S., Kinehara, Y., Naito, Y., Otsuka, T., Kanazu, M., Kuroyama, M., Hamaguchi, M., Koba, T., Futami, Y., Ishijima, M., Suga, Y., Akazawa, Y., Machiyama, H., Iwahori, K., Takamatsu, H., Nagatomo, I., Takeda, Y., Kida, H., Akbay, E. A., Hammerman, P. S., Wong, K. K., Dranoff, G., Mori, M., Kijima, T., Kumanogoh, A., *JCI Insight* 2018, *3*, e59125.

[17] Burova, E., Hermann, A., Waite, J., Potocky, T., Lai, V., Hong, S., Liu, M., Allbritton, O., Woodruff, A., Wu, Q., D'Orvilliers, A., Garnova, E., Rafique, A., Poueymirou, W., Martin, J., Huang, T., Skokos, D., Kantrowitz, J., Popke, J., Mohrs, M., MacDonald, D., Ioffe, E., Olson, W., Lowy, I., Murphy, A., Thurston, G., *Mol. Cancer Ther.* 2017, *16*, 861.

6 Addendum

[2]ProteinSimple, San Jose, CA, USA
[3]Analytical Sciences, Biopharmaceutical Development, R&D, AstraZeneca, Gaithersburg, MD, USA
[4]Analytical Development, Biogen, Cambridge, MA, USA
[5]Bio Process + Analytical Development, Boehringer Ingelheim Pharma GmbH & Co. KG, Biberach an der Riss, Germany
[6]Quality Control/Clinical Supply Transfer, Boehringer Ingelheim Pharma GmbH & Co. KG, Biberach an der Riss, Germany
[7]Global Process Development Analytics, Biologics Development, Bristol Myers Squibb, Devens, MA, USA
[8]Biologics, Catalent Pharma Solutions, Kansas City, MO, USA
[9]Institute of Biologics, Chia Tai Tianqing Pharmaceutical Group Co., Ltd., Jiangsu, P. R. China
[10]Coriolis Pharma Research GmbH, Martinsried, Germany
[11]BioTechnology Discovery Research Lead Optimization, Eli Lilly and Company, Indianapolis, IN, USA
[12]Department of Protein Analytical Chemistry, Genentech, South San Francisco, CA, USA
[13]Key Laboratory of the Ministry of Health for Research on Quality and Standardization of Biotech Products, National Institutes for Food and Drug Control, Beijing, P. R. China
[14]Process Analytical Sciences, Novartis, Mengeš, Slovenia
[15]Novo Nordisk A/S, Hillerød, Denmark
[16]Analytical R&D, Biotherapeutics Pharmaceutical Sciences, Pfizer, Chesterfield, MO, USA
[17]BioProcess Analytics, Sanofi Genzyme, Framingham, MA, USA
[18]Analytical Development, Sanofi Genzyme, Framingham, MA, USA
[19]Analytical Sciences, Seagen Inc., Bothell, WA, USA
[20]Analytical Science and Development, Shanghai Henlius Biotech Inc., Shanghai, P. R. China
[21]Quality Research Department and Quality Control Department, Sichuan Kelun-Biotech Biopharmaceutical Co., Ltd., Sichuan, P. R. China
[22]Analytical Development, Takeda, Lexington, MA, USA
[23]Shanghai Analytical Sciences, WuXi Biologics, Shanghai, P. R. China
[24]Immunodiagnostic Reagents Business Unit, Medix Biochemica, Espoo, Finland

Received: 11 May 2022 | Revised: 11 August 2022 | Accepted: 13 August 2022

DOI: 10.1002/elps.202200123

ELECTROPHORESIS

RESEARCH ARTICLE

Two quality and stability indicating imaged CIEF methods for mRNA vaccines

Finja Krebs[1] | **Udo Burger**[2] | **Susanne Dörks**[2] | **Markus Kramer**[3] | **Hermann Wätzig**[1]

[1]Institute of Medicinal and Pharmaceutical Chemistry, Technische Universität Braunschweig, Braunschweig, Germany

[2]ProteinSimple, a Bio-Techne brand, Wiesbaden-Nordenstadt, Germany

[3]CureVac AG, Tübingen, Germany

Correspondence
Hermann Wätzig, Institute of Medicinal and Pharmaceutical Chemistry, Technische Universität Braunschweig, Beethovenstraße 55, 38106 Braunschweig, Germany.
Email: h.waetzig@tu-bs.de

Color online: See the article online to view Figures 1–2 in color.

Abstract

Two imaged capillary isoelectric focusing methods were developed to provide insight into the quality and stability of messenger ribonucleic acid (mRNA) vaccines, specifically, mRNA encapsulated in lipid nanoparticles (LNPs). A variety of stressed and lipid composition-modified samples were measured and detected by their UV absorption. The results were supported by the data of an encapsulation assay and particle sizing. One method, using 9 M urea as an additive, shows two broad and jagged peaks in which the peak shape offers detailed information. The summed peak area of both peaks showed RSDs from 2% to 8% when one batch was measured in triplicate and apparently depends on the size of the LNPs. In the second method, a combination of 5.5 M urea and 2 M *N*-ethylurea was used. This method is characterized by a high repeatability of the isoelectric point (p*I*, <0.5%). The repeatable peak area (RSD of 2%–7%) correlates linearly with the mRNA content, which also applies to the first method, and added stress is evident by the change in p*I* and peak area. Furthermore, experiments with the addition of a fluorescent dye were performed (fluorescence detection), which tremendously increased the sensitivity of the methods. Both methods can be used to characterize the stability of mRNA-loaded LNPs, for example, when investigating various storage times at different temperatures and freeze–thaw cycles, as well as the ability of the methods to distinguish lipid compositions and measure batch-to-batch variability.

KEYWORDS
CIEF, lipid nanoparticles, method development, mRNA, vaccines

1 | INTRODUCTION

Messenger ribonucleic acid (mRNA) vaccines generally comprise an mRNA, specific for the therapeutic target, which is encapsulated into a lipid nanoparticle (LNP) for patient delivery. The lipids contained in the LNP form an aqueous core in which the mRNA molecules reside,

Abbreviations: CMA, critical material attributes; CPP, critical process parameters; CQA, critical quality attributes; CS, control strategy; FTC, freeze–thaw cycles; iCIEF, imaged CIEF; LNP, lipid nanoparticle; mRNA, messenger ribonucleic acid; PDI, polydispersity index; TNS, 6-(*p*-Toluidino)-2-naphthalenesulfonic acid sodium salt.

allowing the mRNA to enter the cells in a protected manner [1]. The mRNA is thereby exposed to water, which can explain the low stability of these vaccines in the thawed state, as this can lead to degradation through hydrolysis and oxidation of the mRNA [2]. The theory that the mRNA is located in the core of the LNPs is supported by the RiboGreen assay [3].

Basically, the LNPs for mRNA vaccines need a cationic lipid that interacts with the negatively charged mRNA. Most of the cationic lipid is presumably located with the mRNA in the core of the LNP. In addition, polyethylene glycol (PEG)-lipids should be present to protect the LNPs from aggregation and unwanted interactions, as well as structural lipids, such as phospholipids and cholesterol, that are commonly found in cell membranes [4]. The mRNA-LNP (CureVac AG, Tübingen, Germany) used in this study consists of four lipid components: cholesterol, 1,2-distearoyl-*sn*-glycero-3-phosphocholine, PEGylated lipids, and a cationic lipid (LNP formulation by Acuitas Therapeutics [Vancouver, BC, Canada] [5]). The encapsulated, unmodified mRNA encodes the main rabies virus antigen, the envelope glycoprotein RABV-G [6].

Given the rising importance of modern mRNA vaccines, such as those used against COVID-19, the World Health Organization has proposed new guidance to focus on the relevant properties of mRNA vaccines to assess the quality, safety, and efficacy of mRNA for these vaccines [7]. The document provides regulatory considerations regarding key aspects for mRNA vaccines against infectious diseases in general and is intended to provide initial guidance until more detailed information becomes available [8].

Vaccines, and therefore mRNA vaccines, must be certified to be safe, effective, and of consistent quality. Before the vaccine can be administered, they must also be approved by public health authorities [9]. To learn more about the regulatory pathway for mRNA vaccines against infectious diseases in the EU, see Hinz et al. [10].

To demonstrate the important parameters, analytical methods are required to determine product identity, product- and process-related impurities, product content, and product potency [11]. The first step for this is to characterize the vaccine products to determine the critical quality attributes (CQAs) of the vaccine. Indeed, these are associated with safety, efficacy, and quality. Then, the critical process parameters (CPPs) and critical material attributes (CMAs) are determined. In addition, proven acceptable ranges (PARs) and design space are established, followed by the definition of a control strategy (CS). To determine and link CQAs, CPPs, CMAs, and PARs, and to establish a CS, analytical testing is essential [12–16].

Crommelin et al. [17] summarized analytical methods to determine and monitor quality attributes and stability of mRNA vaccines, which was adapted from the papers by Poveda et al. [18] and Muralidhara et al. [19]. Among the methods is an assay that leverages fluorescent dyes to assess encapsulation efficiency [17–19]. This approach will be relevant to the work described in this study.

Separation methods for the analysis of mRNA in various contexts have been recently reviewed by Minkner et al. [20]. Several chromatographic separation principles, such as ion exchange, ion-pair reversed-phase, size exclusion and affinity, and capillary electrophoretic approaches such as capillary zone electrophoresis, pulsed-field capillary electrophoresis, capillary gel electrophoresis, and capillary isoelectric focusing (CIEF), have been highlighted, furthermore discussing spin columns, extractions, precipitations, and magnetic nanoparticles [20].

Analytical methods to characterize the particle size, surface charge, lipid composition, particle morphology, and surface hydrophobicity of LNPs are important because LNPs can differ greatly in these aspects, but also because these properties are very important for the effect of the vaccine. For example, they affect the uptake and release of the mRNA. The surface charge of LNPs is correlated with cell toxicity, which makes the analysis of the same, as we do here via imaged CIEF (iCIEF), very important [21–25]. Positively charged LNPs have the advantage that they can better interact with negatively charged mucosal surfaces, which is important for immune activation and uptake into cells. The disadvantage of the positive charged LNPs, however, is that they can have a toxic and, for example, pro-inflammatory effect [21, 26]. Capillary electrophoresis has already proven to be very useful for vaccine analysis. CE in general has expanded viral vaccine testing beyond what was formerly possible, increased the understanding of procedures and products, and enhanced overall safety, efficacy, and quality [16]. Recently, Malburet et al. determined the global charge of LNPs using CE [27].

The CIEF method was introduced in the 1980s by Hjertén et al. [28, 29]. In this method, a pH gradient is established in a capillary via carrier ampholytes, in which the analytes migrate until they remain in the pH zone corresponding to their isoelectric point (p*I*). For detection, an online imaging detection system that does not require a mobilization of the analytes after focusing can be used today [30]. The performance of this approach has been characterized in comparison to other charge-dependent separation techniques by Kahle et al. [31]. We recently used the method to determine the p*I* values of various commercially available severe acute respiratory syndrome coronavirus 2 (SARS-CoV-2) proteins [32].

2 | MATERIALS AND METHODS

2.1 | Materials

Experiments were performed on the Maurice iCIEF system from ProteinSimple, a Bio-Techne brand (San Jose, CA, USA) and analyzed using the associated compass for iCE software (version 2.2.0). For the Maurice CIEF system, the Maurice CIEF cartridges (capillary length: 50 mm, 100 µm id × 200 µm od, silica coated with fluorocarbon) and the Maurice CIEF method development kit (including system suitability kit, fluorescence calibration standard, anolyte (80 mM phosphoric acid in 0.1% methyl cellulose (MC)), catholyte (100 mM NaOH in 0.1% MC), Pharmalyte® carrier ampholytes (manufactured by Cytiva, Marlborough, MA, USA), p*I* markers, SimpleSol protein solubilizer (proprietary formulation), and MC (1%, 0.5%)) were used (provided by ProteinSimple, a Bio-Techne brand). The p*I* markers are peptides with the corresponding p*I* (e.g., 5.85 or 8.40). Carrier ampholytes are low molecular weight molecules of zwitterionic character with a specific p*I* range, which, for example, ranges from p*I* 3 to 10 for Pharmalyte® 3–10. The capillary was automatically calibrated with the fluorescence calibration standard before the samples were measured. In addition, a system suitability test was performed both before and after measuring the samples to ensure that the instrument was working properly. Samples were injected via vacuum for 55 s to be subsequently prefocused at 1500 V for 1 min and focused at 3000 V for varying times. During injection, the capillary is overfilled to waste such that the same ionic strength is present at both electrodes. The focusing time was adapted to the respective methods. UV absorbance was detected at 280 nm. With native fluorescence at an excitation wavelength of 280 nm, emitted light at 320–450 and 458 nm was used for the detection of the samples containing fluorescent dye [33]. Glycerol (≥99.5%) from Sigma-Aldrich (St. Louis, MO, USA), Tween® 20 (molecular biology grade) from VWR Chemicals (Radnor, PA, USA), urea (≥99.5%) from VWR Chemicals (Radnor, PA, USA), *N*-ethylurea (97%) from Sigma-Aldrich (St. Louis, MO, USA), and the fluorescent dye 6-(*p*-Toluidino)-2-naphthalenesulfonic acid sodium salt (TNS, Sigma-Aldrich, St. Louis, MO, USA) were used for the experiments. Ultrapure water for the experiments was obtained from an Arium pro VF system (Sartorius AG, Göttingen, Germany). Determination of encapsulation of LNPs was performed by a Quant-it RiboGreen RNA Assay Kit and a RiboGreen RNA Reagent (Thermo Fisher Scientific, Waltham, MA, USA). Particle sizes and polydispersity indexes (PDI) were determined on a Zetasizer Ultra (Malvern Panalytical, a Spectris company, Malvern, UK).

2.2 | Samples

The mRNA-LNP vaccine against rabies (CureVac AG, Tübingen, Germany) served as sample materials. Both the mRNA loaded LNPs (batch 1) and the unloaded placebo were used for method development. The concentration of the samples was 25 mg/ml based on lipids and 1 mg/ml mRNA, in the case of the loaded LNPs. Stressed and modified samples, respectively, were also measured besides LNP batches 1 and 2 (manufactured at different times) and Placebo-LNPs, using the two final methods (Section 3.4). These were the following samples: LNP batch 1 stored at 5°C for 4 weeks, LNP batch 1 after 10 passed freeze–thaw cycles (FTC), LNP ±20% cationic lipid, and LNP ±20% PEG-lipid. The ±20% refer to mol% of the cationic lipid/PEG-lipid and apply to both the solution during the formulation process and the LNPs formed. All samples were suspended in a 10 mM phosphate buffer (pH 7.2–7.4) containing 75 mM sodium chloride and 150 mM sucrose.

2.3 | Method development

To prepare the samples, a master mix is always first produced. This consists of MC, p*I* markers, carrier ampholytes, and, if necessary, additives and water. This master mix was mixed well and centrifuged (to free the solution from bubbles). The master mix was then pipetted into Eppendorf Tubes®, and the respective sample was added to achieve a total volume of 160 µl. The mixture was again mixed gently and centrifuged so that 100 µl of the solution could then be pipetted into each well of the 96-well-plate (based on the method development guide of ProteinSimple, a Bio-Techne brand [34]). All percentages given are v/v.

The first experiments (1) were carried out with the addition of 10% glycerol, following the experiments of Loughney et al. [35]. Subsequently, 27 different test combinations were prepared to screen for optimal separation of LNP samples. These included varying sample concentration, carrier ampholytes (ratio and overall total %), and solubilizers (urea, *N*-ethylurea, Tween® 20, glycerol, SimpleSol). For a tabulated listing of all test mixes used in the study, see Table S1.

The focusing times varied between 10 and 30 min, depending on the type and amount of additives. In some cases, the focusing time was 30 min to see if the analytes would keep their focusing position at some point. As only 2 of the 27 methods showed stable separation (shown in the next section), the individual times of the other methods are not mentioned.

TABLE 1 Composition of master mixes A and B

	A		B	
	V (µl)	Content	*V* (µl)	Content
1% MC	–	–	12	0.075%[a]
Pharmalyte® 3–10	6	3.75%[a]	8	5%[a]
Pharmalyte® 5–8	2	1.25%[a]	-	–
p*I* marker 5.85	2	1.25%[a]	2	1.25%[a]
p*I* marker 8.40	2	1.25%[a]	2	1.25%[a]
Water	–	–	44	–
10 M urea in water	32	2 M urea[b]	–	–
10 M urea in 0.5% MC	112	7 M urea[b] 0.35%[a] MC	88	5.5 M urea 0.275%[a] MC
Sample	4	0.625 mg/ml lipid	4	0.625 mg/ml lipid
Total	160		160	

[a](v/v).
[b]2 M plus 7 M urea add up to the final concentration of 9 M urea.
Note: In each case, the master mix was first prepared for the corresponding number of samples to be measured, and 156 µl of the master mix was then mixed with 4 µl of the sample. In the case of master mix B, 28.1952 mg *N*-ethylurea per sample to be measured was added to the tube beforehand.
Abbreviation: MC, methyl cellulose; p*I*, isoelectric point.

2.4 | Final methods

Two methods showed the most stable and repeatable separations and were used to measure the stressed and modified LNP samples. During method development, it was noticed that the addition of 9 M urea (A) or 5.5 M urea +2 M *N*-ethylurea (B) showed the best results. For these two methods, the best carrier ampholyte (mixture) and the optimum focusing time were further optimized. Finally, a focusing time of 15 min was chosen for both methods. The exact final sample compositions for master mix A and B can be seen in Table 1.

For the experiments with the fluorescent dye TNS, a 1.9 mM aqueous TNS solution was first prepared. In the case of method A, this solution was then used in combination with 1% MC to prepare the 10 M urea with which the master mix ended up containing 0.35% MC and 1.0 mM TNS. Thus, the 144 µl of 10 M urea for one master mix consisted of 88 µl of 1.9 mM TNS and 56 µl of 1% MC. For method B, on the other hand, 44 µl of the 1.9 mM TNS solution were added to the master mix instead of water, and the 10 M urea solution was prepared from 1% MC and TNS (50/50, v/v) to similarly arrive at a final concentration of 1.0 mM TNS.

2.5 | Size and encapsulation data assessment

To determine the mRNA encapsulation of the LNPs, the commercially available Quant-it RiboGreen RNA Assay Kit was used according to the instructions of the provider. An RNA standard calibration curve was prepared by diluting the RNA provided with the kit to a concentration range of 0.02–0.6 µg/ml. The total RNA concentration of the LNPs was 1 g/L and diluted accordingly in Tris–EDTA buffer. Triton-X 100 in a concentration of 0.2% (v/v) was used to break the LNPs apart and release the encapsulated RNA.

Particle sizes and PDI were determined on a Malvern Zetasizer Ultra. The samples were diluted in water and measured. The measurement is performed at 22°C in the "General Mode" of the software. The *Z* average is given as "size (nm)," which is the intensity-weighted mean hydrodynamic size of the ensemble collection of particles measured by dynamic light scattering. Furthermore, the PDI is given. PDI values greater than 0.25 determined at 174.7° suggest a broad particle size distribution, which is one sign of low quality materials. This can be seen, for example, after an extended storage of the LNPs, as the PDI is increasing over time as the aggregation of particles occurs. Freshly produced LNP batches show PDI values smaller than 0.2, which shows a much narrower particle size distribution and therefore a homogenous formulation process.

3 | RESULTS AND DISCUSSION

Highly selective methods are desirable for the characterization and statements on the quality and stability of mRNA vaccines. Thus, an iCIEF method should be developed. We were inspired by the paper of Loughney et al.

[35] who developed an iCIEF method that reproducibly measures the apparent p*I* of mRNA-loaded LNPs. In our measurements, the samples were each measured three times in succession, that is, as replicates. Peak areas and p*I*s were calculated using measurements of the samples immediately after thawing. The RSDs given always refer to three measurements of the same batch directly in succession. Subsequently, the samples were stored at 5°C in the refrigerator and measured again after 1 week.

In addition to the iCIEF measurements, the Zetasizer measurements and the RiboGreen assay described in Section 2.5 were performed with the samples. The results can be found in Table S2.

Our paper shows the progress of the method development so far, yet a complete interpretation of the data is still relatively challenging. Nevertheless, the data provide initial insights and show how promising this methodology could be.

3.1 | Method development

For reproducible results over iCIEF, it is important that the analytes remain at their p*I* after the selected separation time and keep their focusing position. Glycerol has previously been known as a common substance for stabilizing proteins in iCIEF [36]. As Loughney et al. [35] showed that LNPs for iCIEF can be stabilized very well in 10% glycerol, we similarly started with a master mix containing 10% glycerol. The samples we investigated were not sufficiently stabilized in the electric field by the addition of 10% glycerol. The p*I* and peak shape changed permanently and the resulting electropherogram could only be regarded as a snapshot. An example of this insufficient stabilization of the LNP can be seen in master mix 3 during a 15-min focusing in Video S1. For this reason, we continued to search for a more suitable master mix. Other glycerol concentrations (5%–20%) did not bring success either. The addition of SimpleSol resulted in the baseline becoming somewhat smoother, it had no effect on the LNP peaks. Addition of Tween® 20 apparently destroyed the LNPs in the electric field, no signals were detectable anymore. The exact master mixes tested can be found in Table S1. The breakthrough in method development was achieved by the addition of the strong denaturing and structure-breaking reagents urea and *N*-ethylurea. Urea is a very suitable and thus frequently used denaturing agent in CIEF. The aim is to stabilize a special conformation of LNP, which are large particles with charges on the surface. It seems that urea interacts with the polar groups of the lipids. This leads to urea partially replacing water at the lipid membrane surface or penetrating into the LNP. This is thought to lead to the stabilization of the lipid membrane under osmotic stress and, in our case, could lead to sharper separation of the LNPs [37, 38]. In the presence of a pH gradient, it is mandatory that the sum of these LNP charges does not change and that the entire complex migrates stably to the p*I* position. A chaotropic molecule should therefore help stabilize this LNP complex. The chaotropic effect of *N*-ethylurea is much stronger, which is precisely the reason why it is often used in combination with urea for proteins that are difficult to denature [39, 40]. The addition of 9 M urea, the highest concentration tested, resulted in an interesting, stable electropherogram with two peaks, which allows great opportunities for interpretation and further method development. Addition of 5.5 M urea and 2 M *N*-ethylurea, the ratio that showed the most stable results in our measurements, gave an electropherogram with one sharp, almost Gaussian main peak, which impresses with high repeatability in the p*I* value and a decent one of the peak area. After finding the best additives, that is, 9 M urea for method A and 5.5 M urea with 2 M *N*-ethylurea for method B, we continued to look for the best sample concentration and the most suitable carrier ampholytes, which are important for resolution. The conditions found to be the best are shown in Table 1.

3.2 | Results for method A with 9 M urea as additive

The mRNA-loaded LNPs very repeatably show two main separated peaks (Figure 1A). When the samples were injected in triplicate, the standard deviation of the total peak area of batch 1 was 3.7% (see Table 2). The total peak areas behave linearly with mRNA loading, as shown by measurements of batch 1 mixed with different amounts of the placebo (rations of 0:100, 25:75, 50:50, 75:75, and 100:0 [v/v] LNP placebo/batch 1, data not shown). This linear correlation was also previously shown by Loughney et al. [35]. mRNA is negatively charged and this certainly plays a role in surface charge of loaded LNPs. It is therefore assumed that the left peak (p$I \approx 6.8$) is mostly mRNA-loaded LNP and supported because the peak area of this peak is strongly influenced by the mRNA amount. Looking at the electropherogram of the placebo using this method (Figure 1C), the LNP alone gives these two peaks. Apparently, there are two different LNP species in the sample, only one of which carries the mRNA, since only the peak area of the left peak (p$I \approx 6.8$) correlates with the mRNA content. This would at least be a possible explanation for this phenomenon. The peak pattern shows an interesting fine structure, possibly due to a varying number of mRNA molecules within each LNP. One week later, while storing the samples at 5°C, the stationary spikes on the left peak (p$I \approx 6.8$) become higher (Figure 1B). Accordingly, the

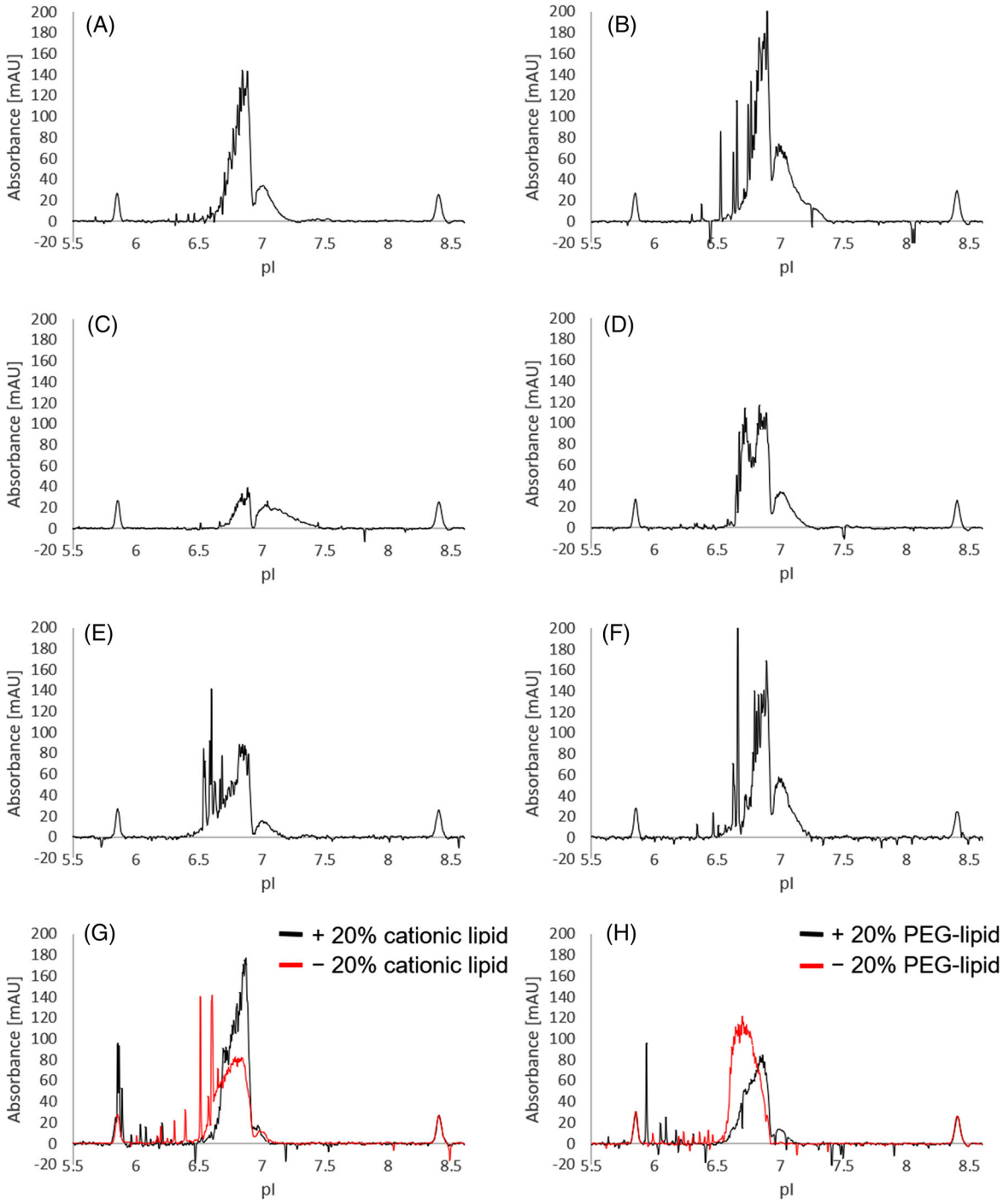

FIGURE 1 Electropherograms of the samples measured with method A, that is, 9 M urea as additive after 15-min separation time: (A) batch 1, (B) batch 1 stored at 5°C for 1 week, (C) lipid nanoparticle (LNP) placebo, (D) batch 2, (E) batch 1 stored at 5°C for 4 weeks, (F) batch 1 after 10 freeze–thaw cycles, (G) batch 1 ±20% cationic lipid, (H) batch 1 ±20% polyethylene glycol (PEG)-lipid. Peaks at isoelectric point (p*I*) 5.85 and 8.40 are the respective p*I* markers

method reveals even the smallest changes that occur after samples have been stored in the refrigerator for 1 week. As RSDs below 5% are acceptable for repeatability in the RiboGreen assay, the difference in encapsulations of the samples cannot be considered substantial, but the trend is in the same direction (Table S2). The sharp, high spikes could be due to UV absorption of the mRNA at the surface of the LNP, which is then no longer shielded by the scattering lipids.

This method provides a lot of information about the sample due to the peak shape, even if they cannot yet be fully interpreted, and is very repeatable as the LNPs are

TABLE 2 Peak areas for all samples measured with methods A and B

	A		B			
Sample LNP	**Area (mAU × pixel)**	**RSD (%)**	**p*I***	**RSD (%)**	**Area (mAU × pixel)**	**RSD (%)**
Batch 1	9920.5	3.69	6.45	0.53	12883.6	4.55
Placebo	4264.9	5.13	6.44	0.04	5850.6	2.36
Batch 2	9875.8	8.04	6.45	0.16	11086.6	2.28
Batch 1, stored at 5°C for 4 weeks	8625.2	2.26	6.41	0.19	9748.4	3.70
Batch 1, after 10 FTC	11489.5	7.01	6.42	0.15	10886.8	2.17
Batch 1% +20% cationic lipid	11160.3	2.05	6.50	0.31	10885.9	4.57
Batch 1% −20% cationic lipid	9496.6	4.61	6.41	0.31	8987.8	3.45
Batch 1 +20% PEG lipid	6865.7	3.63	6.42	0.26	7660.9	3.48
Batch 1% −20% PEG lipid	10574.3	3.29	6.37	0.19	11083.9	6.60

Note: Mean values from three measurements (replicates, one aliquot three times in succession) and the corresponding RSDs. For method B, the p*I* values with the associated RSDs are also included.

Abbreviations: FTC, freeze–thaw cycle; LNP, lipid nanoparticle; PEG, polyethylene glycol; p*I*, isoelectric point.

well stabilized. Loughney et al. suggested that this broad, jagged peak is likely caused by polydispersity in the formation of various LNP structures and sizes during the fabrication process [35]. To see how the LNP batch 1 is focused, please watch Video S2.

3.2.1 | Measurements of the stressed and modified samples with method A

Comparing LNP batch 1 with batch 2 (Figure 1D), it is noticeable that the left peak (p$I \approx 6.8$) has a different shape, which could result from a different mRNA distribution in the LNPs. The peak areas of batches 1 and 2 are very similar, differing by only 0.45%, indicating similar mean mRNA loading. However, looking at the results from the RiboGreen assay and the Zetasizer, batch 2 has less mRNA encapsulated and has larger particles, even if the differences are minimal. Larger particles would produce more scattered light and effect the signal as would an increased absorption due to a higher mRNA loading, with the result that these effects would compensate each other. The relationship between particle size and light scattering is described by the Mie theory [41]. After 1 week, the electropherogram of batch 2 (data not shown) looks almost like that of batch 1, so the batches seem to have equalized, possibly in mRNA or lipid distribution.

If the sample LNP batch 1 stored at 5°C for 4 weeks is considered (Figure 1E), clearly more high stationary spikes toward the left side are noticeable. These were previously observed after 1 week of storage in the refrigerator. In this sample, it is also remarkable that the right peak (p$I \approx 7$) is relevantly smaller compared to the non-stressed sample. This may be due to instability of the LNPs that contain little to no mRNA, as they lack a countercharge, and this proportion thus decreases during storage. As the right peak (p$I \approx 7$) initially became larger after 1 week of storage (Figure 1B), it is quite possible that first mRNA goes out of the LNPs, more empty LNPs are formed, but these are unstable and decay with time. In addition, added stress on the samples causes the PEG lipid to diffuse out of the LNPs, resulting in LNP fusion or aggregation. In cryo-electron microscopy images, many fusion products can be seen, where one half of the LNPs is empty [42]. It is challenging to determine whether this has also happened with the measured samples and how it may have affected the measurements. The total area of both peaks is also reduced by 13% due to storage, which is equally indicative that mRNA may be degraded and consistent with the results of the RiboGreen assay.

After 10 FTC, the electropherogram (Figure 1F) looks even more like that of the non-stressed sample, with only a few high stationary spikes visible. It was therefore reasonable to assume that this is less of a problem for the samples than prolonged storage at 5°C. However, it can also be assumed that LNP aggregates are formed by FTC despite the addition of sucrose to the buffer containing the LNPs [43]. The larger particle size would produce more stray light, which is then not detected, leading to an apparently higher absorbance of the sample. This could explain the 16% larger peak area of this sample, compared to the unstressed one. This assumption is confirmed by the measurements of the Zetasizer, which showed that the particles are larger in this sample, whereas the RiboGreen assay showed that less mRNA is encapsulated in (Table S2). In this case, it may therefore be challenging to determine how much mRNA may have been released by the FTC using iCIEF alone.

The electropherograms of the modified LNPs with ±20% of the cationic lipid (Figure 1G) show expected results.

With +20% cationic lipid, the peak is shifted to the right, because there are more positive charges in the LNP; with −20%, the p*I* is somewhat lower, so the peak is shifted further to the left. In addition, it is noticeable that with both modifications many spikes occur in the entire area to the left of the peak, because presumably mRNA-containing aggregates leave the LNPs, as they are not stable in this way. In addition, the peaks are strongly collapsed after 1 week and have a remarkably smaller peak area (data not shown). It is difficult to make general statements about the correlation between peak area and mRNA content for the modified samples, as the lipid content also affects UV absorbance and the particles are smaller than in the non-modified samples. However, that less mRNA is encapsulated than in the non-modified samples is also shown by the RiboGreen assay (Table S2).

The influence of PEG-lipid content was also considered using modified LNPs (Figure 1H). The p*I* value of the peak for the sample with +20% PEG lipid is slightly higher than that of the sample with −20% PEG lipid. At +20% PEG-lipid in LNP, the signal is remarkably smaller than at −20%. In general, it has been previously shown that a higher PEG content shields the surface charge of LNPs [44]. As can now be seen in the iCIEF measurements, PEG may have a slight effect on the overall surface charge, as the p*I* is slightly changed with the varied PEG content. Another explanation for the small shift and the different peak areas could be that less PEG-lipid in the LNP allows more mRNA to be encapsulated, which would then explain the larger peak area and the drift to the left, compared to +20% PEG-lipid. Overall, however, at −20% PEG-lipid, still less mRNA is encapsulated than in the unmodified sample (Table S2).

3.3 | Results for method B with 5.5 M urea and 2 M *N*-ethylurea as additives

The second method, using 2 M *N*-ethylurea and 5.5 M urea as additives, shows only one approximately Gaussian signal with high repeatability of both peak area and p*I* value (see Table 2). In this method, the peak area also correlates linearly with the mRNA content of the sample (data not shown). It should be noted that moving spikes without a fixed p*I* value prevented the correct setting of the p*I* marker 5.85 in some measurements and the p*I* thus sometimes appears slightly altered. However, the effects are minimal, and the p*I* still shows a great repeatability with RSDs below 0.53% for all measured samples (see Table 2). For the sample LNP batch 1 (Figure 2A) the RSD of the peak area is 4.6%, for the placebo 2.4% (Figure 2C). The peak area of the placebo is equivalent to 45% of the peak area of the mRNA loaded LNP, which is similar (43%) to method A. Thus, slightly more than half of the absorption is caused by the mRNA. For this method, as well, a strong change of the peak in the electropherogram can be seen after only 1 week of storage in the refrigerator (Figure 2B). A remarkable feature of the measurements is that moving spikes occur in the measurements of the mRNA-loaded samples, originating from the large peak and slowly moving toward the anode. These are therefore species without a fixed p*I* value, possibly mRNA-containing aggregates, because these moving spikes do not occur with the placebo. The migration spikes could also reflect an ongoing change in the LNP composition, which drives them toward the anode. The electropherograms are only snapshots, the migrating spikes leave the capillary toward the anode and typically are not detected any longer at the end of the separation (see Video S3).

3.3.1 | Measurements of the stressed and modified samples with method B

If we compare batch 1 (Figure 2A) with batch 2 (Figure 2D) with this method, we notice that the peak area of batch 2 is 14% smaller, while it was only 0.45% smaller in method A. One explanation for this would be that the peak area in this method is not as strongly influenced by scattering or by particle size as in method A. This is possibly because the particles are all very close to one point of the capillary in method B and they are more widely distributed in method A, so scattering may play a greater role. An explanation for the wider distribution in method A is the addition of the narrow range carrier ampholyte (Pharmalyte® 5–8) that entails a broadening of the pH gradient in this region and thus causes broader peaks. The fact that the light scattering in method B has a smaller effect on the absorption measured would also explain why the peak of the sample after 10 FTCs (Figure 2F) has a smaller peak area with this method than the unstressed sample (Figure 2A), unlike the case with method A. Similar to method A, this method also produces high spikes when the samples are subjected to stress. In contrast to method A, however, the spikes in this method move toward the anode and do not remain stationary on the main peak. The sample stored at 5°C for 4 weeks (Figure 2E) also shows a much smaller peak area than the unstressed sample by this method, and despite the higher mRNA content than the sample after 10 FTC, also shows a smaller peak area. Thus, the particle size still seems to have an influence on the detection, albeit to a lesser extent than in method A. This can also be seen when comparing the sample stored at 5°C for 4 weeks with batch 2. Both samples have very similar mRNA content, but the peak area of batch 2 is 14% larger, presumably due to the larger particle size.

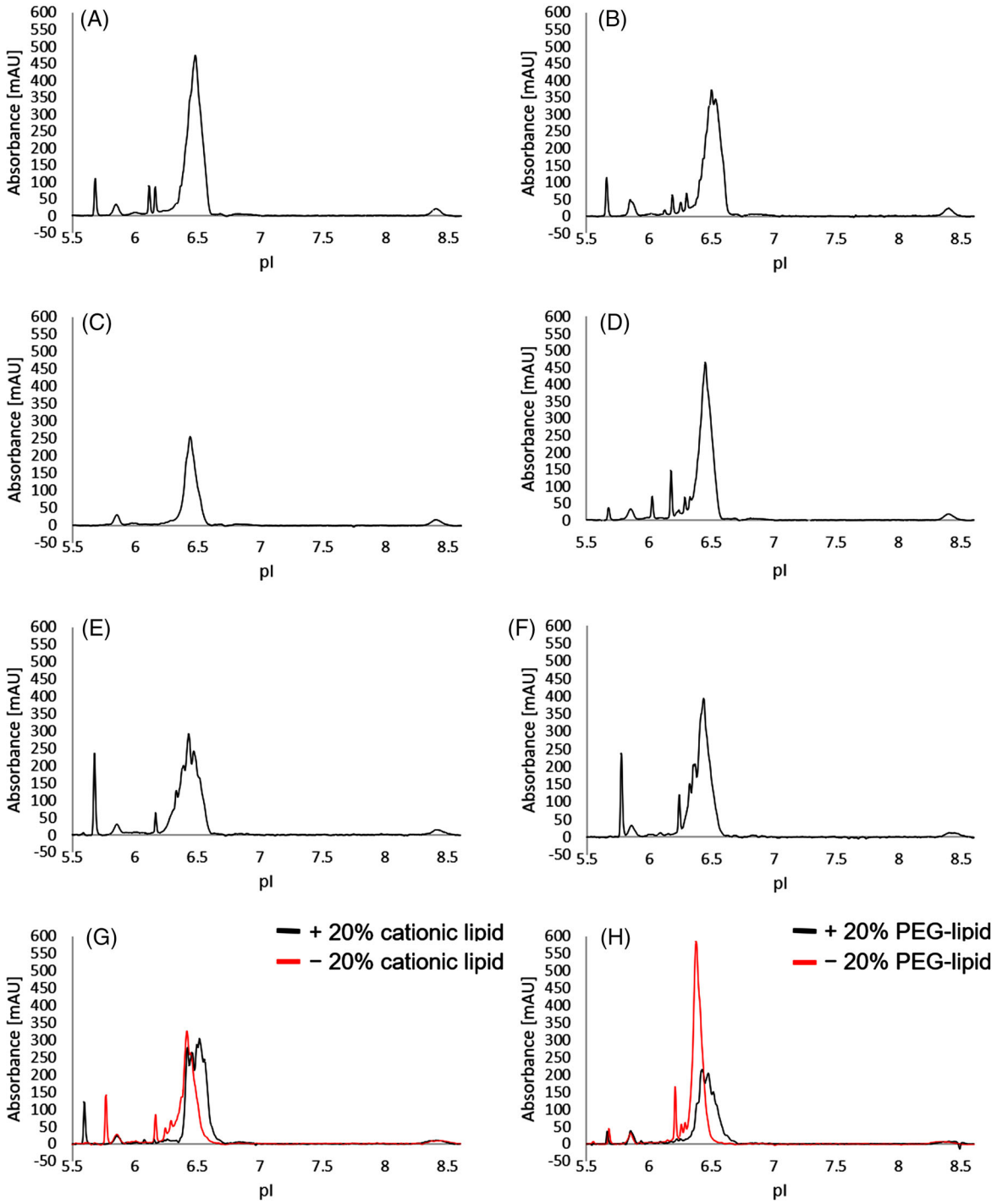

FIGURE 2 Electropherograms of the samples measured with method B, that is, 5.5 M urea and 2 M *N*-ethylurea as additives after 15-min separation time: (A) batch 1, (B) batch 1 stored at 5°C for 1 week, (C) lipid nanoparticle (LNP) placebo, (D) batch 2, (E) batch 1 stored at 5°C for 4 weeks, (F) batch 1 after 10 freeze–thaw cycles, (G) batch 1 ±20% cationic lipid, (H) batch 1 ±20% polyethylene glycol (PEG)-lipid. Peaks at isoelectric point (p*I*) 5.85 and 8.40 are the respective p*I* markers

The results of the samples with ±20% of the cationic lipid show expected results consistent with method A: the p*I* of the "normal" sample (batch 1, Figure 2A) is 6.45, that of the sample +20% cationic lipid is slightly above, at 6.50 and that of the sample with −20% of the lipid at 6.41 is slightly below (Figure 2G). In addition, the peak area of the sample with −20% cationic lipid is again somewhat smaller.

As in method A, the sample with +20% PEG lipid shows the smallest peak area of all mRNA-loaded samples (Figure 2H). The reason for this could be mRNA loss, but also that the added PEG lipid shields the mRNA so

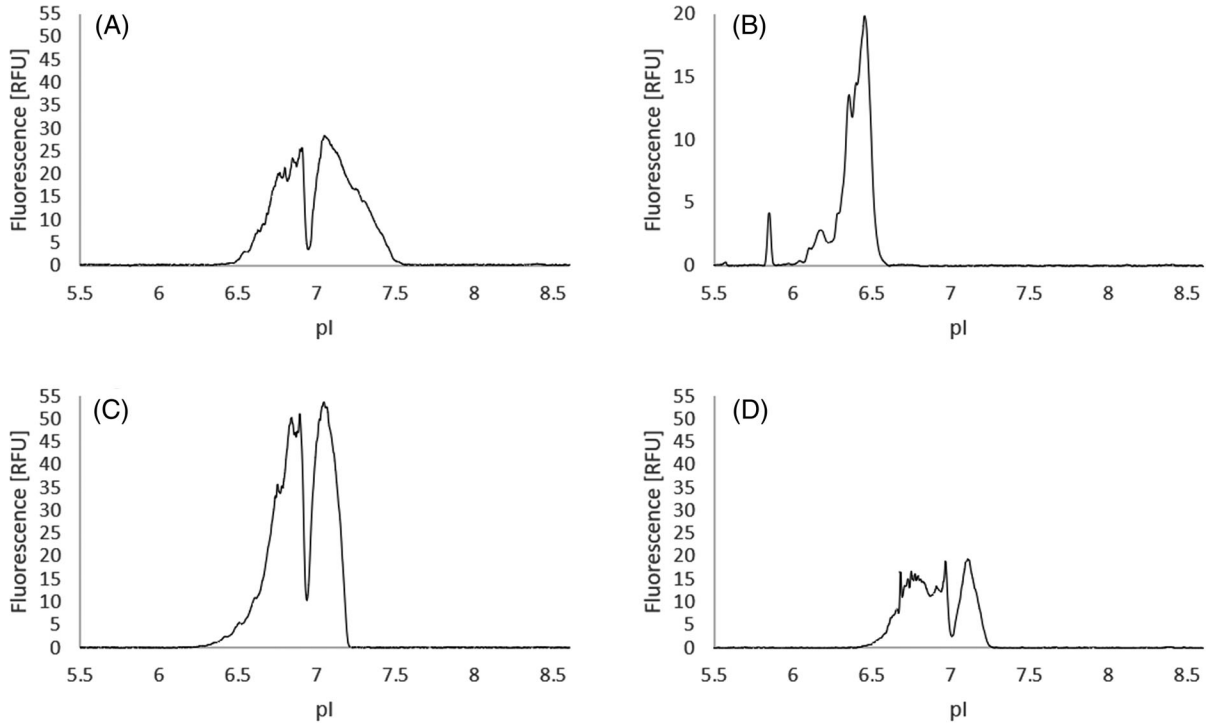

FIGURE 3 Electropherograms of the samples measured with the addition of the fluorescence dye 6-(*p*-Toluidino)-2-naphthalenesulfonic acid (TNS). Emission was detected at 458 nm with 1-s exposure time: (A) batch 1, method A, (B) batch 1, method B, (C) lipid nanoparticle (LNP) placebo, method A, (D) batch 1 stored at 5°C for 4 weeks, method A

that it absorbs less UV light. A very sharp, high peak is shown by the sample with 20% less PEG lipid. Thus, the reduction in PEG content causes the p*I* values of the LNPs to differ less and appear lower than those of the unmodified sample, which might also be explained by the shielding effect of the PEG-lipid on the surface charge [44]. The peak area is similar to that of the LNP batch 2.

3.4 | Experiments using the fluorescent dye TNS

Although the previous results were all detected with the absorption mode of the instrument, in the following experiments the fluorescence of the sample is detected after the addition of the fluorescent dye TNS. The negatively charged fluorescent dye TNS fluoresces when associated with the surface of positively charged membranes, in this case with the cationic lipid. However, it does not fluoresce when it is free in solution [45]. It is added as an aqueous solution to the master mix and applied at a final concentration of 1 mM. During detection, the sample is exposed to a wavelength of 280 nm. The emitted light is detected in the wavelength range of 320–450 or 458 nm. As can be seen in Figure 3, the addition of TNS leads to a massive increase in sensitivity. Tremendously large peaks are already detectable at an exposure time of only 1 s, from an exposure time of 3 s they are even cut off at the top, as there is a detection maximum at 60 relative fluorescence units. This detection method thus offers the possibility to extremely reduce the LNP concentration.

Looking at the results of batch 1 with method A in Figure 3A, it is noticeable that compared to the experiments without the addition of TNS, the right peak (p$I \approx 7.2$) is larger. This is the peak that was previously related to no or very low mRNA loading. Additionally, by adding the fluorescent dye, the placebo shows a larger peak area than the mRNA loaded sample (Figure 3C). Together, these data suggest that due to the lack of mRNA, which is negatively charged, more of the negative fluorescent dye binds. This seems logical, as TNS does not have to compete with mRNA for the positive charges of the cationic lipid. As the mRNA does not fluoresce, mRNA loading does not influence fluorescence detection itself. The method is therefore not suitable for making statements about this. However, statements about the quality and the stability of the LNPs can probably still be made, as the peak shape changes considerably, as can be seen in Figure 3D, for example, due to 4 weeks of storage in the refrigerator. In method B, the same effects as in method A were seen, which is why only the electropherogram of fresh batch 1 (Figure 3B) is shown. Furthermore, a small peak at about p*I* 5.7 is noticeable, which was already visible in the measurements without

fluorescent dye (Figure 2), except for the placebo sample. This peak therefore seems to contain both mRNA and cationic lipid, as without the cationic lipid, it would not be visible by an addition of TNS in fluorescence mode.

In general, the TNS experiments are exploratory but are worth pursuing further. Due to the enormously increased sensitivity, the sample concentration can be considerably reduced. As the analytes usually also act as ampholytes in the iCIEF, they affect the pH gradient formed. This can lead to broader peaks if too high analyte concentrations are used. Alternatively, LNP aggregation could be promoted under these conditions, which also supports the use of lower LNP concentrations.

Changes in the samples due to stress and lipid modifications can also be seen with the addition of TNS, although they are not yet be fully understood. Further research in this area looks very promising.

4 | CONCLUDING REMARKS

Two iCIEF methods have been developed, both having their strengths, and united providing many insights into the quality and stability of mRNA vaccines. The highly repeatable methods offer a lot of very valuable information about the preparation, and at the same time they are flexible to optimize them for various kinds of loaded LNPs. Method A, in which 9 M urea was used as an additive, shows two broad and jagged peaks in which the peak shape changes substantially when stress is added to the samples, and therefore detailed information can be derived about stability. Furthermore, the peak pattern exhibits an interesting fine structure, possibly due to different numbers of mRNA molecules within the individual LNPs. The peak area of the sum of both peaks, with RSDs from 2% to 8% when measured in triplicate, very well correlates linearly with the mRNA content and also apparently depends on the size of the LNPs, as was shown by the additional examinations of the stressed samples with the Zetasizer. In method B, a combination of 5.5 M urea and 2 M *N*-ethylurea was used for LNP separation by iCIEF. This method is characterized by a high repeatability of the p*I* value (<0.5%). Again, the well repeatable peak area (2%–7%) correlates linearly with the mRNA content, and added stress is evident by the change in p*I* and peak area. Particle size does not seem to have a strong effect on peak area with this method. Both methods, particularly method A, allow one to characterize LNP stability investigating different storage times and FTCs, and to distinguish between different preparations, including changing lipid compositions and batch-to-batch variability. The developed methods are very sensitive in showing even the smallest changes in the samples, as evident from the measurements of the samples after 1 week of storage in the refrigerator. In addition, empty and loaded LNPs can be clearly differentiated. Therefore, the presented methods offer several advancements compared to previously established physicochemical methods.

These results are consistent with the established models for mRNA encapsulated in LNPs [2, 46]. Most of the mRNA resides in the center of the LNPs, interacting with the cationic lipid of opposite charge. More detailed information is certainly available by analyzing different variants of the LNP recipes by methods A and B.

The addition of the fluorescent dye TNS resulted in a massive increase in the sensitivity of both methods and should indeed be considered further for use in iCIEF.

Overall, this paper shows that iCIEF analysis is very well suitable for the characterization of mRNA vaccines. This approach is an important analytical tool for the ongoing pandemic and beyond. After widespread use for COVID-19, mRNA vaccines as such convinced competent authorities, and we can expect many more pharmaceuticals of this type in the future, and in addition exceptional options for mRNA-based cancer treatments.

ACKNOWLEDGMENTS

We would like to offer our special thanks to ProteinSimple, a Bio-Techne Brand, for the provision of the Maurice as well as the respective consumables. In this context, we are particularly grateful for the advice and support given by Sibylle Molt, Chris Heger and Carsten Lück. Also, we would like to thank Michael Sonntag (CureVac AG) for providing modified LNPs, Benedikt Ritter and Pirkko Wenzel (CureVac AG) for performing additional stability studies and analytics. Finally, we wish to acknowledge the critical proofreading by Sophie Hartung.

CONFLICT OF INTEREST

The authors have declared no conflict of interest. For transparency, we like to mention that Markus Kramer is an employee of CureVac AG, and Susanne Dörks and Udo Burger are employees of ProteinSimple, a Bio-Techne brand.

DATA AVAILABILITY STATEMENT

The data that support the findings of this study are available from the corresponding author upon reasonable request.

ORCID

Finja Krebs https://orcid.org/0000-0003-1821-5408
Hermann Wätzig https://orcid.org/0000-0002-7456-0612

REFERENCES

1. Reichmuth AM, Oberli MA, Jaklenec A, Langer R, Blankschtein D. mRNA vaccine delivery using lipid nanoparticles. Ther Delivery. 2016;7:319–34.
2. Schoenmaker L, Witzigmann D, Kulkarni JA, Verbeke R, Kersten G, Jiskoot W, et al. mRNA-lipid nanoparticle COVID-19 vaccines: structure and stability. Int J Pharm. 2021;601:120586.
3. Yanez Arteta M, Kjellman T, Bartesaghi S, Wallin S, Wu X, Kvist AJ, et al. Successful reprogramming of cellular protein production through mRNA delivered by functionalized lipid nanoparticles. Proc Natl Acad Sci USA. 2018;115:E3351–60.
4. Eygeris Y, Gupta M, Kim J, Sahay G. Chemistry of lipid nanoparticles for RNA delivery. Acc Chem Res. 2022;55:2–12.
5. Lutz J, Lazzaro S, Habbeddine M, Schmidt KE, Baumhof P, Mui BL, et al. Unmodified mRNA in LNPs constitutes a competitive technology for prophylactic vaccines. NPJ Vaccines. 2017;2:29.
6. Aldrich C, Leroux-Roels I, Huang KB, Bica MA, Loeliger E, Schoenborn-Kellenberger O, et al. Proof-of-concept of a low-dose unmodified mRNA-based rabies vaccine formulated with lipid nanoparticles in human volunteers: a phase 1 trial. Vaccine. 2021;39:1310–8.
7. Knezevic I, Liu MA, Peden K, Zhou T, Kang H-N. Development of mRNA vaccines: scientific and regulatory issues. Vaccines (Basel). 2021;9:81.
8. World Health Organization. Evaluation of the quality, safety and efficacy of messenger RNA vaccines for the prevention of infectious diseases: regulatory considerations. Geneva: World Health Organization; 2021.
9. U.S. Food and Drug Administration (USFDA). Process validation: general principles and practices. Maryland: U.S. Food and Drug Administration (USFDA).
10. Hinz T, Kallen K, Britten CM, Flamion B, Granzer U, Hoos A, et al. The European regulatory environment of RNA-based vaccines. Methods Mol Biol. 2017;1499:203–22.
11. European Medicines Agency. ICH guideline Q 2 (R1) on validation of analytical procedures: CPMP/ICH/381/95. Amsterdam: European Medicines Agency. **1995.**
12. Yu LX, Amidon G, Khan MA, Hoag SW, Polli J, Raju GK, et al. Understanding pharmaceutical quality by design. AAPS J. 2014;16:771–83.
13. European Medicines Agency. ICH guideline Q8 (R2) on pharmaceutical development: EMA/CHMP/ICH/167068/2004. Amsterdam: European Medicines Agency. **2017.**
14. European Medicines Agency. Guideline on process validation for finished products–information and data to be provided in regulatory submissions: EMA/CHMP/CVMP/QWP/BWP/70278/2012-Rev1,Corr.1. **2016.**
15. Hakemeyer C, McKnight N, St John R, Meier S, Trexler-Schmidt M, Kelley B, et al. Process characterization and design space definition. Biologicals. 2016;44:306–18.
16. Geurink L, van Tricht E, van der Burg D, Scheppink G, Pajic B, Dudink J, et al. Sixteen capillary electrophoresis applications for viral vaccine analysis. Electrophoresis. 2022;43:1068–90.
17. Crommelin DJ, Anchordoquy TJ, Volkin DB, Jiskoot W, Mastrobattista E. Addressing the cold reality of mRNA vaccine stability. J Pharm Sci. 2021;110:997–1001.
18. Poveda C, Biter AB, Bottazzi ME, Strych U. Establishing preferred product characterization for the evaluation of RNA vaccine antigens. Vaccines (Basel). 2019;7:131.
19. Muralidhara BK, Baid R, Bishop SM, Huang M, Wang W, Nema S. Critical considerations for developing nucleic acid macromolecule based drug products. Drug Discovery Today. 2016;21:430–44.
20. Minkner R, Boonyakidab J, Park EY, Wätzig H. Oligonucleotides separation techniques for purification and analysis: what can we learn for today's tasks? Electrophoresis. 2022; manuscript submitted for publication.
21. Mizrahy S, Hazan-Halevy I, Landesman-Milo D, Ng BD, Peer D. Advanced strategies in immune modulation of cancer using lipid-based nanoparticles. Front Immunol. 2017;8:69.
22. Lin PJC, Tam YYC, Hafez I, Sandhu A, Chen S, Ciufolini MA, et al. Influence of cationic lipid composition on uptake and intracellular processing of lipid nanoparticle formulations of siRNA. Nanomedicine. 2013;9:233–46.
23. Kou L, Sun J, Zhai Y, He Z. The endocytosis and intracellular fate of nanomedicines: implication for rational design. Asian J Pharm Sci. 2013;8:1–10.
24. Kedmi R, Ben-Arie N, Peer D. The systemic toxicity of positively charged lipid nanoparticles and the role of Toll-like receptor 4 in immune activation. Biomaterials. 2010;31:6867–75.
25. Zhang J, Pei Y, Zhang H, Wang L, Arrington L, Zhang Y, et al. Assessing the heterogeneity level in lipid nanoparticles for siRNA delivery: size-based separation, compositional heterogeneity, and impact on bioperformance. Mol Pharm. 2013;10:397–405.
26. Verma A, Stellacci F. Effect of surface properties on nanoparticle-cell interactions. Small. 2010;6:12–21.
27. Malburet C, Leclercq L, Cotte J-F, Thiebaud J, Bazin E, Garinot M, et al. Size and charge characterization of lipid nanoparticles for mRNA vaccines. Anal Chem. 2022;94:4677–85.
28. Hjertén S, Liao J-L, Yao K. Theoretical and experimental study of high-performance electrophoretic mobilization of isoelectrically focused protein zones. J Chromatogr A. 1987;387:127–38.
29. Hjertén S, Zhu M. Adaptation of the equipment for high-performance electrophoresis to isoelectric focusing. J Chromatogr A. 1985;346:265–70.
30. Wu J, Pawliszyn J. Universal detection for capillary isoelectric focusing without mobilization using concentration gradient imaging system. Anal Chem. 1992;64:224–7.
31. Kahle J, Wätzig H. Determination of protein charge variants with (imaged) capillary isoelectric focusing and capillary zone electrophoresis. Electrophoresis. 2018;39:2492–511.
32. Krebs F, Scheller C, Grove-Heike K, Pohl L, Wätzig H. Isoelectric point determination by imaged CIEF of commercially available SARS-CoV-2 proteins and the hACE2 receptor. Electrophoresis. 2021;42:687–92.
33. ProteinSimple, a Bio-Techne brand. Maurice CIEF specification [Internet] [cited 2022 Jan 18]. Available from: https://www.bio-techne.com/instruments/ice
34. ProteinSimple, a Bio-Techne brand. cIEF Method Development Guide: Maurice and Maurice C. 046–296 RevD. **2019.**
35. Loughney JW, Minsker K, Ha S, Rustandi RR. Development of an imaged capillary isoelectric focusing method for characterizing the surface charge of mRNA lipid nanoparticle vaccines. Electrophoresis. 2019;40:2602–9.
36. Wu J, Li S-C, Watson A. Optimizing separation conditions for proteins and peptides using imaged capillary isoelectric focusing. J Chromatogr A. 1998;817:163–71.

37. Pham QD, Wolde-Kidan A, Gupta A, Schlaich A, Schneck E, Netz RR, et al. Effects of urea and TMAO on lipid self-assembly under osmotic stress conditions. J Phys Chem B. 2018;122:6471–82.
38. Assaf KI, Nau WM. The chaotropic effect as an assembly motif in chemistry. Angew Chem Int Ed. 2018;57:13968–81.
39. Gervais D, King D. Capillary isoelectric focusing of a difficult-to-denature tetrameric enzyme using alkylurea-urea mixtures. Anal Biochem. 2014;465:90–5.
40. Righetti PG, Gelfi C, Bossi ML. Hydrophobic interaction between alkaline immobilines and ferritin during isoelectric focusing in immobilized pH gradients. J Chromatogr A. 1987;392:123–32.
41. Mie G. Beiträge zur Optik trüber Medien, speziell kolloidaler Metallösungen. Ann Phys. 1908;330:377–445.
42. Brader ML, Williams SJ, Banks JM, Hui WH, Zhou ZH, Jin L. Encapsulation state of messenger RNA inside lipid nanoparticles. Biophys J. 2021;120:2766–70.
43. Ball RL, Bajaj P, Whitehead KA. Achieving long-term stability of lipid nanoparticles: examining the effect of pH, temperature, and lyophilization. Int J Nanomed. 2017;12:305–15.
44. Kumar V, Qin J, Jiang Y, Duncan RG, Brigham B, Fishman S, et al. Shielding of lipid nanoparticles for siRNA delivery: impact on physicochemical properties, cytokine induction, and efficacy. Mol Ther Nucleic Acids. 2014;3:e210.
45. Jayaraman M, Ansell SM, Mui BL, Tam YK, Chen J, Du X, et al. Maximizing the potency of siRNA lipid nanoparticles for hepatic gene silencing *in vivo*. Angew Chem Int Ed Engl. 2012;51:8529–33.
46. Viger-Gravel J, Schantz A, Pinon AC, Rossini AJ, Schantz S, Emsley L. Structure of lipid nanoparticles containing siRNA or mRNA by dynamic nuclear polarization-enhanced NMR spectroscopy. J Phys Chem B. 2018;122:2073–81.

SUPPORTING INFORMATION

Additional supporting information can be found online in the Supporting Information section at the end of this article.

Electrophoresis 2019, *40*, 2602–2609

John W. Loughney
Kevin Minsker
Sha Ha
Richard R. Rustandi

Vaccine Analytical Research & Development, Merck and Co. Inc., West Point, PA, USA

Received January 27, 2019
Revised June 9, 2019
Accepted June 10, 2019

Research Article

Development of an imaged capillary isoelectric focusing method for characterizing the surface charge of mRNA lipid nanoparticle vaccines

Lipid nanoparticles (LNPs) have been employed for drug delivery in small molecules, siRNA, mRNA, and pDNA for both therapeutics and vaccines. Characterization of LNPs is challenging because they are heterogeneous mixtures of large complex particles. Many tools for particle size characterization, such as dynamic and static light scattering, have been applied as well as morphology analysis using electron microscopy. CE has been applied for the characterization of many different large particles such as liposomes, polymer, and viruses. However, there have been limited efforts to characterize the surface charge of LNPs and CIEF has not been explored for this type of particle. Typically, LNPs for delivery of oligonucleotides contain at least four different lipids, with at least one being an ionizable cationic lipid. Here, we describe the development of an imaged capillary isoelectric focusing method used to measure the surface charge (i.e., pI) of an LNP-based mRNA vaccine. This method is capable of distinguishing the pI of LNPs manufactured with one or more different ionizable lipids for the purpose of confirming LNP identity in a manufacturing setting. Additionally, the method is quantitative and stability-indicating making it suitable for both process and formulation development.

Keywords:
Cationic lipid / Imaged capillary isoelectric focusing / Isoelectric point (pI) / Lipid nanoparticles / Maurice / mRNA vaccine DOI 10.1002/elps.201900063

1 Introduction

Drug and vaccine development in which the active drug substance is encapsulated with a lipid nanoparticle (LNP) has gained momentum over the past decade as an efficient drug delivery system [1, 2]. Several lipid-based delivery systems have been clinically approved to deliver small drug molecules such as doxorubicin and vincristine [3]. In 2018, the first LNP-based drug containing small interfering RNA (siRNA) named Patisiran was approved for the treatment of hereditary transthyretin-mediated amyloidosis [4]. Additional LNPs are being evaluated clinically for delivery of a wide variety of nucleic acids, including siRNA, messenger RNA (mRNA), and plasmid DNA, for both therapeutic and vaccine purposes [5–7]. LNPs that encapsulate nucleic acid macromolecules are generally comprised of four components: (1) an ionizable amino lipid (cationic lipid); (2) a zwitterionic phospholipid such as 1,2-distearoyl-sn-glycero-3-phosphocholine (DSPC) or 1,2-dipalmitoyl-sn-glycero-3-phosphocholine (DPPC); (3) a neutral lipid such as cholesterol; and (4) a polyethylene glycol-lipid (PEG-lipid) [8]. The ionizable cationic lipid plays a principal role, for example, in siRNA transfection, by mediating cytosolic delivery of the siRNA through facilitated endosomal escape after LNP endocytosis. Neutral lipids, such as DSPC, 1,2-dipalmitoyl-sn-glycero-3-phosphocholine, and cholesterol, are selected to modulate the fluidity and phase behavior of the LNP, whereas PEG-lipids are utilized to improve particle circulation half-life and systemic exposure [9].

LNPs are produced through a self-assembly process and can be made to have a particle size ranging from 70 to 110 nm depending on the target delivery purpose [10]. LNPs can have a complex structure with respect to particle size, surface charge, lipid composition, particle morphology, and surface hydrophobicity [11, 12]. All of these attributes can affect the uptake of LNP and release of the RNA drug in various cell types [13]. In addition to the transfection efficiency, the surface charge may be correlated with cell toxicity [14, 15]. Last, a guideline from the FDA recommends the physiochemical characterization of liposomes, including a stability assessment should be completed [16]. Zhang et al., have described

Correspondence: John W. Loughney, 770 Sumneytown Pike, P. O. Box 4, WP42A-30, West Point, PA 19486, USA
Email: John_Loughney@merck.com
Fax: +1 (215) 993 2244

Abbreviations: **DSPC**, 1,2-distearoyl-sn-glycero-3-phosphocholine; **iclEF**, imaged capillary isoelectric focusing; **LNP**, lipid nanoparticle; **mRna**, messenger RNA; **PEG-lipid**, polyethylene glycol-lipid; **siRNA**, small interfering RNA

Color online: See the article online to view Figs. 1–5 in color.

how to characterize size and morphology of LNPs using techniques such as dynamic light scattering, cryoelectron microscopy, high performance size exclusion chromatography, and asymmetric flow field-flow fractionation [12, 17]. However, there is a lack of tools to measure the surface charge of LNPs. Currently, zeta potential is the only method routinely used and available to measure surface charge of LNPs.

Liposome protein interactions have been studied using imaged capillary isoelectric focusing (icIEF) [18] and CE has been applied to study other types of large particles such as bacteria, viruses, colloidal/nanoparticles, and polymeric particles [19–24]. However, CE has not been used to effectively measure the surface charge of LNPs. Here, we describe for the first time, using CE for characterizing LNPs that encapsulate nucleic acids using icIEF separation.

Earlier publications have described traditional gel isoelectric focusing to analyze the size of colloidal nanoparticles and gold nanoparticles [25, 26]. However, these gel-based electrophoretic techniques are labor intensive and qualitative in nature. This study describes an icIEF method to measure the pI of LNPs for the process and formulation development of an mRNA-based vaccine. This method is capable of distinguishing the pI of LNPs manufactured with different cationic lipids, is quantitative, and is stability-indicating.

2 Material and methods

2.1 Chemicals and reagents

All methylcellulose containing solutions, Maurice icIEF fluorescence calibration standards, system suitability standards, pI markers (5.85 and 8.40), Servalyt pH 2–9 ampholytes, and icIEF cartridges were obtained from ProteinSimple (Santa Clara, CA, USA). Pharmalyte ampholytes pH 3–10 and pH 5–8 were purchased from GE Healthcare (Uppsala, Sweden). Glycerol and sucrose were purchased from Sigma–Aldrich (St. Louis, MO, USA).

2.2 LNP preparation

LNPs containing mRNA were prepared in-house as previously described [27]. Briefly, LNP preparation includes (i) with, or without (empty LNP) mRNA, drug substance, (ii) a cationic lipid, (referred to here as Cationic Lipid-1 or Cationic Lipid-2), which is an ionizable lipid that complexes with mRNA to promote the formation of LNPs, (iii) one or more commercially available lipids, such as cholesterol, DSPC, and 1,2-dimyristoyl-rac-glycero-3-methylpolyoxyethylene, that contribute to the overall pharmaceutical properties of LNP. A lipid stock solution was prepared by dissolving the cationic lipid, cholesterol, phospholipid, and 1,2-dimyristoyl-rac-glycero-3-methylpolyoxyethylene in ethanol in a molar ratio of 50–58:30–38:10:1–2.

2.3 icIEF sample preparation

The icIEF sample preparation has been previously described [28, 29]. Unless specified otherwise, the ampholytes solution was prepared by combining two parts of the ampholytes (pH 5–8) with 1 part of the ampholytes (pH 3–10). The sample was prepared by combining 70 µL of 0.5% methylcellulose, 8 µL of ampholytes solution, 16µL of glycerol (99%), 1 µL of each pI marker 5.85 and 8.40 with various volumes of LNP (0.5 to 2.5 µL) to make consistent cationic lipid concentrations, and various amounts of water to obtain a final volume of 160 µL. The samples were centrifuged at 5 000 g for 5 min before 120 µL was transferred to the 96-well plate.

2.4 icIEF instrument and software

Maurice is an instrument from ProteinSimple that is similar to iCE280 and iCE3 instruments except the capillary is provided in a preassembled cartridge. The IEF separation capillary is 50 mm in length and is 100 µm ID x 200 µm OD silica coated with fluorocarbon. The catholyte consists of 0.1 M NaOH in 0.1% methylcellulose and the anolyte consists of 0.08 M phosphoric acid in 0.1% methylcellulose. All other reagents, such as system suitability standard, fluorescence calibration standard, and 0.5% methylcellulose, were prepared according to vendor recommendations. The capillary is automatically calibrated with a fluorescence standard preconditioned with a system suitability control to ensure the capillary is functioning properly. The samples were injected using the default pressure setting for 55 s and were prefocused for 1 min at 300 V/cm, followed by focusing time for 8 min at 600 V/cm. All electropherograms were detected with UV absorbance at 280 nm. All data analyses were performed using vendor software called *Compass for iCE*. The *Compass* software aligns each electropherogram using the pI markers so that the *x*-axis is displayed as a normalized pI for each injection.

3 Results and discussion

3.1 Apparent pI measurement of LNPs

Development of an icIEF method for LNPs was initiated using broad range ampholytes to determine the apparent pI. Two different broad range ampholytes (Servalyt pH 2–9 and Pharmalyte pH 3–10) were tested and compared initially as shown in Fig. 1A (trace A and B, respectively). The Servalyt ampholytes profile showed many sharp irreproducible peaks indicating possible LNP precipitation or aggregation. The Pharmalyte mixture showed an inconsistent broad peak shape. Glycerol is known to be a stabilizing additive for protein cIEF method development [30], and was tested with the Pharmalyte mixture. The addition of 10% glycerol helped to consistently and reproducibly focus the LNP as illustrated

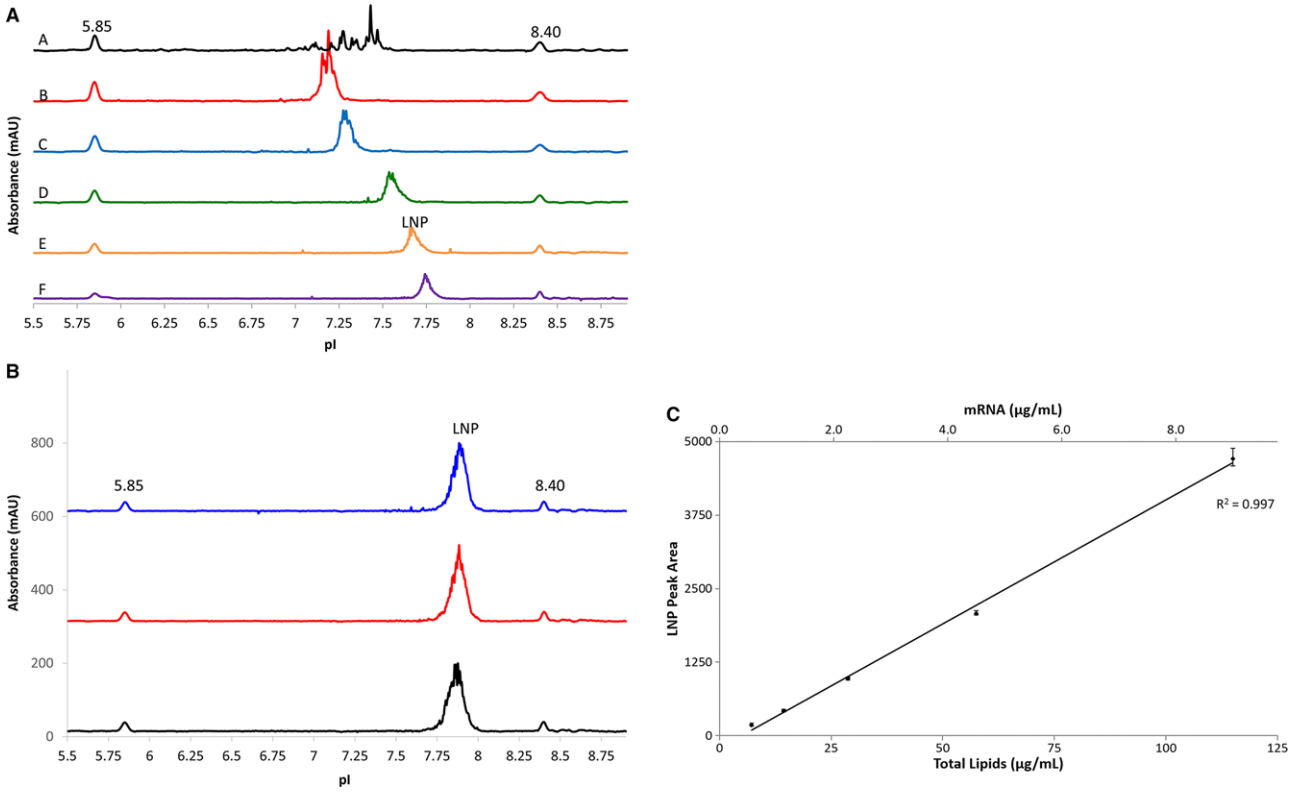

Figure 1. (A) Electropherograms of an LNP using various ampholytes and additives. Traces A and B show high background or precipitation and LNP containing sharp peaks using the broad range Servalyt pH 2–9 and Pharmalyte ampholytes pH 3–10, respectively. Trace C shows a focused LNP with an apparent pI of approximately 7.3 using pH 3–10 Pharmalyte ampholytes containing 10% glycerol. Trace D uses a mixture of 33.3% ampholyte pH 5–8 and 66.6% ampholytes pH 3–10 with 10% glycerol. Trace E uses a 66.6% ampholyte pH 5–8 and 33.3% ampholytes pH 3–10 with 10% glycerol. Trace F uses ampholyte pH 5–8 containing 10% glycerol. The pI of the LNP shifts to approximately 7.6–7.8 in traces D, E, and F. Two pI markers are 5.85 and 8.40. (B) Electropherogram of an LNP prepared in triplicate. An LNP sample was prepared in triplicate for the icIEF experiment. The LNP has an apparent pI of approximately 7.89 and peak shape was consistent for the three replicates. (C) Calibration curve of LNP, which ranges from 7.2–115 µg/mL of total lipids. LNP samples were diluted in icIEF ampholyte mixtures from 0.56 to 9.0 µg/mL of mRNA (equivalent to 7.2 to 115 µg/mL of total lipid). This linear range has a coefficient of determination (R^2) ≥ 0.997.

in Fig. 1A trace C. Higher percentages (20% and 40%) of glycerol noticeably increased the viscosity and, thus, decreased the ability of the LNP to be focused in the tested separation time (data not shown). Based on the initial observation using the broad range ampholytes mixture, the estimated pI of the LNP was approximately 7.3 (Fig. 1 trace C).

The separation was further optimized by mixing different amounts of narrower range Pharmalyte ampholytes pH 5–8 into the Pharmalyte ampholytes pH 3–10. As the percentage of the narrow range ampholytes increased from 33% to 100%, the apparent pI shifted from approximately 7.6 to 7.8 (Fig. 1A trace D, E, and F, respectively). Figure 1A trace F showed the best LNP peak shape, yet the separation was more reproducible and consistent using the conditions shown in trace E. Trace E was the final ampholyte mixture used in all remaining experiments.

The ampholyte screening and optimization, shown in Fig. 1A, was performed with an LNP containing Cationic Lipid-1, which had an apparent pI of 7.7. The LNP peak was relatively broad and not quite as homogeneous as normally observed for proteins. This broad peak shape is consistent with published gel IEF methods analyzing gold nanoparticles [25]. We believe this broad, jagged peak is likely caused by the polydispersity of generating different LNP structures and sizes during the manufacturing process. It is important to note that mixing the broad range and narrow range ampholytes can introduce different pH slopes, thus, shifting the apparent pI. This phenomenon was observed in Fig. 1A traces C to F; the different ampholyte mixture showed a pI shift of approximately 0.5 units. Regardless, using the final ampholytes mixture, the pI and peak shape remained consistent between three individual preparations of a different LNP samples (Fig. 1B). Precision of the pI was evaluated with this LNP sample over 16 independent runs; the LNP had an average pI of 7.89 ± 0.028 (RSD < 0.4%).

Last, five concentrations of an LNP sample ranging from 0.56 to 9.0 µg/mL of mRNA (equivalent to 7.2 to 115 µg/mL of total lipids) were tested by icIEF and the pI was determined. Using linear regression analysis, the peak area of the standard (LNP) was plotted against the mRNA concentration (µg/mL). This linear range has a coefficient of determination (R^2) ≥ 0.997 showing strong linearity and demonstrating

the ability of this technology to perform quantitative analysis (Fig. 1C).

3.2 Effect of lipid concentration on the pI

The pI of an LNP sample was found to vary when loading different quantities of LNP based on mRNA concentration into the ampholytes mixture; samples of higher LNP concentration display a higher apparent pI. To further investigate if the pI variation was caused by the cationic lipid or the mRNA concentration, both parameters were examined. Four different LNP batches were formulated and each batch contained a different cationic lipid to mRNA ratio (mole/mole). The four LNP batches had cationic lipid to mRNA ratios of 3.1, 6.6, 12.2, and 20.1. The LNP batches were diluted to five different cationic lipid concentrations and subjected to icIEF. The apparent pIs for all prepared LNPs were plotted against cationic lipid and mRNA concentrations.

The apparent pI was found to have a strong correlation to cationic lipid concentration with an $R^2 = 0.956$, using a logarithmic fit (Fig. 2A). The apparent pI has a weaker correlation with an $R^2 = 0.653$, using a logarithmic fit to mRNA concentration (Fig. 2B). Results of this experiment indicate that icIEF sample loading should be normalized according to cationic lipid concentration rather than to mRNA concentration to maintain consistent pI results between different LNP batches. This data correlate well with the hypothesis that the cationic lipid is at the surface of the LNP and the mRNA is located inside of the LNP. This hypothesis is reasonable as the LNP acts as a protective hydrophobic barrier to protect the mRNA.

3.3 UV-Vis spectrum of LNP with and without mRNA

The icIEF instrument detects the LNP at 280 nm and the instrument does not allow this wavelength to be altered. To better understand how the LNP was being detected by the icIEF instrument, the absorbance spectrum of LNPs (containing Cationic Lipid-1) formulated with and without mRNA was measured using an Agilent 8453 ultraviolet-visible spectrophotometer. The LNPs were prepared in two different matrices: Tris buffer (10 mM Tris with 10% sucrose) and cIEF ampholytes matrix. The Tris buffer was measured because ampholytes used in cIEF are known to have interference at wavelengths below 280 nm. In addition, the samples prepared in Tris buffer serve as a control

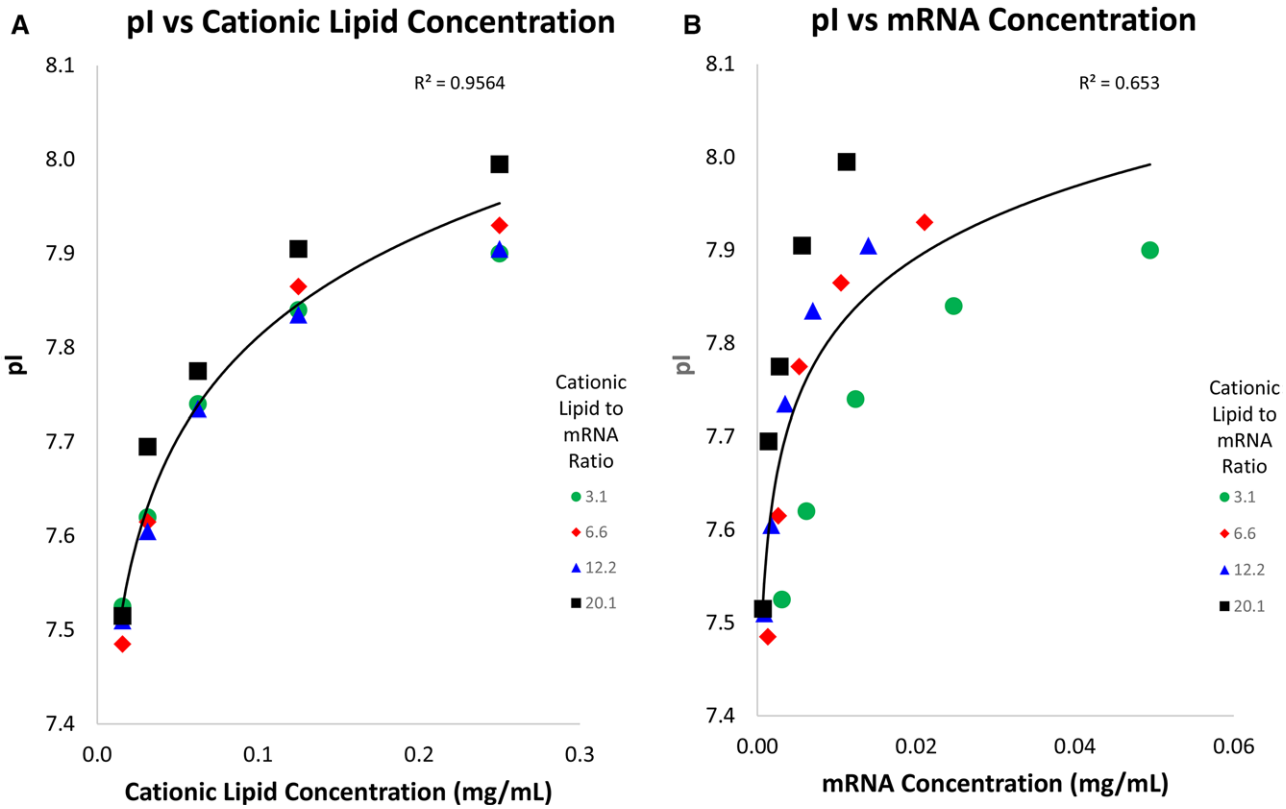

Figure 2. LNP pI plotted by cationic lipids and mRNA concentration: different LNP batches were formulated to contain different cationic lipid to mRNA ratios. These LNPs were then diluted to five different lipid concentrations and subjected to icIEF. The pI (*y*-axis) was plotted against cationic lipid concentration (Fig. 2A) and the mRNA concentration (Fig. 2B). A strong correlation of pI to cationic lipid concentration was observed ($R^2 = 0.956$; logarithmic fit, left graph) compared to a weaker correlation of pI to mRNA concentration ($R^2 = 0.653$; logarithmic fit, right graph).

spectrum of intact LNPs. Figure 3A shows UV spectra for each matrix measured from 210 nm to 600 nm.

The UV spectra of LNPs containing mRNA for both Tris and ampholyte matrices showed an elevated UV absorbance from 240 to 290 nm, with an absorbance maximum at 260 nm. The absorbance at 260 nm is due to the mRNA component of the LNP. In addition, both LNPs formulated with and formulated without mRNA have significant light scatter throughout the wavelengths collected.

Comparing the UV spectra of LNPs without mRNA for both Tris and ampholyte matrices, the spectra showed only broad-spectrum light scattering. No defined UV absorbance was observed within 240–290 nm. These data suggest that observed icIEF signal at 280 nm results from a combination of both the mRNA absorbance and light scattering of the approximately 100 nm LNP. Thus, mRNA is not needed to obtain a signal at 280 nm.

Last, LNPs measured in the ampholyte matrix displayed inconsistent signal from 210 to 256 nm. This inconsistency was expected due to interfering components in the ampholyte matrix resulting in higher background below 250 nm [30]. Regardless, both the Tris buffer matrix and the ampholyte matrix absorbance traces were identical at wavelengths higher than 260 nm. These data also suggest that LNPs formulated with or without mRNA are stable and intact in the final ampholyte matrix (Fig. 3A).

The apparent pIs of LNPs formulated with or without mRNA were subsequently measured by icIEF. Figure 3B shows that LNPs with and without mRNA have similar pIs at approximately 7.7. As expected, the peak areas for LNPs containing mRNA are larger than those for LNPs without mRNA. These data further support the conclusion that the observed signal is a combination of both scattered light and mRNA absorbance.

3.4 Effect of cationic lipid type on LNP pI

The LNPs contain several ionizable groups that can contribute to the apparent pI: the phosphate backbone of the mRNA, the cationic lipid, the zwitterionic phospholipid, and potential degradants from the various lipids (e.g., fatty acids resulting from hydrolysis of DSPC or the PEG-lipid). The contribution of the phosphate backbone within the mRNA is negligible as shown in Fig. 2B and 3B.

To demonstrate the apparent pI of the LNP is dependent on the cationic lipid used in the LNP, a second LNP was evaluated containing Cationic Lipid-2. Cationic Lipid-2 has a pKa of approximately 0.4 units higher than that of Cationic Lipid-1. Figure 4 trace A shows an LNP containing Cationic Lipid-1 with a pI of approximately 7.75. The LNP containing Cationic Lipid-2 demonstrated a higher apparent pI of approximately 8.1, as illustrated in Fig. 4 trace B, which suggests the pKa of the cationic lipid is the main contributing factor for the observed pI. When a mixture of these two LNPs was prepared and analyzed by icIEF, both LNPs were baseline resolved as shown in Fig. 4 trace C. A slight basic shift for both LNP peaks was observed; at this time, the mechanism for this observation is not known and further investigation is required. Regardless, this finding suggests the method is capable of separating LNPs by their pI based on the discrete cationic lipid pKa values (Fig. 4). The results demonstrate that the icIEF method can be used to confirm the identity of the cationic lipid present within a given LNP sample.

3.5 Detecting LNP stability

The new icIEF method can detect changes in LNP stability upon heat stress as shown in Figs 5A and B. In Fig. 5A, when

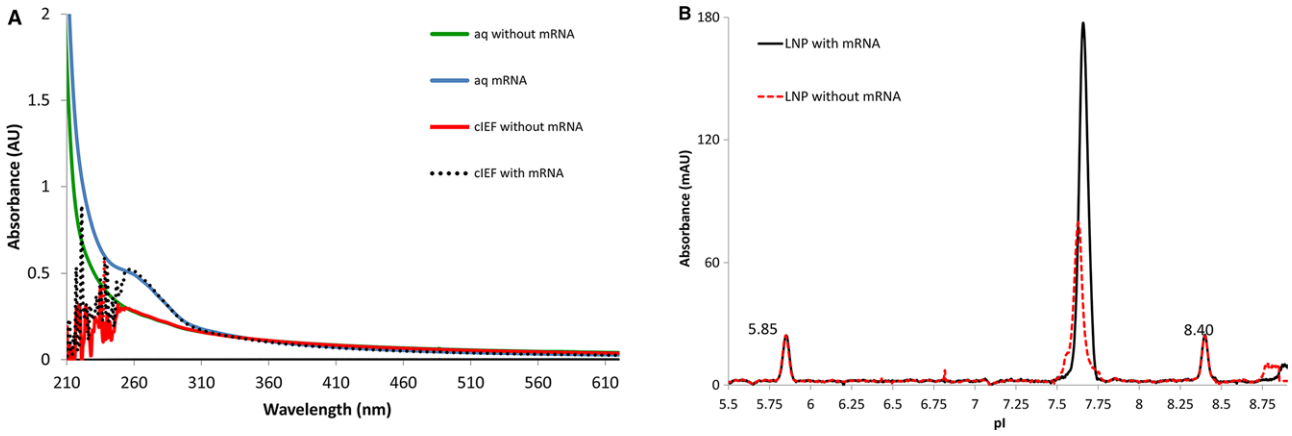

Figure 3. (A) UV absorbance of LNPs in both aqueous and icIEF ampholyte mixtures. LNPs containing mRNA were tested in Tris buffer (blue trace) and icIEF ampholyte mixture (black dash trace). LNPs without mRNA were tested in Tris buffer (green trace) and icIEF ampholyte mixture (red dash trace). LNPs containing mRNA show an absorbance max at 260 nm compared to LNP without mRNA, which lack a peak at 260 nm. Both aqueous and icIEF ampholyte mixtures absorbance traces were identical when comparing the wavelengths at 260 nm demonstrating that with or without mRNA, LNPs are stable and intact in the final cIEF ampholyte mixture. (B) Electropherogram of LNP formulated with and without mRNA. LNPs without mRNA (red dashed trace) have a similar pI to LNPs formulated with mRNA (black solid trace). The pI of both LNPs is approximately 7.6–7.7. Two pI markers were 5.85 and 8.40.

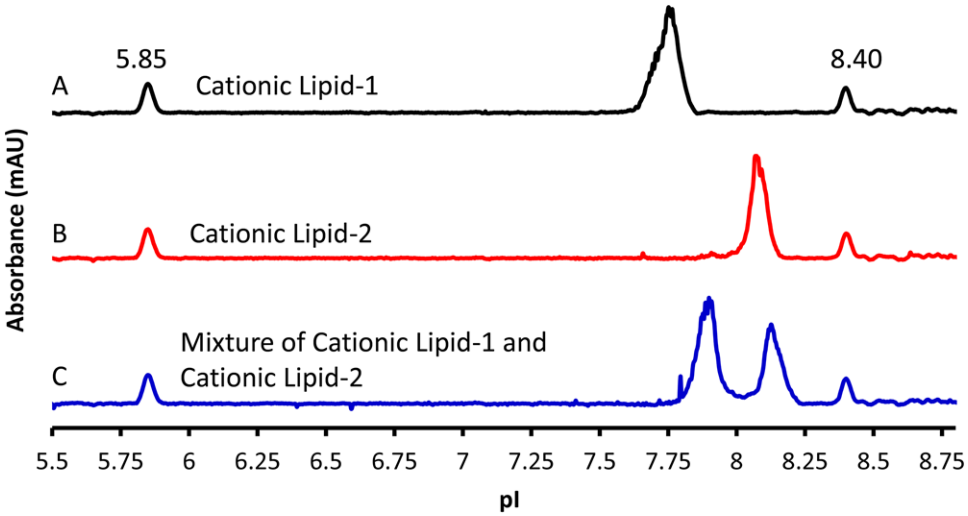

Figure 4. LNP with different cationic lipids have unique pIs. Trace A shows an LNP containing Cationic Lipid-1with a lower pKa value has a pI of 7.6–7.7. (B) LNP containing Cationic Lipid-2 with a higher pKa value has a pI of 8.1. (C) Separation of a mixture of LNP containing different cationic lipids. Two pI markers were 5.85 and 8.40.

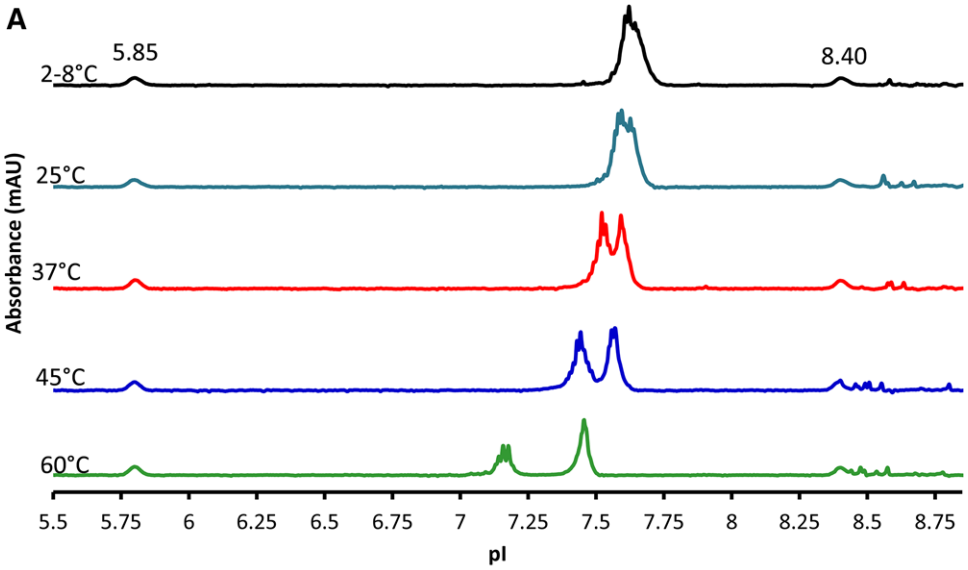

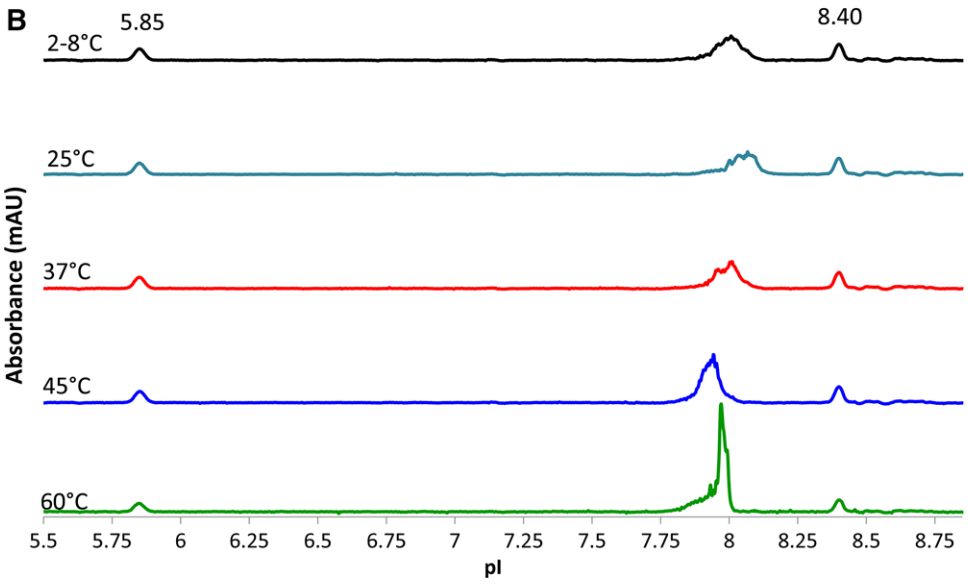

Figure 5. (A) Stability of LNPs containing mRNA. The LNPs containing mRNA were exposed to elevated temperatures for 24 h. The LNP stored at 2–8°C showed a symmetrical peak shape with a pI of approximately 7.7. As the temperature increased, the LNP with mRNA peaks became more acidic and split into two distinct peaks. (B) Stability of empty LNPs. LNPs without mRNA stored at 2–8°C showed a symmetrical peak shape with a pI of approximately 8.0. As the temperature increased, the LNP without mRNA showed a different degradation pattern compared to the LNPs containing mRNA. Two pI markers were 5.85 and 8.40.

an mRNA-containing LNP sample was stressed at 37°C for 24 h, the entire LNP profile shifts to lower apparent pI values and a new peak is detected (analogous to acidic variants in the context of protein analysis). Moreover, the "acidic variants" became more acidic with increasing temperature. At 60°C, the "acidic variants" were baseline separated from the main peak with a pI of 7.4 (Fig. 5A). This suggests that the higher the stress temperature, the greater the "acidic variant."

The LNP stability experiment described above was repeated using LNPs that were formulated without mRNA. The corresponding electropherograms shown in Fig. 5B had a different degradation pattern compared to the LNPs containing mRNA. At 45°C after 24 h, the empty LNP peak showed a slight acidic shift of approximately 0.1 pI units. A sample stressed at 60°C for 24 h showed an uncharacteristic peak profile containing a sharp spike in absorbance, which may indicate LNP destabilization or aggregation. Unlike the mRNA-containing LNPs, these preparations did not show splitting into two peaks or generation of "acidic variants." It is conceivable that the previously seen acidic peak could be due to the mRNA being exposed on the surface of the LNP. Future work employing LC ion exchange could be exploited to further investigate the behavior of these stressed samples.

4 Concluding remarks

Characterization of LNPs is challenging because they are heterogeneous mixtures of large complex particles. There are limited methods for surface charge LNP characterization that have been explored including CE. To better characterize the surface charge of LNP drug delivery systems, we have developed a new icIEF method. This method uses a commercially available cIEF instrument and can measure the pI of LNPs formulated with or without mRNA. The icIEF method can reproducibly measure the apparent pI of LNPs, provided that the cationic lipid concentration is known. With detection at 280 nm, the observed signal is proportional to the LNP concentration. Surface charge of an LNP is found to be primarily driven by the cationic lipid, implying that this lipid is at the surface of the LNP. In addition, this method is capable of differentiating LNPs containing different cationic lipids and is suitable as a test for LNP identity. More importantly, it is a stability-indicating assay, which can be used to support process and formulation development for LNP-based mRNA vaccines. To the best of our knowledge, this is the first reported use of icIEF applied to an LNP-based drug delivery system.

We would like to thank our colleagues, specifically Dave Boyd in Vaccine Process Development for providing the LNP samples, Jessica Raffaele for generating stability samples, Katrina Fritts for dynamic light scattering technical guidance, and Alyssa Deiss for grammatical suggestions. We also would like to thank Richard Peluso for his support. The authors report one patent related to the characterization of LNPs using the cIEF method described in this work: US Patent serial number 62/756302 (case 24665).

The authors have declared no conflict of interest.

5 References

[1] Allen, T. M., Cullis, P. R., *Science* 2004, *303*, 1818–1822.

[2] Guan, S., Rosenecker, J., *Gene Ther.* 2017, *24*, 133–143.

[3] Mayer, L. D., Bally, M. B., Loughrey, H., Masin, D., Cullis, P. R., *Cancer Res.* 1990, *50*, 575.

[4] Adams, D., Gonzalez-Duarte, A., O'Riordan, W. D., Yang, C.-C., Ueda, M., Kristen, A. V., Tournev, I., Schmidt, H. H., Coelho, T., Berk, J. L., Lin, K.-P., Vita, G., Attarian, S., Planté-Bordeneuve, V., Mezei, M. M., Campistol, J. M., Buades, J., Brannagan, T. H., Kim, B. J., Oh, J., Parman, Y., Sekijima, Y., Hawkins, P. N., Solomon, S. D., Polydefkis, M., Dyck, P. J., Gandhi, P. J., Goyal, S., Chen, J., Strahs, A. L., Nochur, S. V., Sweetser, M. T., Garg, P. P., Vaishnaw, A. K., Gollob, J. A., Suhr, O. B., *N. Engl. J. Med.* 2018, *379*, 11–21.

[5] Zatsepin, T. S., Kotelevtsev, Y. V., Koteliansky, V., *Int. J. Nanomed.* 2016, *11*, 3077–3086.

[6] Midoux, P., Pichon, C., *Expert Rev. Vaccines* 2015, *14*, 221–234.

[7] Brito, L. A., Chan, M., Shaw, C. A., Hekele, A., Carsillo, T., Schaefer, M., Archer, J., Seubert, A., Otten, G. R., Beard, C. W., Dey, A. K., Lilja, A., Valiante, N. M., Mason, P. W., Mandl, C. W., Barnett, S. W., Dormitzer, P. R., Ulmer, J. B., Singh, M., O'Hagan, D. T., Geall, A. J., *Mol. Ther.* 2014, *22*, 2118–2129.

[8] Gindy, M. E., Feuston, B., Glass, A., Arrington, L., Haas, R. M., Schariter, J., Stirdivant, S. M., *Mol. Pharmaceutics* 2014, *11*, 4143–4153.

[9] Foged, C., *Curr. Top. Med. Chem.* 2012, *12*, 97–107.

[10] Jeffs, L. B., Palmer, L. R., Ambegia, E. G., Giesbrecht, C., Ewanick, S., MacLachlan, I., *Pharm. Res.* 2005, *22*, 362–372.

[11] Lin, P. J., Tam, Y. Y., Hafez, I., Sandhu, A., Chen, S., Ciufolini, M. A., Nabi, I. R., Cullis, P. R., *Nanomed. Nanotechnol. Biol. Med.* 2013, *9*, 233–246.

[12] Zhang, J., Pei, Y., Zhang, H., Wang, L., Arrington, L., Zhang, Y., Glass, A., Leone, A. M., *Mol. Pharmaceutics* 2013, *10*, 397–405.

[13] Kou, L., Sun, J., Zhai, Y., He, Z., *Asian J. Pharm. Sci.* 2013, *8*, 1–10.

[14] Kedmi, R., Ben-Arie, N., Peer, D., *Biomaterials* 2010, *31*, 6867–6875.

[15] Mizrahy, S., Hazan-Halevy, I., Landesman-Milo, D., Ng, B. D., Peer, D., *Front. Immunol.* 2017, *8*, 69.

[16] FDA, Liposome drug products chemistry, manufacturing, and controls; human pharmacokinetics and bioavailability; and labeling documentation; guidance for industry. Office of communications, division of drug information, center for drug evaluation and research; food and drug administration; 2018.

[17] Zhang, J., Haas, R. M., Leone, A. M., *Anal. Chem.* 2012, *84*, 6088–6096.

[18] Bo, T., Pawliszyn, J., *Electrophoresis* 2006, *27*, 852–858.

[19] Rodriguez, M. A., Armstrong, D. W., *J. Chromatogr. B* 2004, *800*, 7–25.

[20] Rustandi, R. R., Wang, F., Hamm, C., Cuciniello, J. J., Marley, M. L., *Electrophoresis* 2014, *35*, 1072–1078.

[21] Wiedmer, S. K., Hautala, J., Holopainen, J. M., Kinnunen, P. K., Riekkola, M. L., *Electrophoresis* 2001, *22*, 1305–1313.

[22] Owen, R. L., Strasters, J. K., Breyer, E. D., *Electrophoresis* 2005, *26*, 735–751.

[23] Riley, K. R., Liu, S., Yu, G., Libby, K., Cubicciotti, R., Colyer, C. L., *J. Chromatogr. A* 2016, *1463*, 169–175.

[24] van Tricht, E., Geurink, L., Pajic, B., Nijenhuis, J., Backus, H., Germano, M., Somsen, G. W., Sanger-van de Griend, C. E., *Talanta* 2015, *144*, 1030–1035.

[25] Arnaud, I., Abid, J. P., Roussel, C., Girault, H. H., *Chem. Commun.* 2005, 787–788.

[26] Gole, A. M., Sathivel, C., Lachke, A., Sastry, M., *J. Chromatogr. A* 1999, *848*, 485–490.

[27] Abrams, M. T., Koser, M. L., Seitzer, J., Williams, S. C., DiPietro, M. A., Wang, W., Shaw, A. W., Mao, X., Jadhav, V., Davide, J. P., Burke, P. A., Sachs, A. B., Stirdivant, S. M., Sepp-Lorenzino, L., *Mol. Ther.* 2010, *18*, 171–180.

[28] Anderson, C. L., Wang, Y., Rustandi, R. R., *Electrophoresis* 2012, *33*, 1538–1544.

[29] Loughney, J. W., Ha, S., Rustandi, R. R., *Anal. Biochem.* 2017, *534*, 19–23.

[30] Wu, J., Li, S. C., Watson, A., *J. Chromatogr. A* 1998, *817*, 163–171.

Electrophoresis 2021, *42*, 1521–1531

Christin Scheller‡
Finja Krebs‡
Rebecca Wiesner
Hermann Wätzig
Imke Oltmann-Norden

Institute of Medicinal and Pharmaceutical Chemistry, Technische Universität Braunschweig, Braunschweig, Germany

Received March 17, 2021
Revised April 22, 2021
Accepted April 27, 2021

Research Article

A comparative study of CE-SDS, SDS-PAGE, and Simple Western—Precision, repeatability, and apparent molecular mass shifts by glycosylation

SDS gel electrophoresis is a commonly used approach for monitoring purity and apparent molecular mass (Mr) of proteins, especially in the field of quality control of biopharmaceutical proteins. The technological installation of CE-SDS as the replacement of the slab gel technique (SDS-PAGE) is still in progress, leading to a continuous improvement of CE-SDS instruments. Various CE-SDS instruments, namely Maurice (CE-SDS/CE-SDS PLUS) and Wes by ProteinSimple as well as the microchip gel electrophoresis system LabChip® GXII Touch™ HT by PerkinElmer were tested for precision and repeatability compared to SDS-PAGE (Bio-Rad). For assessing these quality control parameters, standard model proteins with minor post-translational modifications were used. Overall, it can be concluded that the CE-SDS-based methods are similar to SDS-PAGE with respect to these parameters. Quality characteristics of test systems gain more significance by testing proteins that do not behave like model proteins. Therefore, glycosylated proteins were analyzed to comparatively investigate the influence of glycosylation on Mr determination in the different instruments. In some cases, high deviations were found both among the methods and with regard to reference values. This article provides possible explanations for these findings.

Keywords:
CE-SDS / Glycoproteins / Molecular mass determination / Precision / SDS-PAGE
DOI 10.1002/elps.202100068

Additional supporting information may be found online in the Supporting Information section at the end of the article.

1 Introduction

For more than 20 years, CE-SDS has been increasingly used as an analytical method for characterizing and measuring sample purity, especially for the investigation of biopharmaceuticals and is replacing the previously used SDS-PAGE. The principle of both techniques is the same: heat denaturation of proteins, in presence of SDS and reducing agents, which leads to protein unfolding and stretching. SDS ideally binds in a ratio of 1.4 mg SDS/mg protein and consequently, the charge density of the protein becomes nearly constant. Next, the SDS-protein-complexes are separated electrophoretically according to their Stokes radii and, therefore, by their relative molecular masses (Mrs) [1]. In contrast to the traditional planar SDS-PAGE, in which slab gels consisting of polyacrylamide are used, noncross-linked entangled polymer networks, for example, dextran, pullulan, polyvinyl alcohol, polyethylene oxide, or polyethylene glycol, are utilized as separation matrices in CE-SDS [2–6]. Another exciting advancement of SDS-PAGE is the method called SDS-PAGE focusing. Here, a gradient of positive charges is attached to the polyacrylamide matrix, which causes the Mr and relative migration distances to behave more linearly than in conventional SDS-PAGE. Since the Mr determination in SDS-PAGE is carried out via linear regression, it becomes more accurate. This method will not be examined here, as we are only concerned with the comparison of SDS-PAGE with various CE-SDS instruments [7]. Kahle et al. give an impression about the

Correspondence: Dr. Imke Oltmann-Norden, Institute of Medicinal and Pharmaceutical Chemistry, Technische Universität Braunschweig, Beethovenstraße 55, 38106 Braunschweig, Germany
Email: i.oltmann-norden@tu-bs.de

Abbreviations: **AA**, amino acid; **β-ME**, β-mercaptoethanol; **EPO**, Erythropoietin; **Mrs**, relative molecular masses; **PNGase F**, Peptide-N-glycosidase F; **r-Mr**, reference molecular mass; **SST**, system suitability test

‡Christin Scheller and Finja Krebs are equal contributors of this work.
Color online: See article online to view Fig. 1 in color.

state-of-the-art performance of some recently developed CE-SDS instruments [8]. CE-SDS is a well-established approach to determine the purity of monoclonal antibodies [8–14]. Thus, several studies have evaluated CE-SDS platforms, and have been largely focused on improving and investigating the performance for antibody analysis. The focus of these studies is more on the enhancement of resolution, sensitivity, and linearity, and not on apparent Mr determination [8, 15–17].

The publication by Wiesner et al. illustrates the influences of sample preparation and the choice of the Mr marker on the apparent Mr determination of proteins by comparing CE-SDS instruments with SDS-PAGE [18]. The present publication is a follow-up study to this previously mentioned work, comparing the precision, repeatability, and apparent Mr shifts by glycosylation on Mr determination. Specifically, the Maurice CE-SDS/CE-SDS PLUS and Wes by ProteinSimple as well as the LabChip® GXII Touch™ HT by PerkinElmer were investigated and compared to the conventional SDS-PAGE following the Laemmli procedure [19]. Precision experiments were conducted using carbonic anhydrase, ovalbumin, BSA, and phosphorylase B by analyzing them individually using ten independent preparations. For repeatability, 60 measurement replicates were performed with one preparation mixture of all four proteins.

The second part of this article deals with the comparison of the instruments concerning the Mr determination of post-translationally modified proteins. It is already known that specific side groups like carbohydrates, lipids, or other prosthetic groups can cause abnormal migration behaviors in SDS electrophoresis due to an irregular binding of SDS resulting in inaccurate estimates of the apparent Mr [1, 20–24]. Engel et al. analyzed proteins varying in their glycan moieties by microchip gel electrophoresis and found deviations in sizing proteins compared to SDS-PAGE [25]. Moreover, Wang et al. investigated various mammalian glycoproteins using CE-SDS and SDS-PAGE under reduced and nonreduced conditions and revealed substantial reduction in electrophoretic mobility under the capillary mode: while Mrs determined by SDS-PAGE were close to the theoretical values, the Mrs determined by CE-SDS appeared to be more than 10 kDa higher per glycan site in average [26].

In the present work, the apparent Mr shifts caused by glycosylation of proteins in SDS-PAGE and various CE-SDS instruments were investigated by analyzing several glycosylated proteins (ovalbumin, α-2-macroglobulin, Matuzumab, CD74, Erythropoietin (EPO), SynCAM1, *N*-Cadherin) before and after enzymatic deglycosylation. It includes an insight into the reasons that may explain the discrepancies found.

2 Materials and methods

2.1 Materials

2.1.1 Instrumentation

The CE-SDS systems Simple Western (Wes) and Maurice (both from ProteinSimple, a Bio-Techne Brand, San Jose, CA, USA), the gel electrophoresis system Mini-PROTEAN® Tetra System by Bio-Rad (Bio-Rad Laboratories GmbH, Feldkirchen, Germany), a Vilber Lourmat Peqlab FUSION SL gel documentation system 2012 (Vilber Lourmat Deutschland GmbH, Eberhardzell, Germany), and the LabChip® GXII Touch™ HT by PerkinElmer, Inc. (Waltham, MA, USA) were used.

2.1.2 Chemicals and reagents

Tris (ultrapure grade (>99.9%), Sigma-Aldrich Chemie GmbH, Steinheim, Germany) and SDS (Dodecylsulfate-Na-salt, electrophoresis grade, SERVA Electrophoresis GmbH, Heidelberg, Germany) were used for buffer preparation. As reducing agents, 14.2 M β-mercaptoethanol (β-ME, 99%, Carl Roth GmbH, Karlsruhe, Germany) and 400 mM DTT out of the Simple Western EZ Standard Pack (ProteinSimple, a Bio-Techne Brand) were used. For deglycosylation experiments, following enzymes were used: Peptide-*N*-glycosidase F (PNGase F) by Promega GmbH (Walldorf, Germany) and the Protein Deglycosylation Mix II (New England Biolabs, Ipswich, MA, USA). An additional reagent for deglycosylation was Tergitol™ solution type NP-40 (ω = 70% in H_2O) from Sigma-Aldrich (St. Louis, MO, USA). The ultrapure water used in all experiments was produced by an arium pro VF system (Sartorius AG, Göttingen, Germany). Amicon® Ultra 0.5 mL centrifugal filter units with an Ultracel® 10 K Membrane (Merck Millipore Ltd., Tullagreen, Ireland) were needed for protein sample concentration and buffer exchange.

For the SDS-PAGE, Bio-Safe™ Coomassie G-250 Stain, 10× tris/glycine/SDS buffer, 2× Laemmli Sample Buffer, Mini-PROTEAN® TGX™ Gels 7.5% 10-well, 30 μL and Mini-PROTEAN® TGX™ Gels 10% 10-well, 30 μL precast gels for use with tris/glycine buffers (all from Bio-Rad Laboratories GmbH) were used.

For performing CE-SDS experiments on the Maurice, the CE-SDS or the CE-SDS PLUS system was used in combination with the respective CE-SDS (PLUS) Size Application Kits (ProteinSimple, a Bio-Techne Brand) containing reagents and consumables. For more detailed information about the content of the kits, see Wiesner et al. or ProteinSimple's website [18, 27]. Regarding the kits, CE-SDS and CE-SDS PLUS differ from each other in CE-SDS PLUS using another cartridge as well as a different sample buffer. Maurice CE-SDS IgG Standard and Maurice CE-SDS Molecular Weight Markers were also obtained from ProteinSimple.

For performing Simple Western experiments on the Wes, the 12–230 kDa Wes Separation Module, containing 8 × 25 capillary cartridges, reagents, and consumables, was used. For more detailed information about the content of the kit, see Wiesner et al. or ProteinSimple's website [18, 28].

To perform experiments on the LabChip® GXII Touch™ HT, the ProteinEXact™ assay reagent kit and the ProteinEXact™ assay HT LabChip® were used [29].

2.1.3 Proteins

The following proteins were used in this study: carbonic anhydrase from bovine erythrocytes (29.0 kDa, SERVA Electrophoresis GmbH), albumin from chicken egg white (ovalbumin, lyophilized, 42.7 kDa, glycosylated: 44.3 kDa), BSA (66.0 kDa), and phosphorylase B from rabbit muscle (97.0 kDa) from Sigma-Aldrich Chemie GmbH. Additional proteins for deglycosylation experiments were: α-2-macroglobulin from human plasma (163.3 kDa, glycosylated: 179.0 kDa, Sigma-Aldrich Chemie GmbH), recombinant human *N*-Cadherin Fc Chimera (89.2 kDa, catalog number: 1388-NC, [30]), recombinant human CD74 (19.3 kDa, catalog number: 3590-CD, [31]), recombinant human EPO (ultrapure, 21 kDa, catalog number: 286-EP, [32]), and recombinant human IGSF4A/SynCAM1 (38.4 kDa, catalog number: 3519-S4, [33]), all from R&D Systems, Inc., a Bio-Techne Brand (Minneapolis, MN, USA) and Matuzumab (Patent WO 2009/04 3490 A1 [34], light chain 23.63 kDa and heavy chain 49.66 kDa), provided by Merck KGaA (Darmstadt, Germany) as a 10 mg/mL stock solution.

2.2 Methods

2.2.1 General procedure for sample preparation and deglycosylation

For precision and repeatability experiments, the protein stock solutions were prepared by dissolving an appropriate amount of each protein mentioned in Section 2.1.3 in a 100 mM tris buffer (pH 8.0) containing 1% SDS to achieve a concentration of 1 mg/mL. While single protein samples were used for the precision measurements, mixtures of the four investigated proteins were utilized for the repeatability experiments. Repeatability experiments were conducted by measuring one single protein mix about 60 times. For precision, ten samples were all prepared independently. For more detailed information about the individual sample preparations, see the respective chapter of the instrument (2.2.2–2.2.5).

For deglycosylation experiments, ovalbumin and α-2-macroglobulin were dissolved according to the procedure for the precision and repeatability experiments, but to a concentration of 4 mg/mL. The Matuzumab stock solution was diluted with 100 mM tris buffer (pH 8.0) containing 1% SDS to reach this concentration as well. A higher starting concentration of protein is required because the deglycosylation reaction requires subsequent dilution steps which otherwise would lead to very low final concentrations. Due to this fact, it was necessary to concentrate the proteins *N*-Cadherin, CD74, EPO, and SynCAM1 (concentrations at hand were 0.315, 0.623, 1.33, and 0.462 mg/mL) by using Amicon® Ultra 10K centrifugal filter units. The concentrates were replenished with the above-mentioned buffer to a concentration of 3 mg/mL.

The deglycosylation of ovalbumin, α-2-macroglobulin, and Matuzumab with PNGase F was conducted based on the enzyme manufacturer's protocol. Briefly, to 10 μL of each stock solution ($\rho = 4$ mg/mL), 1 μL 14.2 M β-ME was added, and the sample was denatured by heat at 95°C for 5 min. After cooling for 5 min, 5 μL of 100 mM tris buffer (pH 8), 2 μL of NP-40 ($\omega = 10\%$), and 2 μL of PNGase F (respective amount of water added in case of nondeglycosylated controls) were added, resulting in a protein concentration of 2 mg/mL. Incubation was performed at 37°C for 3 h.

Deglycosylation of *N*-Cadherin, CD74, EPO, and SynCAM1 with the Deglycosylation Mix II was conducted based on the manufacturer's protocol (New England Biolabs). First, 40 μL of each stock solution ($\rho = 3$ mg/mL) was mixed with 6 μL Deglycosylation Mix Buffer 2 and denatured by heat at 95°C for 5 min. After cooling for 5 min, 6 μL of Deglycosylation Mix II (or water for nondeglycosylated controls) were added, resulting in a protein concentration of 2.31 mg/mL. Incubation was performed at 25°C for 30 min in the first step and at 37°C for 24 h in the second step.

2.2.2 SDS-PAGE (Bio-Rad)

Sample preparation was performed by diluting the stock solution 1+1 with Laemmli sample buffer, addition of the Maurice CE-SDS 25× Internal Standard (10 kDa) and a reduction and denaturation step in the presence of β-ME (710 mM), while heating to 95°C for 5 min. The Maurice CE-SDS Molecular Weight Markers were used to calculate the Mr. For the precision measurements, the final protein concentration was 0.5 mg/mL each, while the concentration of each protein in the repeatability measurements was 0.125 mg/mL. Loading quantities onto the gel were 10 μL per sample or 7.5 μL of the Maurice CE-SDS Molecular Weight Markers respectively (due to the unknown concentration, no information can be provided regarding the protein amount). The final protein concentration in the sample for the deglycosylation experiments of ovalbumin, α-2-macroglobulin, and Matuzumab was 1 mg/mL, while it was 1.155 mg/mL for *N*-Cadherin, CD74, EPO, and SynCAM1. Loading quantities onto the gel were 5 μg per protein and 7.5 μL of the Maurice CE-SDS Molecular Weight Markers. SDS-PAGE experiments were carried out using 10% (for Mrs < 100 kDa) and 7.5% (for Mrs > 100 kDa) polyacrylamide gels, whereby precast gels by Bio-Rad were used to ensure reproducibility. The electrophoresis itself, carried out according to the Laemmli procedure [19], and the subsequent calculation of Mrs have been described in detail in the previous work [18]. To briefly summarize: SDS-PAGEs were performed on a Mini-PROTEAN® Tetra System by Bio-Rad in a tris/glycine/SDS running buffer (25 mM tris, 192 mM glycine, 0.1% SDS, pH 8.3) while applying a voltage of 200 V (29.9 V/cm), resulting in a current of about 50 mA. After completion of the electrophoresis, the gels were washed with deionized water, subsequently stained with Bio-Safe™ Coomassie G-250 Stain for at least 2 h and destained with deionized water overnight. Transmitted light photos were taken for documentation using an imager (Vilber Lourmat Peqlab

FUSION SL gel documentation system 2012) connected to the program Infinity by Vilber Lourmat (version 15.06). These were evaluated using the image processing program ImageJ 1.52a (Wayne Rasband, National Institutes of Health, Bethesda, MD, USA) which works with grayscale analysis. The Maurice CE-SDS 25× Internal Standard (10 kDa) added to every sample, was used to calculate relative migration distances, which in turn are used for Mr calculation.

2.2.3 CE-SDS and CE-SDS PLUS (Maurice by ProteinSimple)

The sample preparations and experiments were performed with the respective kits and according to the manufacturer's protocols [35, 36], which mainly contain a dilution step of the stock solution with sample buffer, an addition of the Maurice CE-SDS 25× Internal Standard (10 kDa), and a reduction and denaturation step with β-ME (710 mM), while heating to 95°C for 5 min. For the precision measurements, the final protein concentration was 0.5 mg/mL each, while the concentration of each protein in the repeatability measurements was 0.125 mg/mL. The final protein concentration in the sample for the deglycosylation experiments of ovalbumin, α-2-macroglobulin, and Matuzumab was 1 mg/mL, while it was 1.155 mg/mL for *N*-Cadherin, CD74, EPO, and SynCAM1.

The cartridges used contain a capillary with an effective length of 15 cm and an inner diameter of 50 μm. The sample injections were conducted electrokinetically for 20 s at 4600 V. A reduced IgG (included in the kit) was used as system suitability test (SST) at the beginning and end of each sequence. Regarding the precision and repeatability experiments, the Maurice CE-SDS Molecular Weight Markers and the protein samples with Mrs of more than 70 kDa were separated for 35 min at 5750 V, while the reduced IgG and protein samples with Mrs of less than 70 kDa were separated for 25 min at the same applied voltage. All protein samples of the deglycosylation experiments were separated for 40 min at 5750 V. Detection was done UV-metrically at a wavelength of 220 nm. Data were analyzed using Compass for iCE 2.1.0.

2.2.4 Simple Western (Wes by ProteinSimple)

The sample preparations and experiments were performed with the respective kit and according to the manufacturer's protocol [37]. For the precision measurements, the final protein concentration was 0.2 mg/mL each, while the concentration of each protein in the repeatability measurements was 0.05 mg/mL. The experiments were conducted under reducing conditions (40 mM DTT). The final protein concentration in the sample for the deglycosylation experiments of ovalbumin, α-2-macroglobulin, and Matuzumab was 0.75 mg/mL, while it was 0.8663 mg/mL for *N*-Cadherin, CD74, EPO, and SynCAM1. Separation took place at 375 V for 25 min. Afterwards, the proteins were immobilized on the capillary wall, covalently labelled with biotin for 30 min, washed, and incubated for 30 min with Streptavidin Horseradish peroxidase conjugate followed by chemiluminescence detection. Evaluation was conducted by Compass for SW 4.1.0.

2.2.5 Microchip CE-SDS (LabChip® GXII Touch™ HT by PerkinElmer)

The ProteinEXact™ assay was used and the sample preparations and experiments were performed according to the manufacturer's protocol [29]. For the precision measurements, the final protein concentration was 0.05 mg/mL each, while the concentration of each protein in the repeatability measurements was 0.0125 mg/mL. All experiments were conducted under reducing conditions (161 mM β-ME). The final protein concentration in the sample for the deglycosylation experiments of ovalbumin, α-2-macroglobulin, and Matuzumab was 0.1 mg/mL, while it was 0.1155 mg/mL for *N*-Cadherin, CD74, EPO, and SynCAM1. The samples were separated for 65 s and detected by fluorescence. Afterwards, the data were analyzed using the LabChip® GX Reviewer by PerkinElmer (software version 5.5.2312.0).

3 Results and discussion

3.1 Precision

To compare the methods described in Section 2.2, ten repeat measurements were conducted with independent sample preparations of the four investigated proteins to calculate the precision afterwards. The precision results for the instruments regarding RSDs are all <3.1% which can be seen from Table 1. Remarkably low are the RSDs on the LabChip® in combination with the ProteinEXact™ assay, which are ≤0.6% for all four examined proteins. The CE-SDS PLUS system on the Maurice also produced high precision, where all RSDs are <1.6%. The CE-SDS PLUS shows improvements over the original CE-SDS system for all four proteins, where RSDs previously ranged from 1.0 to 3.1%. Overall, CE-SDS and SDS-PAGE are similar in their precision in the conducted experiments. Additionally, the RSDs for BSA on SDS-PAGE and CE-SDS are slightly higher than for the other proteins. This could be due to the fact that BSA can be present in several isoforms [38]. This heterogeneity leads to band/peak broadening resulting in more imprecise calculations of the Mr. This kind of broadening has been observed for BSA in CZE and described by Dolnik and Gurske in 2011 [39]. An influence of the separation matrix on the separation efficiency was described by Karim et al. [40]. This might also explain why some observed effects are not observed across all examined instruments. Specifically, the two CE-SDS methods (CE-SDS and CE-SDS PLUS) tend to show slightly higher deviations for larger proteins, while the effect on the Wes seems to be exactly the opposite.

It is important to note that these data do not provide information about the trueness of the results, as this was

Table 1. The precision experiment's results of the proteins measured via SDS-PAGE, Maurice CE-SDS, Maurice CE-SDS PLUS, Wes, and PerkinElmer LabChip® (ProteinEXact™ assay); shown are the respective mean calculated Mrs ($n = 10$) for each protein; reference Mrs: 29.0 kDa for carbonic anhydrase, 44.3 kDa for ovalbumin, 66.0 kDa for BSA, and 97.0 kDa for phosphorylase B

	SDS-PAGE		CE-SDS		CE-SDS PLUS		Wes		LabChip®	
	Mean (kDa)	RSD (%)	Mean (kDa)	RSD (%)	Mean (kDa)	RSD (%)	Mean (kDa)	RSD (%)	Mean (kDa)	RSD (%)
Carbonic anhydrase	28	1.6	32	1.0	32	0.0	37	1.1	28	0.6
Ovalbumin	45	1.7	45	1.1	46	1.1	49	2.0	45	0.4
BSA	68	3.0	68	3.1	68	1.1	63	1.0	77	0.5
Phosphorylase B	99	1.7	102	2.6	104	1.6	102	0.7	105	0.2

Table 2. The repeatability experimental results of the proteins measured via SDS-PAGE, Maurice CE-SDS, Maurice CE-SDS PLUS, Wes, and PerkinElmer LabChip® (ProteinEXact™ assay); reference Mrs: 29.0 kDa for carbonic anhydrase, 44.3 kDa for ovalbumin, 66.0 kDa for BSA, and 97.0 kDa for phosphorylase B

	SDS-PAGE		CE-SDS		CE-SDS PLUS		Wes		LabChip®	
	Mean (kDa)	RSD (%)	Mean (kDa)	RSD (%)	Mean (kDa)	RSD (%)	Mean (kDa)	RSD (%)	Mean (kDa)	RSD (%)
Carbonic anhydrase	30	1.5	31	1.2	31	1.5	36	1.0	29	0.8
Ovalbumin	46	1.7	45	1.6	46	1.1	48	1.2	46	0.5
BSA	72	1.7	68	1.9	69	0.7	63	0.6	77	0.6
Phosphorylase B	101	1.7	102	2.3	105	1.8	99	1.1	105	0.4

determined in the previous work [18]. For example, both carbonic anhydrase (on Simple Western) and BSA (on LabChip®), exhibit larger deviations in apparent Mr compared to the reference molecular mass (r-Mr) even though the precision is more than acceptable.

3.2 Repeatability

In addition to the precision investigated in Section 3.1 when testing samples from independent preparations, it was also investigated how repeatable the result of one and the same sample is when measuring it several times. Concerning repeatability (Table 2), the results are similar to those in Section 3.1. The RSDs on SDS-PAGE for all four proteins range between 1.5 and 1.7%. As already similarly observed in the precision experiments, the RSDs received with CE-SDS increase with higher Mrs. This effect was not seen on the CE-SDS PLUS system. Again, lowest RSDs are obtained with the LabChip® ranging between 0.4 and 0.8%, which overlaps with Simple Western (RSDs 0.61.2%).

Additional effects become apparent when looking at the control charts in Fig. 1. The first observation is the wavy course of the measurements on the SDS-PAGE (Fig. 1A). Seen from left to right, there are always nine points belonging to one gel (protein mix loaded to nine lanes while the Maurice CE-SDS Molecular Weight Markers were loaded to one of the middle lanes). Thus, when looking at the course of a gel from left to right, it is noticeable that the measuring points obtained in the middle of the gel, especially directly next to the lane with the Maurice CE-SDS Molecular Weight Markers, tend to result in higher Mrs than the values in other lanes further to the edges. This effect can be observed in nearly the same way for all proteins, sometimes more or less pronounced. There is a suspicion concerning the reason for this effect: the sample of the Maurice CE-SDS Molecular Weight Markers in the middle of the gel is of lower ionic strength than the other protein samples and, thus, of lower conductivity. When starting the electrophoresis by applying voltage to the gel, the differing conductivities would lead to an unequally distributed resulting current. Related to this effect, the temperature development throughout the gel is expected to be unequal as well. These effects cause the running distances to be different. In lanes with lower ionic strength, the conductivity, the resulting current, and the temperature is lower and samples in these lanes will migrate slightly slower than in lanes with samples of higher ionic strength. An example of a gel making this effect visible is shown in Fig. S1 of the Supporting information. In this context, it is important to mention that such effects are usually only noticeable macroscopically if one and the same sample is applied several times to a gel. Similar effects are also shown by See et al. who investigated the effects of different salt concentrations on Mr determination in SDS-PAGE [41].

The second effect can be observed in Fig. 1B in the control charts of the measurements on CE-SDS. The experiments were conducted in two batches of 30 repeats each with fresh reagents. Two batches were necessary because only 48 injections are possible in one batch. At the beginning of each batch, the calculated Mrs are higher and seem to get closer to a minimum asymptotically with each run. This effect can be observed for all proteins. A lower calculated Mr is a

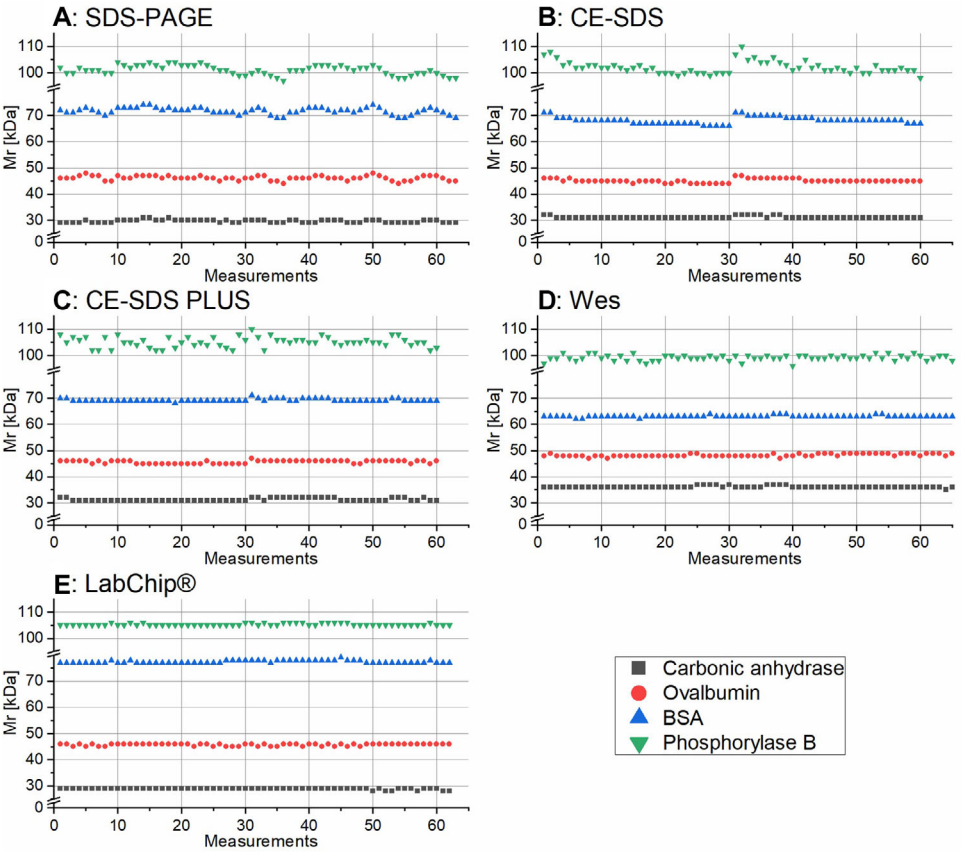

Figure 1. Control charts of the repeatability results. All single measurement values of the four examined proteins phosphorylase B, BSA, ovalbumin, and carbonic anhydrase are plotted according to their calculated Mr. (A) results obtained by SDS-PAGE (Bio-Rad, repetitions = 63); (B) results obtained by Maurice CE-SDS (repetitions = 60); (C) results obtained by Maurice CE-SDS PLUS (repetitions = 60); (D) results obtained by Wes (repetitions = 66); (E) results obtained by the PerkinElmer LabChip® GXII Touch™ HT (ProteinEXact™ assay, repetitions = 62).

result of a shorter migration time. One reason for this might be temperature changes. An increase in temperature leads to lower viscosities of liquids, in this case, for example, of the separation matrix. The effect of temperature and viscosity on sieving media in capillary gel electrophoresis was already described in 1996 by Nakatani et al. [6]. It would be conceivable that the temperature of the capillary as well as of the instrument's interior is not yet constant at the beginning of a new batch and only settles at a temperature over time. This would lead to the separation matrix experiencing viscosity changes which in turn lead to differences in migration. In this context, it is critical to consider that the SST and Maurice CE-SDS Molecular Weight Markers are running at the beginning of a batch. According to the assumption that the test parameters are not yet constant at this point, it might be suboptimal to run the markers, which represent the calculation basis for all subsequent measurements, if fluctuations are still present. It remains to be noted that such systematic effects usually become visible only when a series of consecutive measurements of the same sample is evaluated. However, on CE-SDS PLUS the effect is much less pronounced (Fig. 1C). As the CE-SDS and CE-SDS PLUS platforms on Maurice differ in the sample buffer, the cartridge, and software, it would be reasonable to assume that these differences result in this improvement. Regarding the measurements on Wes and on the LabChip®, no special observations could be made in terms of any abnormalities (Fig. 1D and E). While these observations are intriguing, the overall apparent Mr RSD across all platforms is ≤2.3%.

3.3 Apparent molecular mass shifts by glycosylation

3.3.1 Measured differences between various approaches

To investigate whether (and if so to what extent) a possible glycosylation of a protein has an influence on the Mr determination using different methods, seven proteins were measured in their glycosylated and deglycosylated state. The corresponding results are shown in Table 3. The respective RSDs of the individual experiments can be found in Table S1 of the Supporting information.

In some cases, there are striking differences in Mr determination, both between the glycosylated/deglycosylated variants and between the methods or instruments used. In most cases, the Mr is rather over- than underestimated compared to the r-Mr. The lowest apparent Mr differences are observed for ovalbumin, where the calculated Mrs of the glycosylated ovalbumin show quite similar values between 43 and 46 kDa across all instruments (r-Mr for glycosylated ovalbumin with 44.3 kDa). There is a decrease in the calculated Mr after deglycosylation with PNGase F, with CE-SDS showing the lowest value with 33 kDa and SDS-PAGE the

Table 3. Results of the deglycosylation experiments on CE-SDS and CE-SDS PLUS (Maurice, ProteinSimple), SDS-PAGE (Bio-Rad), Simple Western (Wes, ProteinSimple), LabChip® GXII Touch™ HT (ProteinEXact™ assay, PerkinElmer); shown are the respective mean calculated Mrs ($n = 3$) for each of the seven proteins in their glycosylated (glyc) and deglycosylated (deglyc) state, for the origin of the r-Mr data see Section 2.1.3

		Mr (kDa)					
		CE-SDS	CE-SDS PLUS	SDS-PAGE	Wes	LabChip®	r-Mr (kDa)
Ovalbumin	glyc	43	44	45	45	46	44.3
	deglyc	33	35	42	39	41	42.7
α-2-macroglobulin	glyc	245	241	144	132	221	179
	deglyc	165	164	136	111	180	163.3
Matuzumab light chain	glyc	25	26	27	31	27	23.63
	deglyc	23	26	27	30	27	
Matuzumab heavy chain	glyc	63	67	57	56	68	49.66
	deglyc	53	57	53	51	61	
CD74	glyc	81	82	34	48	63	
	deglyc	34	35	23	31	32	19.3
EPO	glyc	97	101	40	56	74	
	deglyc	21	18	20	27	17	21
SynCAM1	glyc	343	345	74	123	194	
	deglyc	62	59	50	54	65	38.4
N-Cadherin	glyc	262	253	117	121	195	
				101			
	deglyc	134	127	108	99	164	89.2
		108	103	94	82	143	

highest one with 42 kDa. The r-Mr calculated from the amino acid (AA) sequence for ovalbumin without glycosylation is 42.7 kDa.

α-2-Macroglobulin, on the contrary, shows more distinct differences. For example, when the glycosylated protein is measured by CE-SDS, CE-SDS PLUS, and LabChip®, the values range from 221 to 245 kDa, whereas values of 144 and 132 kDa are obtained on SDS-PAGE and Wes, respectively. Thus, absolute differences of approximately 100 kDa between methods occur. If α-2-macroglobulin is deglycosylated and measured again, a significant reduction in Mr is seen, in some cases by up to 80 kDa (CE-SDS). Since each glycosylated glycan site is assumed to add 2.5 kDa to the Mr of the protein in average, this is much more than can be explained by the mass of the sugar chains [42, 43]. It can be assumed that the Mrs of the glycosylated proteins are sometimes significantly overestimated by CE-SDS-based methods (effect appears less pronounced when using Simple Western). After deglycosylation of α-2-macroglobulin, the Mrs determined using CE-SDS and CE-SDS PLUS are very close to the r-Mr of 163.3 kDa at 165 and 164 kDa, respectively.

Antibodies are well known to carry significant glycosylation. Therefore, an antibody (Matuzumab) was also studied. After reduction with β-ME, it is present separately in light and heavy chains. Values between 25 and 31 kDa were measured for the light chain before deglycosylation, with the r-Mr being 23.63 kDa. Since the light chain is not glycosylated, the calculated values with and without PNGase F treatment are nearly identical on all instruments. The heavy chain, on the other hand, undergoes glycosylation. Glycosylated Mrs between 56 kDa (Wes) and 68 kDa (LabChip®) were obtained. On CE-SDS and CE-SDS PLUS, deglycosylation results in a reduction of Mr by 10 kDa, while on SDS-PAGE, Wes, and LabChip® it is somewhat lower with 4, 5, and 7 kDa, respectively.

The proteins discussed in the following, namely CD74, SynCAM1, and *N*-Cadherin, are membrane proteins, whereas EPO is a hormone. Examination of these proteins revealed even greater discrepancies in some cases than for α-2-macroglobulin. Measured values for glycosylated CD74 range from 34 kDa on SDS-PAGE to 82 kDa on CE-SDS PLUS. After deglycosylation according to the procedure in Section 2.2.1, the Mrs calculated using the four CE-SDS-based methods are all close to each other (31–35 kDa), only the SDS-PAGE value is slightly lower at 23 kDa, while the r-Mr is 19.3 kDa. Exemplary electropherograms of the deglycosylation experiments of CD74 are shown in Fig. S2 of the Supporting information. Examination of EPO revealed Mrs between 40 and 101 kDa for the glycosylated form, while Mrs after deglycosylation are between 18 and 27 kDa. The SDS-PAGE and CE-SDS values, at 20 and 21 kDa, respectively, are closest to the r-Mr of 21 kDa.

There were clear differences between the methods when measuring glycosylated SynCAM1. While SDS-PAGE yields a Mr of 74 kDa, the values obtained with CE-SDS-based methods are much higher. For example, Wes shows a Mr of 123 kDa, LabChip® of 194 kDa, and CE-SDS (PLUS) Mrs of above 340 kDa. The calculated Mrs after deglycosylation are in a similar range of 50–65 kDa (r-Mr = 38.4 kDa) for all methods. This provides clear evidence that glycosylation of the protein has a significant effect on Mr determination, to varying degrees depending on the method used.

Finally, *N*-Cadherin, which, along with Matuzumab (heavy chain), CD74 and SynCAM1, is a protein where Mrs, both glycosylated and deglycosylated, tend to be overestimated by all methods examined. The appearance of two bands or peaks of *N*-Cadherin can be explained by immature (nonspliced) and mature *N*-Cadherin [44]. When considering absolute figures, the differences between SDS-PAGE and CE-SDS (PLUS) are highest when measuring the glycosylated proteins SynCAM1 and *N*-Cadherin.

Taken together, glycosylation has a tremendous influence on the migration behavior when size-related separations, such as SDS-PAGE and CE-SDS, are performed.

3.3.2 Effect of sialic acid

After thorough literature research, several possible reasons arise that may explain the above-mentioned phenomena. Assigning a single reason to each protein seems difficult. Rather, one might consider it as an interplay of several factors that have differing effects on the individual methods.

It can also be noted that anomalous migration behavior, specifically of membrane proteins, was already described by Rath et al. in 2009 [45]. As mentioned above, CD74, SynCAM1, and *N*-Cadherin are membrane proteins. Looking at the similarities shared by SynCAM1 and *N*-Cadherin, it is striking that both are cell adhesion proteins, and both were derived from an NS0 cell line. In contrast, EPO and CD74 are derived from CHO cells. Zhang et al. found, using the example of EPO, that sialylation is cell type specific and they postulate that there is less sialic acid bound to NS0-derived proteins than to CHO-derived ones [46]. Sialic acids are deprotonated under the conditions electrophoresis takes place and, thus, contribute to increased negative charge of the protein. On the one hand, the glycans on the protein might prevent complete unfolding and on the other hand, they bind SDS less effectively, often only 0.2 mg/mg glycan [47]. Thus, due to the glycans, the apparent Mr would be higher. However, if sialic acids are present on the glycan, their charge can partially compensate for the fact that less SDS binds. Evidence that sialic acids contribute to electrophoretic mobility can be found in Ref. [48]. Segrest et al. performed SDS-PAGE with sialylated proteins and found that the migration speed decreased, and the apparent Mr increased accordingly after their removal. Fittingly, Karger et al. described that glycoproteins do not conform to the predicted migration behavior both because of the sialic acids and the carbohydrates themselves [49]. Wang et al. deny an influence of sialic acids on protein mobility, but their data only allowed preliminary conclusions [26]. However, if the observed effects were solely a matter of abnormal binding behavior of SDS or sialylation, they would be expected to be similar in magnitude on SDS-PAGE and the CE-SDS-based methods. Since this is not the case, the influence of other factors causing the differences between the methods must be assumed.

The effect of glycosylation is much more pronounced if no sialic acid is included in the sugar chains. Since the degree of sialylation strongly depends on the producing organisms, so does the effect on migration time shifts of proteins produced in these organisms.

3.3.3 Relevance of carbohydrate-carbohydrate interactions

Discrepancies between the CE-SDS-based methods might occur since the methods are based on different compositions of the separation matrices. Here, the fact that SynCAM1 and *N*-Cadherin are cell adhesion proteins comes into play again. Bucior et al. found that cell-cell recognition takes place with the help of the carbohydrates of their cell adhesion proteins, that is, carbohydrate-carbohydrate interactions occur [50]. They found that these glycan interactions can be as strong as antibody-antigen interactions. If one assumes that the separation matrix of a method possibly consists of a carbohydrate, for example, dextran or pullulan (see Section 1, Introduction), it is conceivable that an interaction between the glycan(s) of the protein and the separation matrix may occur. To stay with the example of dextran: interactions between dextran and some proteins were described as early as in 1960 [51]. In addition, some (murine) myeloma proteins appear to show affinities to dextran [52, 53]. An interaction would reduce the migration speed of the proteins concerned and would also explain why the effects can be observed to different extents when comparing the methods. Nonspecific interactions between matrix and (glyco)proteins are also conceivable for separation matrices that are not based on carbohydrates. Since the compositions of the CE-SDS separation matrices used are unknown, further evaluation of these assumptions is not possible but the fact that an interaction between glycoprotein and separation matrix has to be considered has already been addressed by Wang et al. [26].

Some proteins are made to interact strongly with their sugar chains, for example, cell adhesion proteins, such as SynCAM1 and *N*-Cadherin, used in this work. If such an interaction is known or can be assumed, different interactions depending on the gel must also be expected using electrophoretic SDS-based separations by size. Stronger interactions of some proteins will cause a chromatography-like retention and longer migration times, which will be interpreted as an apparently higher Mr. In these cases, the relative Mrs of protein derivatives of the same kind can still be estimated, assuming a similar degree of glycosylation.

3.3.4 Importance of *N*-glycan sites

What could also have an influence on the strength of the observed effect is the number of *N*-glycan sites present. This correlation can be seen in Table 4, which shows the number of predicted glycan sites of the proteins. The *N*-glycan sites should be considered, since *N*-glycans are generally larger than *O*-glycans and, therefore, potentially have a greater influence.

Table 4. Compilation of some of the properties of the proteins studied in the deglycosylation experiments including the isoelectric point (pI), grand average of hydropathicity (GRAVY), proline content, percentage of negative (Asp + Glu) and positive (Arg + Lys) charges in relation to the total number of AAs and the number of *N*- and *O*-glycan sites

	pI	GRAVY	Content proline [%]	Neg. charges [%]	Pos. charges [%]	*N*-glycan sites	O-glycan sites
Ovalbumin	5.19	–0.001	3.6	12.2	9.1	1	0
α-2-macroglobulin	6.03	–0.195	5.3	10.7	9.2	8	0
Matuzumab light chain	6.34	–0.417	4.7	9.0	8.5	N/A	N/A
Matuzumab heavy chain	8.34	–0.552	7.6	9.4	10.3	N/A	N/A
CD74	6.65	–0.654	11.8	11.2	10.7	2	1
EPO	8.30	0.027	5.7	9.8	10.9	3	1
SynCAM1	5.14	–0.430	6.1	12.8	8.2	6	0
N-Cadherin	5.16	–0.405	9.0	11.8	8.4	8	0

The values are taken from a calculation using the ProtParam tool by ExPASy [58], except for the glycan sites, which were taken from the NCBI [59] using the following accession numbers: P01012 (ovalbumin), P01023 (α-2-macroglobulin), NP_0 04346 (CD74), P01588 (EPO), Q9BY67 (SynCAM1), and P19022.4 + P01857.1 (*N*-Cadherin construct); for the origin of the r-Mr data see Section 2.1.3

It is noticeable that α-2-macroglobulin, SynCAM1, and *N*-Cadherin have significantly more *N*-glycan sites than the other proteins. Consequently, the previously described effects would be expected to be stronger if these sites are occupied with glycans. This is consistent with the results in Table 3, where the highest discrepancies are found for these three proteins, as already mentioned above. *N*-Glycan sites show a particularly strong effect.

3.3.5 Influences on SDS-binding properties

What is noticeable as well is that there are also differences in terms of Mr determination after deglycosylation. For Matuzumab, CD74, SynCAM1, and *N*-Cadherin, the Mr after deglycosylation is still overestimated while for the other three proteins it tends to be underestimated. A look at Table 4 also provides an explanation for this phenomenon. Ovalbumin, α-2-macroglobulin and EPO have a higher GRAVY, that is, they are more hydrophobic in nature whereas CD74, SynCAM1, and *N*-Cadherin have a lower GRAVY and are, therefore, more hydrophilic. Shirai et al. found that differences between the predicted and the apparent Mr can occur because of the GRAVY score [54]. Since SDS binding occurs preferentially on hydrophobic parts of the protein, those with a low GRAVY tend to bind less SDS, which is why their electrophoretic mobility decreases and their Mr appears higher. According to this, especially proteins with a higher GRAVY have a higher mobility, which is why the apparent Mr tends to become smaller. Shirai et al. also showed that the isoelectric point of the protein can affect the electrophoretic mobility. This confirms what Guan et al. postulate, namely that proteins with many charges, possibly leading to charge repulsion with SDS, can lead to abnormal migration behavior in electrophoresis [55].

The proline content of a protein should also be considered as a reason for higher apparent Mrs. The presence of proline in a protein, due to the special heterocyclic structure, can lead to "disturbances," in form of kinks in the secondary structure, because the cyclic structure in the proline molecule prevents rotation of the C-N bond. This in turn leads to the protein being unable to be completely stretched after reduction and SDS-binding, which results in an increase of the Stokes radius. Such an effect has already been observed with the proline-rich tumor suppressor protein p53 (proline content: >11%), which has even been named according to its unexpected apparent Mr [56, 57]. It is conceivable that this effect might be also of importance for CD74 (proline content: 11.8%).

All in all, however, all these protein properties must be considered in conjunction with each other to explain their migration behavior in electrophoresis. Hydrophobicity, which can be characterized by the GRAVY score, influences SDS binding and can cause various SDS loads on proteins of the same size. The same applies to the acid/base properties and pI: native protein charges are not ideally equalized by SDS binding. Moreover, proline-rich proteins show particular shapes, which can also mean individual SDS binding properties.

4 Concluding remarks

In the present work, the quality control attributes precision and repeatability were investigated using four model proteins in different SDS-electrophoresis systems. It was shown that the precision and repeatability of CE-SDS-based methods are similar to those of SDS-PAGE.

Glycosylations can have a tremendous effect on Mr determination, with discrepancies to the r-Mr generally increasing with an increase in the number of glycan sites present. The effect of glycosylation is much more pronounced if no sialic acid is included in the sugar chains. *N*-Glycan sites show a particularly strong effect. After deglycosylation, these differences between measured and theoretical Mr are only moderate. They can arise due to increased hydrophilicity or hydrophobicity (GRAVY), high or low pI values associated with

an increased number of charges in the protein or a high percentage of proline.

Some proteins naturally interact strongly with sugar chains, for example, cell adhesion proteins, such as SynCAM1 and *N*-Cadherin, used in this work. If such an interaction is known or can be assumed, different interactions depending on the gel must also be expected using electrophoretic SDS-based separations by size. Stronger interactions of some proteins will cause a chromatography-like retention and longer migration times, which will be interpreted as an apparently higher Mr. These effects can be mostly understood and, therefore, fairly predicted and interpreted.

These effects depend on the separation matrices and the presence of glycosylation on the protein. Therefore, the observed effects are not the same for all instruments and methods. In all cases, the relative Mrs of protein derivatives of the same kind can be estimated, assuming a similar degree of glycosylation.

It remains to join Wang et al. in stating that these aspects are worth for further investigations [26]. The determined Mr depends to a large extent on the properties of the protein and not solely on the used approach. This is also the reason why no general statement can be made about which method and instrument is best. The choice of method must be adapted to the proteins as well as to the needs of the user. Kahle et al. provide a comparative overview of various CE-SDS instruments, both in terms of parameters, such as resolution, linearity, sensitivity, as well as in terms of ease of use, flexibility, etc., which could be helpful in making a good choice [8].

We would like to offer our special thanks to ProteinSimple, a Bio-Techne Brand, for the provision of the Maurice and Wes as well as the respective reagents. In this context, we are particularly grateful for the advices and support given by Udo Burger, Susanne Doerks, and Chris Heger. We would also like to express our appreciation to R&D Systems, Inc., a Bio-Techne Brand, for providing some of the proteins that were studied. Another special thank goes to PerkinElmer, Inc., for providing the LabChip® GXII Touch™ HT and the respective LabChip®. Thanks go to the Institute of Pharmaceutical Biology of the Technische Universität Braunschweig for the provision of the imager and to the working group of Prof. Ott of the Institute of Medicinal and Pharmaceutical Chemistry of the Technische Universität Braunschweig for the loan of the SDS-PAGE system of Bio-Rad. Furthermore, we would like to thank the state Lower Saxony for providing the fellowship for Rebecca Wiesner. Finally, we wish to acknowledge the help and assistance with the experiments by Kristina Grove-Heike, Nordilyn Lorenz and Lena Pohl.

Hermann Wätzig likes to mention, that he stands in close and very friendly contact to ProteinSimple for a long time.

Data availability statement

The data that support the findings of this study are available from the corresponding author upon reasonable request.

5 References

[1] Lottspeich, F., Engels, J. W. (Eds.), *Bioanalytik*, Springer Spektrum, Berlin 2012.

[2] Guttman, A., *Electrophoresis* 1995, *16*, 611–616.

[3] Bean, S. R., Lookhart, G. L., *J. Agric. Food Chem.* 1999, *47*, 4246–4255.

[4] Chung, M., Kim, D., Herr, A. E., *Analyst* 2014, *139*, 5635–5654.

[5] Ganzler, K., Greve, K. S., Cohen, A. S., Karger, B. L., Guttman, A., Cooke, N. C., *Anal. Chem.* 1992, *64*, 2665–2671.

[6] Nakatani, M., Shibukawa, A., Nakagawa, T., *Electrophoresis* 1996, *17*, 1210–1213.

[7] Zilberstein, G., Korol, L., Antonioli, P., Righetti, P. G., Bukshpan, S., *Anal. Chem.* 2007, *79*, 821–827.

[8] Kahle, J., Maul, K. J., Wätzig, H., *Electrophoresis* 2018, *39*, 311–325.

[9] El Deeb, S., Wätzig, H., Abd El-Hady, D., Sänger-van de Griend, C., Scriba, G. K. E., *Electrophoresis* 2016, *37*, 1591–1608.

[10] Rustandi, R. R., Washabaugh, M. W., Wang, Y., *Electrophoresis* 2008, *29*, 3612–3620.

[11] Sänger-van de Griend, C. E., *Electrophoresis* 2019, *40*, 2361–2374.

[12] Tamizi, E., Jouyban, A., *Electrophoresis* 2015, *36*, 831–858.

[13] Lechner, A., Giorgetti, J., Gahoual, R., Beck, A., Leize-Wagner, E., François, Y.-N., *J. Chromatogr. B* 2019, *1122–1123*, 1–17.

[14] Felten, C., Salas-Solano, O., *Quality Control Application for Therapeutic Proteins*, Beckman Coulter Life Sciences, Indianapolis, IN 2016.

[15] Zhang, L., Fei, M., Tian, Y., Li, S., Zhu, X., Wang, L., Xu, Y., Xie, M. H., *J. Pharm. Biomed. Anal.* 2020, *190*, 113527.

[16] Wagner, E., Colas, O., Chenu, S., Goyon, A., Murisier, A., Cianferani, S., François, Y., Fekete, S., Guillarme, D., D'Atri, V., Beck, A., *J. Pharm. Biomed. Anal.* 2020, *184*, 113166.

[17] Salas-Solano, O., Tomlinson, B., Du, S., Parker, M., Strahan, A., Ma, S., *Anal. Chem.* 2006, *78*, 6583–6594.

[18] Wiesner, R., Scheller, C., Krebs, F., Wätzig, H., Oltmann-Norden, I., *Electrophoresis* 2021, *42*, 206–218.

[19] Laemmli, U. K., *Nature* 1970, *227*, 680–685.

[20] Hames, B. D., Rickwood, D. (Eds.), *Gel electrophoresis of proteins: A practical approach*, IRL Press, Oxford 1990.

[21] Bryan, J., *J. Muscle Res. Cell. Motil.* 1989, *10*, 95–96.

[22] Poduslo, J. F., *Anal. Biochem.* 1981, *114*, 131–139.

[23] Frank, R. N., Rodbard, D., *Arch. Biochem. Biophys.* 1975, *171*, 1–13.

[24] Rath, A., Glibowicka, M., Nadeau, V. G., Chen, G., Deber, C. M., *Proc. Natl. Acad. Sci. U.S.A.* 2009, *106*, 1760–1765.

[25] Engel, N., Weiss, V. U., Wenz, C., Rüfer, A., Kratzmeier, M., Glück, S., Marchetti-Deschmann, M., Allmaier, G., *Electrophoresis* 2015, *36*, 1754–1758.

[26] Wang, A. L., Paciolla, M., Palmieri, M. J., Hao, G. G., *J. Pharm. Biomed. Anal.* 2020, *180*, 113006.

[27] ProteinSimple, a Bio-Techne Brand. *Maurice reagents and consumables* 2020. https://www.proteinsimple.com/consumables_maurice.html.

[28] ProteinSimple, a Bio-Techne Brand. *Wes reagents and consumables* 2020. https://www.proteinsimple.com/consumables_sw_wes.html.

[29] PerkinElmer, Inc. *ProteinEXact HR assay user guide for LabChip GXII touch*, P/N CLS150849 Rev. D 2019.

[30] R&D Systems, a Bio-Techne Brand. *Recombinant human N–Cadherin*, Rev. 11/4/2019.

[31] R&D Systems, a Bio-Techne Brand. *Recombinant Human CD74*, Rev. 2/6/2018.

[32] R&D Systems, a Bio-Techne Brand. *Recombinant Human Erythropoietin/EPO*, Rev. 8/8/2019.

[33] R&D Systems, a Bio-Techne Brand. *Recombinant Human IGSF4A/SynCAM1*, Rev. 2/6/2018.

[34] Knoechel, T., Schmiedel, J., Ferguson, K. M., *Crystalline EGFR-Matuzumab complex and Matuzumab mimetics obtained thereof* (WO 2009/043490 A1) 2008.

[35] ProteinSimple, a Bio-Techne Brand. *Maurice CE-SDS Size Application Kit: PS-MAK02*, 046–407_RevC.

[36] ProteinSimple, a Bio-Techne Brand. *Maurice CE-SDS PLUS Size Application Kit: PS-MAK03-S*, PL3-0012, Rev A.

[37] ProteinSimple, a Bio-Techne Brand. *Wes Training Kit: PS-T001*, 031–105 RevJ.

[38] Gabaldón, M., *Int. J. Biol. Macromol.* 2002, *30*, 259–267.

[39] Dolnik, V., Gurske, W. A., *Electrophoresis* 2011, *32*, 2884–2892.

[40] Karim, M. R., Janson, J. C., Takagi, T., *Electrophoresis* 1994, *15*, 1531–1534.

[41] See, Y. P., Olley, P. M., Jackowski, G., *Electrophoresis* 1985, *6*, 382–387.

[42] Montreuil, J., Schachter, H., Vliegenthart, J. F. G., *GlycoproteinsII*, Elsevier, Burlington 1997.

[43] Roth, Z., Yehezkel, G., Khalaila, I., *Int. J. Carbohydr. Chem.* 2012, *2012*, 1–10.

[44] Reinés, A., Bernier, L.-P., McAdam, R., Belkaid, W., Shan, W., Koch, A. W., Séguéla, P., Colman, D. R., Dhaunchak, A. S., *J. Neurosci.* 2012, *32*, 6323–6334.

[45] Rath, A., Glibowicka, M., Nadeau, V. G., Chen, G., Deber, C. M., *Proc. Natl. Acad. Sci. U.S.A.* 2009, *106*, 1760–1765.

[46] Zhang, P., Tan, D. L., Heng, D., Wang, T., Mariati, Yang, Y., Song, Z., *Metab. Eng.* 2010, *12*, 526–536.

[47] Bagger, H. L., Hoffmann, S. V., Fuglsang, C. C., Westh, P., *Biophys. Chem.* 2007, *129*, 251–258.

[48] Segrest, J. P., Jackson, R. L., Andrews, E. P., Marchesi, V. T., *Biochem. Biophys. Res. Commun.* 1971, *44*, 390–395.

[49] Karger, B. L., Chu, Y. H., Foret, F., *Annu. Rev. Biophys.* 1995, *24*, 579–610.

[50] Bucior, I., Scheuring, S., Engel, A., Burger, M. M., *J. Cell Biol.* 2004, *165*, 529–537.

[51] Ponder, E., Ponder, R. V., *J. Gen. Physiol.* 1960, *43*, 753–758.

[52] Takeo, K., Kabat, E. A., *J. Immunol.* 1978, *121*, 2305–2310.

[53] Sugii, S., Kabat, E. A., Shapiro, M., Potter, M., *J. Exp. Med.* 1981, *153*, 166–181.

[54] Shirai, A., Matsuyama, A., Yashiroda, Y., Hashimoto, A., Kawamura, Y., Arai, R., Komatsu, Y., Horinouchi, S., Yoshida, M., *J. Biol. Chem.* 2008, *283*, 10745–10752.

[55] Guan, Y., Zhu, Q., Huang, D., Zhao, S., Jan Lo, L., Peng, J., *Sci. Rep.* 2015, *5*, 13370.

[56] Linzer, D. I. H., Levine, A. J., *Cell* 1979, *17*, 43–52.

[57] Levine, A. J., Oren, M., *Nat. Rev. Cancer.* 2009, *9*, 749–758.

[58] Gasteiger, E., Gattiker, A., Hoogland, C., Ivanyi, I., Appel, R. D., Bairoch, A., *Nucleic Acids Res.* 2003, *31*, 3784–3788.

[59] National Center for Biotechnology Information. *Welcome to NCBI* 1988, https://www.ncbi.nlm.nih.gov/.

A Novel Platform for icIEF Fractionation of Antibody Charge Variants

While imaged capillary isoelectric focusing electrophoresis (imaged cIEF or icIEF) has become the method of choice for monitoring charge variant levels of biotherapeutics, the in-depth characterization of charge variants has been carried out mostly by mass spectrometry (MS).

The MauriceFlex™ system is a new and innovative Maurice platform featuring icIEF-based fractionation for collecting protein charge variants, enabling downstream analysis of these variants with techniques such as MS. The fractionation utilizes a special cartridge to perform isoelectric focusing to separate protein charge variants, and once focused and separated, the charge variants are eluted via chemical mobilization for fraction collection. Compared to ion-exchange chromatography (IEX)-based fractionation, MauriceFlex™ fractionation is fast, with pI-based resolution, and overcomes some of the limitations of direct coupled cIEF-MS, such as the need for a dedicated interface and incompatibility of the background electrolytes with the MS. Moreover, offline fractionation and potential enrichment of charge variants pooled from multiple fractionations offer more flexibility for mass spectrometry characterization, including intact mass, reduced mass and peptide mapping.

In addition to fraction collection, MauriceFlex™ can perform routine CE-SDS and cIEF analysis using the relevant Maurice cartridges, and all data is analyzed using the 21CFR Part 11 compliant Compass for iCE software.

In this spotlight, we demonstrate the fractionation workflow and intact and peptide mapping analysis by liquid chromatography and mass spectrometry (LC-MS) on the NIST mAb (RM 8761 from NIST), which is a common reference standard for assessing new analytical technologies for characterizing monoclonal antibodies (mAbs).

Experimental Methods

The stepwise fractionation workflow on MauriceFlex™ is illustrated below:

1 Setup (~30min)

- Load reagents (kit provided) and NIST mAb (1 mg/mL)
- Insert MauriceFlex cartridge

2 Focusing (45min)

Voltage

- 10 min @500 V
- 10 min @1000 V
- 25 min @1500 V

3 Mobilization (25min)

- Mobilizer: 5 mM NH_4Ac
- Voltage: 1000V

4 Elution (20min)

Collect fraction

- 36 fractions at 25 second/fraction on a 96-well plate
- Each well contains 30 uL 5 mM NH_4Ac

Voltage

- 1000 V (off during transition from well to well)

5 Verification (4-5 hours)

- Check identify and purity of fractions with analytical Maurice icIEF
- 16 fractions checked

For intact mass, the fractions were analyzed directly. For peptide mapping, the charge variant fractions from 10 fractionation runs were pooled, lyophilized on a SpeedVac, and reconstituted prior to tryptic digestion. The digested samples were lyophilized and reconstituted in 40 µL 5 mM ammonium acetate solution.

The LC-MS characterization was performed with a Thermo Scientific™ Vanquish UHPLC coupled to a Q Exactive™ HF Hybrid Quadrupole-Orbitrap™ mass spectrometer. Reverse phase LC separation was used for intact mass analysis and peptide mapping with appropriate gradients of 0.1% formic acid in water and acetonitrile at 0.3 mL/min. The injection volume was 10 µL for both intact and peptide mapping analysis. The data were analyzed using BioPharma Finder 4.1 software.

Results

The method for fractionation of the NIST mAb sample using the MauriceFlex cIEF fractionation cartridge can be developed quickly based on the analytical method on a Maurice cIEF cartridge. **FIGURE 1** shows profiles of analytical icIEF and fractionation focusing runs of NIST mAb. Five charge variants (B2, B1, M, A1, A2) were identified for NIST mAb and their relative abundances were obtained (**FIGURE 1A**). Note that fractionation separation with cIEF fractionation cartridge is designed for maximizing the yield of the fraction collection, and for this purpose, a higher concentration (1 mg/mL) of NIST mAb was loaded. While this resulted in apparently lower resolution with overlapped peaks (**FIGURE 1B**) when compared to charge separation with the regular Maurice cIEF cartridge (**FIGURE 1A**), the same number of charge variants were detected, as seen in **FIGURE 1B**, and were well separated.

As shown in the workflow, the mobilization and elution steps take 45 minutes in total when collecting 36 fractions on a 96-well plate. The Compass for iCE software has a peak prediction feature that provides an estimated range of wells that contain the eluted charged variants. Alternatively, a fluorescence plate reader can be used to select the wells that contain the most abundant charge variant. For NIST mAb, a total of 16 wells of fractions were selected, and their identity and purity were verified with analytical Maurice icIEF. Among the 16 fractions analyzed, 12 were found to contain the charge variants.

FIGURE 2 shows icIEF electropherograms of fraction wells containing individual charge variants with the highest purity. As shown, except for low abundant B2 (0.9%) at 65% purity in fraction #10, fractions containing 100% purity for the four other charge variants were obtained.

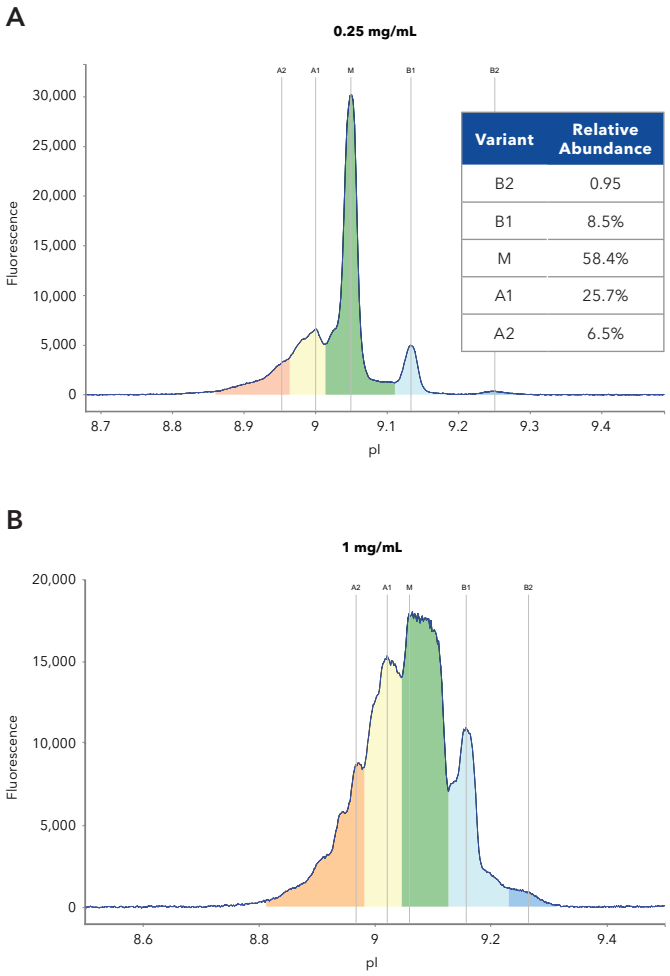

FIGURE 1. icIEF separation of NIST mAB charge variants with the Maurice cIEF cartridge (A) and MauriceFlex™ cIEF Fractionation cartridge (B). Both electropherograms show the same number of charge variants. The relative abundance (%) of each variant was calculated from the peak areas in the analytical run (A) and listed in the table insert.

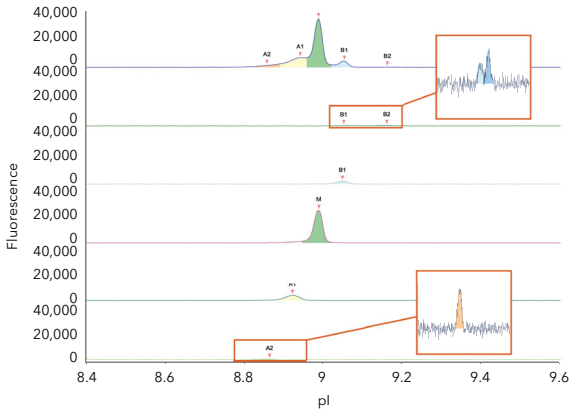

FIGURE 2. Verification of charge variants of representative fractions for identity and purity by Maurice icIEF analytical runs. The numbers assigned represent the fraction numbers.

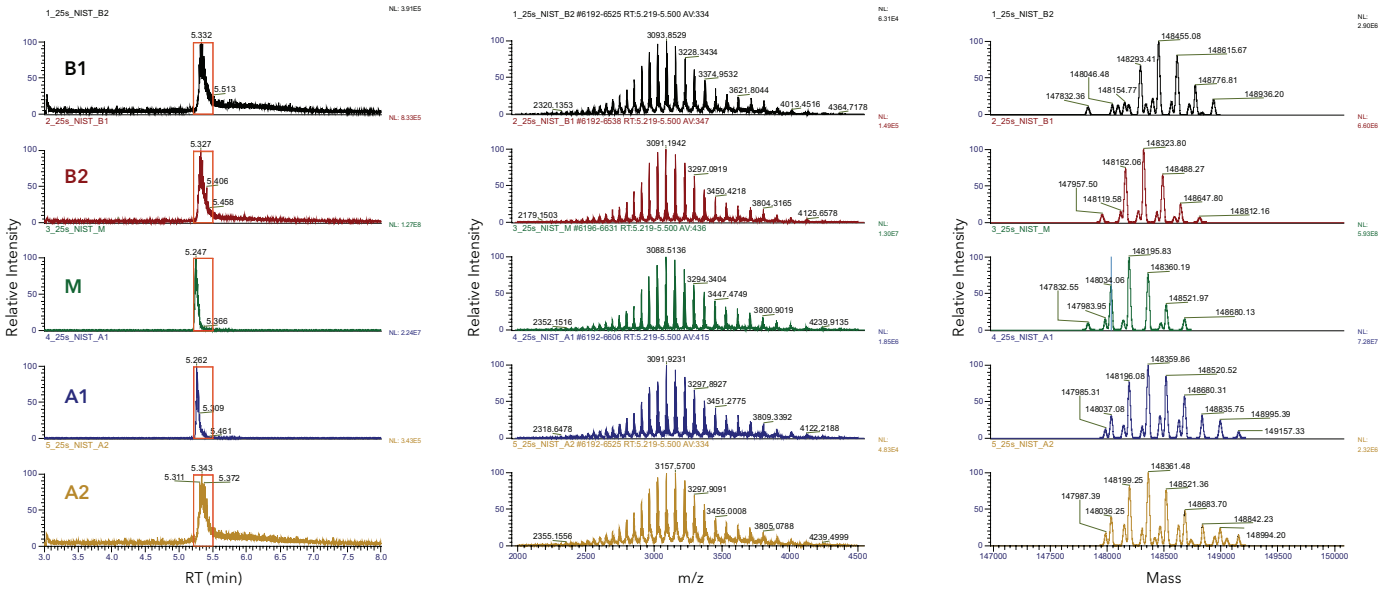

FIGURE 3. LC-MS intact mass analysis of charge variants showing total ion current (TIC) chromatograms (left), mass spectra of the peaks (middle) and the deconvoluted spectra (right).

The LC-MS intact mass analysis on the high purity charge variant fractions are shown in **FIGURE 3** and the modifications identified from the deconvoluted mass spectra for each charge variants are summarized in **TABLE 1**. The results are consistent with the established knowledge of PTMs of the charge variants of NIST mAb.

Peak	Deconvoluted Mass (Da)	Mass Shift (Da)	Modification
B2	148455.08	+259.25	2xC-term K
B1	148323.80	+127.97	C-term K
M	148195.83	0.00	G0F/G1F
A1	148359.86	+164.03	Glycation
A2	148361.48	+165.65	Glycation

TABLE 1. Summary of the identified modifications from intact mass analysis. The mass shifts of each variants are relative to the G0F/G1F glycoform of the M peak.

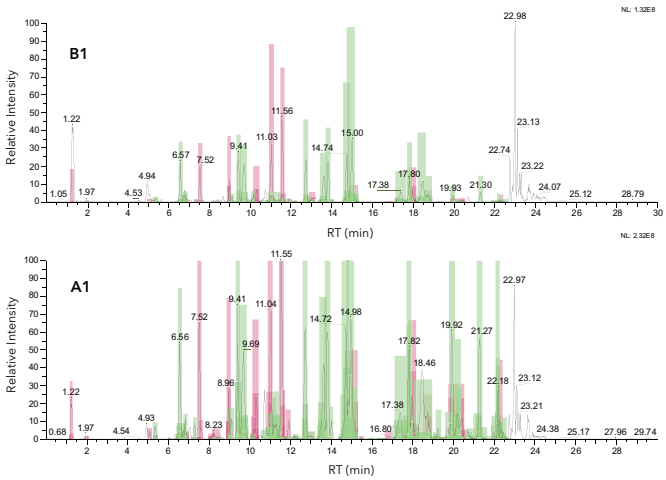

FIGURE 4. Representative chromatograms of the peptide mapping of B1 and A1, and sequence coverage of Light Chain (LC) and Heavy Chain (HC) of all charge variants. The charge variant samples were pooled from 10 fractionation runs.

Peptide mapping is an indispensable tool for characterizing the primary structure of biotherapeutics, and the capability of pooling charge variants from multiple fractionation runs on MauriceFlex™ makes it possible to enrich the charge variants for peptide mapping analysis. **FIGURE 4** demonstrates the peptide mapping results from samples pooled from 10 fractionation runs. As shown, the sequence coverage is above 90% for all variants except for the low abundant B (relative abundance 0.9%) and heavy chain (HC) of the A2 peak.

Sequence Coverage %		
Fraction	LC	HC
B2	84.0	58.9
B1	94.4	92.4
M	95.3	94.0
A1	95.3	92.2
A2	93.9	73.8

Conclusion

By using the NIST mAb sample with the icIEF fractionation feature on the new MauriceFlex™ system, we have demonstrated that:

- High purity fractionation of charge variants can be obtained in a single day
- A single fractionation run provides sufficient charge variant fractions for intact mass analysis
- With enrichment from pooling fractions from multiple runs, charge variants can be analyzed with LC-MS peptide mapping